VALIDATION OF A HYDRODYNAMIC MODEL OF DELAWARE BAY AND THE ADJACENT COASTAL REGION

BY

PHILLIP J. CASTELLANO AND JAMES T. KIRBY

RESEARCH REPORT NO. CACR-11-03
JUNE 2011

This study was supported by the Delaware Sea Grant Program
Project Number NOAA SG0910 R/ETE-17

CENTER FOR APPLIED COASTAL RESEARCH

Ocean Engineering Laboratory
University of Delaware
Newark, Delaware 19716

TABLE OF CONTENTS

LIST OF TABLES

LIST OF FIGURES

ABSTRACT

The goal of this research is to validate a hydrodynamic model of Delaware Bay and the coastal region surrounding it. The aim is to simulate all the major forces over a long period of time, and compare the results to a wide range of available measured data.

The model used here is ROMS, an open source regional model that has been used successfully in similar applications. ROMS has been calibrated and set to run for four years, from January 1st 2006 to December 31st 2009. Tidal, wind, and river forcing are used to drive the simulation.

There is measured data available from high frequency radars set up across the bay mouth, which measures surface currents over a large area outside of the mouth. Also, ADCP measurements were taken around the bay mouth for extended periods of time to provide 3D current data.

Assessment of model and measured data is done with a complex correlation analysis, along with point comparisons. The results of these comparisons show that the model performs almost perfectly under tidal conditions, and still remains very accurate with the wind and river discharge forcing as well. Evaluation of 3D velocity profile data between the model and measured data indicates the model is performing correctly vertically as well.

The large amount of data produced from the simulation allowed for an examination of buoyant plume activity in the area. The model shows the formation and dissolution of freshwater plumes under many discharge and wind conditions.

Chapter 1

INTRODUCTION

1.1 Background

The Delaware Estuary is a major estuary on the East Coast of the United States, a major portion of which is Delaware Bay. Home to millions of people, the estuary drains an area of 420,000 km^2 (Sharp 1984). Its waters create a natural border between the states of New Jersey and Delaware. The Bay is 45 km apart at its widest, and shortens to 18 km wide near the bay mouth (Wong and Münchow 1995). There is a deep channel that extends through much of the bay and out of the bay mouth (Garvine 1991), but it is only about 7m deep on average (Harleman 1966). It is home to a diverse ecosystem, and is used for transportation, commerce, fishing, and recreational activities.

There is a large freshwater input to the bay, which has a tendency to exit out of the bay mouth and travel down the coast under the right conditions. Delaware River provides the majority of the freshwater input, with no other source independently contributing more than 1% (Sharp 1984). Based on information provided by the USGS, the average discharge of the river at the Trenton, NJ stream gage is approximately 350 m^3/s. The coastal jet that forms from this freshwater can transport nutrients, pollutants, and suspended sediment.

1.2 Past Work and Research Objectives

The main goal of this modeling effort is to create an accurate simulation of the hydrodynamics of Delaware Bay and the surrounding area, and validate the results of this simulation with various reliable sources of measured data. Creating an accurate simulation allows access to a robust data set of information on surface, current, salinity, etc. This information can then be utilized to study the waters in and around Delaware Bay.

The dynamics of Delaware Bay have been studied extensively. The observational study by Garvine (1991) examining the interaction with the estuary and the adjacent shelf noticed evidence of a buoyancy-driven coastal current. Prior to this study, it was not known that an estuary as weakly stratified as Delaware Bay could produce a coastal current. This information led to more work being done investigating this phenomenon.

Since that time, the coastal current has been studied at length in works by Garvine, Wong, and Münchow. Data began to be collected over long periods of time, for multiple different studies, to explore the nature of this buoyant outflow. Münchow and Garvine (1993a and 1993b) concluded the downshelf flow of the plume is in semi-geostrophic balance with the across shelf pressure gradient, and that wind forces can heavily modify the plumes behavior.

Other similar studies have been conducted since then. The most recent measurements available are from 1993 and 1994. The results have been published in Sanders (1999) and Sanders and Garvine (2001). The Spring of 1993 showed a buoyant plume that extended far downshelf of the bay mouth due to a large amount of precipitation that created very high river discharge.

This previous work on the dynamics of the Delaware Bay, most notably relating to the buoyant outflow, led to the work of Whitney (2003). His goal was to model the bay and adjacent coastal region in order to simulate and study the coastal current that travels down the flanks and exits out the bay mouth, and compare his results to the 1993 and 1994 data. This was accomplished using the ECOM3d model.

To run this simulation Whitney (2003) created a grid containing Delaware Bay and a significant portion of the Atlantic Ocean out to the 100m isobath. The grid uses a variable resolution to give more detailed information around the bay, yet still remain efficient. To force the model he used tide, wind, and river discharge information as input. These conditions created a realistic environment on the appropriate scale to examine the coastal jet. The jets produced by his model were found to compare well with observed data.

More recent modeling efforts have been done using ROMS (Shchepetkin and McWilliams, 2005). ROMS is very useful for accurately modeling nearshore environments. It has been successfully used in many realistic scenarios. Marchesiello et. al. (2003) used ROMS to measure the equilibrium structure of the Pacific Ocean region around California. Choi and Wilkin (2006) examined the wind effects on the plume from the Hudson River in New York. Kosters (2006) investigated the transport of dense water through the Denmark Strait. These are just a few of the myriad examples of ROMS being used to study realistic phenomena, and reinforcement of why it is an appropriate choice for modeling Delaware Bay.

Newer simulations of Delaware Bay using ROMS, which is the model used in this study, preceded the present endeavor. The first of these simulations was completed by Qin et, al. (2005). ROMS was run over short periods of time with the

grid used in Whitney (2003), and with I/O coupling to a third generation numerical wave model, SWAN. The focus here was simulating wave activity at Fourteen Ft. Bank Lighthouse, which showed positive results. There was some comparison of the currents produced by ROMS with current data from an ACDP over short periods of time. Though a small sample, the currents here compared fairly well.

Chen (2010) also used the grid from Whitney (2003) to model Delaware Bay in ROMS. This study used ROMS together with SWAN as well, but this time the models were coupled with the Model Coupling Toolkit (MCT) explained in Warner et. al. (2008). This work improved the communication between ROMS and SWAN, but still only offered a localized data comparison over the course of a few days.

In the past few years a large amount of measured data has been gathered around the bay in the form of 3D ADCP profiles, and 2D surface current measurements from a pair of HF radars. This information will prove integral in evaluating and assessing the accuracy of model results. The radar is running continuously and collects current information at the surface over a large area; the 3D ADCP data has been collected from numerous deployments in recent years, and at multiple locations around the bay mouth.

This most recent effort modifies and builds on the previous work. Notably, these prior tests have been for shorter periods of time, the previous ROMS work did not include freshwater input from the Delaware River, and did not have the large amount of measured data that will be used in the current modeling effort for validation.

1.3 Overview

This document provides information on the model used to run simulations, the setup and output of these model runs, comparison on model results to measured data, where the measured data is coming from, and an examination of buoyant plumes escaping from Delaware Bay.

Chapter 2 concentrates on information about the model and model setup. The equations and boundary conditions used within the model will be presented. Settings used on input, as well as the generation of those settings are assessed. Information on the domain, bathymetry, and forcing applied is also handled here.

Chapter 3 is an exploration on where the data used to compare to model results comes from, as well as an explanation about the correlation method used to compare model and measured data.

Chapter 4 centers on comparing model data to the measured data described in the previous chapter. Model data is compared to the 2D radar data source with a large sampling footprint, and 3D ADCP data at specific locations.

Chapter 5 is an exploration of the salinity conditions in the bay and conditions when a buoyant plume escapes out of the bay mouth. The salinity information from the model results is used to examine when this phenomenon occurs, as well as the structure of the plume.

Chapter 2

MODEL SETUP AND IMPLEMENTATION

2.1 Choice of Model

To best simulate the conditions present in Delaware Bay, the Regional Ocean Modeling System, or ROMS as it will be referred to in the rest of this document, was chosen. ROMS is a three dimensional ocean circulation model that solves primitive equations with the Boussinesq approximation and a hydrostatic momentum balance in the vertical using a split-explicit time stepping scheme (Shchepetkin and McWilliams, 2005). This allows for multiple 2D time steps for each 3D one, which makes the model much more efficient. Though not used in the present work, ROMS is also capable of numerous other applications such as biogeochemical (Power et al., 2006; Fennel et al., 2006), bio-optical (Bissett et al., 1999), sediment (Warner et al., 2006), and sea ice (Budgell, 2005).

The ROMS code is executed according to numerous C-preprocessing options specified prior to running the model. It can be run in either serial or parallel, for both shared and distributed memory. ROMS has the capability to be coupled with other models such as the wave formation and propagation model SWAN (Booij et al., 1999) via the Model Coupling Toolkit (Warner et al., 2008). The bulk parameterization of the atmospheric forcing from Fairall et al. (1996) is the basis for the air-sea interaction in ROMS. To better specify these values, ROMS is being

coupled to an atmospheric model, WRF (Skamarock et al., 2005). This is currently working, but not available for public release (Warner et al., 2010).

ROMS has been successfully used in many different studies over the last decade (Haidvogel et al., 2000, Marchesiello et al., 2003, Wilkin et al., 2005, and many more). It should prove ideal for both present and future modeling efforts in Delaware Bay.

2.2 Equations of Motion

The primitive equations solved by ROMS will be shown in this section. This information comes directly from the ROMS wiki.

The momentum balance, in Cartesian coordinates, is

$$\frac{\partial u}{\partial t} + \vec{v} \cdot \nabla u - fv = -\frac{\partial \phi}{\partial x} - \frac{\partial}{\partial z}(\overline{u'w'} - \nu \frac{\partial u}{\partial z}) + F_u + D_u \tag{2.1}$$

$$\frac{\partial v}{\partial t} + \vec{v} \cdot \nabla v + fu = -\frac{\partial \phi}{\partial y} - \frac{\partial}{\partial z}(\overline{v'w'} - \nu \frac{\partial v}{\partial z}) + F_v + D_v \tag{2.2}$$

In this equation ϕ represents the dynamic pressure.

The progression of a tracer variable such as salinity is dealt with by the advective diffusive equation

$$\frac{\partial C}{\partial t} + \vec{v} \cdot \nabla C = -\frac{\partial}{\partial z}(\overline{C'w'} - \nu_\theta \frac{\partial C}{\partial z}) + F_C + D_C \tag{2.3}$$

Where the equations are closed by parameterizing the tracer flux ($\overline{C'w'}$) and Reynolds stresses ($\overline{(u,v)'w'}$).

The equation of state is

$$\rho = \rho(T, S, P) \tag{2.4}$$

The vertical momentum balance in the hydrostatic and Boussinesq approximations is:

$$\frac{\partial \phi}{\partial z} = -\frac{\rho g}{\rho_o} \tag{2.5}$$

Continuity for an incompressible fluid is given by

$$\frac{\partial u}{\partial x} + \frac{\partial v}{\partial y} + \frac{\partial w}{\partial z} = 0 \tag{2.6}$$

Table 2.1 Variables used in the equations of motion.

D_u, D_v, D_C	Diffusive terms
F_u, F_v, F_C	Forcing terms
$f(x, y)$	Coriolis parameter
g	Acceleration of gravity
$h(x, y)$	Bottom depth
ν, ν_Θ	Molecular viscosity and diffusivity
P	Total pressure $P \sim \rho_o g z$
$\phi(x, y, z, t)$	Dynamic pressure $\phi = (P/\rho_o)$
$\rho_o + \rho(x, y, z, t)$	Total *in situ* density
$S(x, y, z, t)$	Salinity
t	time
$T(x, y, z, t)$	Potential temperature
u, v, w	The (x, y, z) components of vector velocity $\vec{v}$ (u, v, w)
x, y	Horizontal coordinates
z	Vertical coordinate

Vertical boundary conditions at the surface are the Reynolds stress parameterization balancing out the surface stress induced by the wind, the turbulent tracer flux balancing out a surface concentration flux of the tracer, and the vertical velocity as the rate of change of the free surface. At the bottom the Reynolds stress parameterization balances a bottom stress based on a chosen bottom stress type and

coefficient, and the tracer flux is zero. The options for conditions at the horizontal boundaries will be covered in the following chapter.

2.3 Curvilinear Coordinates

In order to better adapt to irregular boundaries and locally increased grid resolution, ROMS adopts a curvilinear grid. The formally x, y oriented coordinates are now expressed as a function of $\eta(x,y)$ and $\xi(x,y)$. This will change the equations of motion, which can be rewritten according to Arakawa and Lamb (1977), while the boundary conditions stay the same.

2.4 Vertical Coordinates

To represent the different vertical levels at each point in the grid, ROMS uses terrain following vertical s-coordinates (Song and Haidvogel, 1994). This flattens out the boundary at the bottom of the water column and simplifies the vertical velocity boundary by having it equal to zero at the upper and lower bounding surfaces of the vertical coordinate transformation. Similar coordinate systems have long been used in both meterorology and oceanography (Phillips 1957, Freeman et al. 1972).

2.5 Domain

The area contained by the grid used in running the model simulations covers Delaware Bay and much of the surrounding region. The reach of this domain expands far offshore to the 100 m isobath, and extends 340 km from North to South. For application of the tidal forcing it is critical to have the offshore boundary lie along an isobath. The domain extends 110 km upshelf from Delaware Bay and terminates along a boundary located directly across shelf of the Jersey Shore northward of Atlantic City to the 100 m isobath. Downshelf, it stretches 230 km and stops at the

Chesapeake Bay. This can be seen in figure 2.1, where grid boundary geometry is superimposed on an image from Google Earth. There are many small inlets and geographic features such as Chincoteague Bay, Assawoman Bay, Indian River Bay, Great Egg Harbor, Great Bay, and the previously mentioned Chesapeake Bay that are contained in the domain, but not represented in the grid. In order to focus on the dynamics of Delaware Bay and minimize the influence from boundaries these features were intentionally omitted (Whitney, 2003).

The grid was created with the Gridpack grid generation software (Wilkin and Hedstrom, 1991). In order for the offshore boundary to be able to follow the isobath, curvilinear coordinates must be used. Approximately half the cells have a land mask applied to them, and the landward boundary is kept straight. It is not possible within the constraints of the grid to perfectly follow the coastline. Also, the Delaware River had to be bent in order to keep it within the limits of the grid, but this does not affect the results as it only has local effects (Whitney, 2003).

2.6 Bathymetry

The data for the bathymetry of Delaware Bay, along with the rest of the model domain, was provided on CD by the NOAA National Geophysical Data Center, and passed through a median filter in order reduced noise and create a low-passed data set of bathymetry information that can be used in the model (Whitney, 2003). The minimum water depth in the grid is 3 m, so the 3 m isobath becomes the location of the land boundary for the purposes of the simulation. Figure 2.2 illustrates the bathymetry information of the total domain, while figure 2.3 shows the data for Delaware Bay only.

Depth, volume, and width of the Bay have been kept as realistic as possible in order to accurately represent the dynamics of the region. However, the 3 m isobath within the Bay lies too far offshore for the size of Delaware Bay to be sensible, so the land boundary in the Bay is set at the 1.5 m isobath. The depth for these water cells are artificially set to 3 m. This causes a less than 2% increase in volume within the Bay, yet keeps the Bay width much closer to the actual values.

Accurate information on the Delaware River can not be provided by the NOAA bathymetry data, so this information is obtained from Thatcher and Harleman (1981). As best as is possible due to the restrictions of the grid, the width and depth of the Delaware River is represented based on this data.

2.7 Grid Resolution

The grid employed by the model is 300 by 150 cells, and rotated into η and ψ coordinates in order to correctly follow the coastline. The resolution employed is variable because larger spacing can be accepted far enough offshore, and the computational efficiency is greatly improved by not having a full grid at the smallest resolution needed. Due to the transformation into curvilinear coordinates the size of the cells will have some variation. The density of grid points can be seen in figure 2.4. Just outside Delaware Bay and the surrounding area has the highest resolution with 0.75 km cell size before the transformation. The rest of the Bay has 0.75 km cell size across the bay, and 1.5 km along it before the transformation. The bathymetry in the area is highly variable, making the smaller cells in this area necessary. This is important because the densest portion of the grid overlaps with the valid portion of CODAR coverage, which will be discussed in a later section. It is vital to have the smaller grid cells in more critical areas in order to properly resolve any instabilities or

eddies that are of smaller scale than the larger grid cells. The largest of these grid cells are located far offshore and are up to 8 km (Whitney, 2003).

The vertical structure of the grid consists of 10 terrain following, vertical levels. This type of vertical structure used by ROMS was discussed earlier in the chapter. The use of *s*-levels allows all measurements at the *s*-level closest to the surface to happen at roughly the same depth, regardless of the bathymetry of the area. An example of this can be seen in figure 2.5, which shows the *s*-levels for a horizontal slice of the grid from inside the Bay to offshore.

2.8 Typical Settings

In order to run simulations in ROMS, there are many initial settings that need to be prescribed. These settings are vital to obtaining accurate output from the model.

The baroclinic time step is set to be 150 seconds for 3D calculations. This number was reached through testing to provide a stable environment for the simulation to run. In the absence of river outflow this time step could be doubled, but needed to be reduced in order to maintain stability through times of higher discharge. Since ROMS allows a split time step between the 2D and 3D, many barotropic steps can be resolved for each baroclinic step without sacrificing a large amount of efficiency. In this case, there are 30 2D iterations for every 3D step. While the time step is 150 s, the model is set to provide output only ever hour. This still gives an accurate picture of tidal oscillations for current and free surface, while greatly saving on storage space.

Quadratic bottom drag is used, and the coefficient is set to 5.0×10^{-3}. This value was reached through starting the coefficient at a typical value of 2.5×10^{-3}, and increasing this number until the tidal amplitude from the model best matched with that

from observed data. Tests were done at values of $2.5\text{x}10^{-3}$, $3.0\text{x}10^{-3}$, $3.5\text{x}10^{-3}$, $4.0\text{x}10^{-3}$, $5.0\text{x}10^{-3}$, and $5.5\text{x}10^{-3}$. Comparisons to available data show the value of $5.0\text{x}10^{-3}$ to produce amplitudes that best agree with observed conditions in Delaware Bay. This number is higher than the standard value, but still realistic when looking at the friction coefficient estimate in Mellor (1998) of

$$C_d = \frac{\kappa^2}{(\ln(\frac{H}{2z_0}))^2} \tag{2.7}$$

Where C_d is the friction coefficient, κ is the von Kármán constant, H is the water depth, and z_o is the bottom roughness. The bottom stress is then calculated

$$\tau_{u_B} = C_d u_B \mid \vec{v}_B \mid \tag{2.8}$$

$$\tau_{v_B} = C_d v_B \mid \vec{v}_B \mid \tag{2.9}$$

Where $\vec{v}_B$ is the velocity vector closest to the bed, and (u_B, v_B) are its components. Though ROMS applies a constant friction coefficient regardless of factors such as water depth, in the shallower areas where the bottom friction is most critical a value of $5.0\text{x}10^{-3}$ provides reasonable values for water depth and bottom roughness.

Initial conditions are set so the ocean starts at rest and the free surface and all velocities are zero. The salinity in the ocean and bay is set at 35 psu at all *s*-levels at the outset. While this is an appropriate value for the surrounding ocean, it is obviously not the case for much of Delaware Bay due to freshwater discharge. The model is given ample time to develop the salinity field in the bay before any meaningful comparisons are made. Temperature is set at 10 degrees Celsius, and no temperature variation is included in the model so this will never change. Since the

temperature is kept constant it will not affect the density field, but locations that experience large salinity changes will see changes in density for those areas.

In order to transport the salinity tracer in the simulation, the Akima fourth order advection scheme is used (Akima, 1984). This advection is used in the ROMS river plume examples. It produced good results during testing of different types of advection, though there was not a large difference between different advection schemes. The vertical mixing chosen is a non-local closure scheme based on K-profile boundary layer formation (Large et al. 1994). This was used because it is the closure of choice in the header files of the ROMS river plume examples provided with the model. Testing in Robertson (2010) between ten different types of closure showed very little difference in the velocity field for each.

2.9 Boundary Conditions

In the simulation there are three open boundaries out in the ocean to contend with, plus the land boundary. The land masked points are treated as a wall, which applies a zero gradient for surface elevation and tracers and no flow for normal velocity. The wall boundary is allowed to be free slip for tangential velocities.

At the open boundaries ROMS offers a wide array of conditions. For the free surface the Chapman condition is used, which takes gravity wave propagation into account (Chapman, 1985). The momentum at the boundary is handled by the Flather condition. Variations from exterior values of the normal 2D velocity are radiated out at the speed of the external gravity waves (Flather, 1976). This condition requires that external momentum forces must be supplied. For 3D momentum and tracers (salinity in this case), a radiation condition first proposed by Orlanski (1976) and then modified

by Raymond and Kuo (1984) is used. This only allows fluxes to radiate out, and applies a zero gradient if anything is trying to radiate in.

For realistic applications, these are typically the best choices for boundary conditions. The Chapman and Flather conditions work well in tandem, and the radiation condition performs similar to a simple zero gradient at the boundary, but in this case it is important to allow salt to leave out of the bottom of the domain. The other choice for tidal forcing would be to prescribe a free surface and clamp that to the boundary; however this does not perform as well as the Chapman condition (Mori 2007).

2.10 Model Forcing

In order to force the simulations, the three main forces in the area have been included. The most important is the tidal forcing, which is the main contribution to the oscillations in free surface and current. Wind forcing also plays a large role, especially during periods of strong wind events, which can create significant non-tidal currents. Lastly there is river discharge. The momentum from this can propagate along the south side of the bay, all the way out of the bay mouth. It also pumps fresh water into the domain. All of these forcings are given to ROMS in the form of NetCDF files (Rew and Davis 1990).

As in Whitney (2003), types of forcing on a larger scale, such as seasonal effects and shelf circulation, are not considered. Relatively, they are much less important to the simulation than the included forcing.

Model runs are carried out for a total of four years, from 2006-2009. The simulation is allowed to run for a year before any meaningful data is recorded, starting in 2007. This spin up period is ample time for the salinity field in the bay to develop.

2.10.1 Tidal Forcing

Since the tidal forcing plays such an important role in the dynamics of the bay, it must be included as accurately as possible. This was accomplished by using the ADCIRC tidal database (Luettich et al. 1992). To do this, the appropriate database must be downloaded from the ADCIRC website, and the information needs to be extracted that pertains to Delaware Bay grid.

This can be done by using appropriate software obtained from the Rutgers Marine Science department found here (http://marine.rutgers.edu/~hunter/roms/tides/otps/), which will extract the relevant tidal information from ADCIRC and save it as a ROMS forcing file. The scope of the ADCIRC database is more than sufficient to cover all the boundaries of the domain.

The tidal constituents used are M6, M4, K2, S2, M2, N2, K1, O1, and Q1. As is required by the boundary conditions, both the phases and amplitudes for the free surface and velocity are prescribed in the forcing file. The most dominant of the constituents for Delaware Bay is M2, and a picture of the elevation amplitude and phase information resulting from the information in the database can been seen in figures 2.6 and 2.7 respectively. Though the information is displayed for the whole grid, it is only used at the boundary. Data for the other constituent's elevation, velocity, and phase are provided in the same fashion.

2.10.2 Wind Forcing

Forcing from the wind is applied for the whole grid. For Delaware Bay it has been demonstrated that using a spatially uniform or spatially varying wind field from the available wind information does not make a large difference in wind speed in the relevant areas in and around the bay (Qin 2005). For this application a spatially

uniform approach is taken. This has the advantage of being able to update the wind information constantly with a relatively small input file. In this case new surface forcing from the wind is fed to the model every hour.

Out of the available stations to gather wind speed and direction in the area, none have a flawless data record over the lengthy four year simulation. To remedy this, a composite of three different wind gages was formulated and used. These are the anemometer at the Brandywine Lighthouse located on the Brandywine Shoal, one in Lewes, DE, and NDBC buoy 44009. The locations of these stations can be seen in figure 2.8. These locations were chosen because of their close proximity to the area chiefly targeted by the data comparisons in a later chapter. The data taken from these locations is given hourly.

Ideally, NDBC 44009 would be used as the main wind record because it is out in the ocean undisturbed by natural boundaries, but the information is too unreliable and it will randomly skip over time steps. For this reason the lighthouse station was used as the base wind record for its stability. It is located in the middle of the bay, and fairly high in the air. The speed and direction of the wind records in these locations generally agree well, though some scaling is required. The base speed for the data was chosen to be the 10 meter wind speed at buoy 44009 because it represents a wind measurement out in the open ocean, which is where the majority of data comparisons will be made during later analysis. The buoy reports wind at a height of 5 m, and the 10 m speed is found using a simple power law described by Johnson (1999). The data from the lighthouse is taken at a higher elevation of approximately 18 m, and due to the slowdown from the nearby land it is just about a one-to-one ratio with the 10 m buoy data based on a comparison of the velocities from both sensors.

The data from Lewes requires the biggest correction. As a whole over the entire record, the wind speed for 10 m elevation at the buoy is about 1.4 times faster than the speed at Lewes. However, this relationship is partially dependant on how fast the wind is blowing, so different ratios were applied to transform the Lewes data depending on the velocity of the wind. These ratios were found by separating all reported speeds at Lewes, DE into groups of less than 3 m/s, 3-6 m/s, 6-10 m/s, 10-15 m/s, and greater than15 m/s. The average speed for each group was then compared to the average speed of the concurrent measurements from the Brandywine, DE sensor for each group. As mentioned above, the measurements from the Brandywine sensor are in a one-to-one ratio with the 10 m speed at buoy 44009. The ratio of the averages is displayed in table 2.2.

Table 2.2 Conversion factors for wind speed from the sensor at Lewes, DE to the 10 m wind speeds at buoy 44009.

Wind speed at Lewes, DE sensor (m/s)	Conversion factor to 10 m 44009 speed
< 3	2
3-6	1.5
6-10	1.3
10-15	1.15
>15	1.05

The lighthouse data is checked for bad values, and if missing or bad data is found, it is replaced with data from either buoy or Lewes. When using data from the buoy, care must be taken to make sure the date numbers match, because of the time steps completely omitted from the data record at random. Data from Lewes must be scaled to be at the appropriate speed. By using three separate locations there is rarely a

time when wind information can not be found, which makes for a much more complete and accurate record than if only one location was used.

The combined wind record is used to force ROMS through the formulation of surface wind stress. These are calculated with a simple parameterization that requires only the wind speed as input (Large and Pond 1981). This formulation calculates a drag coefficient based on wind speed and uses this to calculate stress. The drag coefficient formulations are as follows:

$$C_D = \frac{1.2}{10^3} \qquad U_{10} \le 11 m/s \tag{2.10}$$

$$C_D = \frac{0.49 + 0.065\,|U_{10}|}{10^3} \qquad U_{10} \ge 11 m/s \tag{2.11}$$

where U_{10} is the 10 meter wind speed in m/s, and C_D is the drag coefficient. The wind stress is then found:

$$\tau_{u_{10}} = 10^3 u_{10} \rho C_D \frac{|U_0|}{1 + \frac{\sqrt{C_D}\ln(\frac{z_0}{10})}{.41}} \tag{2.12}$$

$$\tau_{v_{10}} = 10^3 v_{10} \rho C_D \frac{|U_0|}{1 + \frac{\sqrt{C_D}\ln(\frac{z_0}{10})}{.41}} \tag{2.13}$$

where τ is stress, ρ is the density of the air, z_0 is the height of the measurement, U_0 is the wind speed vector at z_0, and u_{10} and v_{10} are the 10m wind speed components.

A plot of the wind speed and direction for each year of the simulation can be seen in figures 2.9 - 2.12. This data is used to find the surface stresses and then written into a NetCDF file with the NetCDF toolbox for Matlab, so it may be read by

ROMS as input. Since the stress is not being specified at each individual grid point, it should be input as true East and North. ROMS will automatically rotate to the local coordinates for each point.

2.10.3 River Forcing

Records of the river discharge over the four year simulation period are taken from the Delaware River gage at Trenton, NJ, maintained by the USGS (http://waterdata.usgs.gov/de/nwis/uv/?site_no=01463500&PARAmeter_cd=00065,00060,62619,62620). The data is obtained in a text file as a daily time series. This discharge is 58% of the freshwater that flows into Delaware Bay (Sharp 1984). Using this information, the data from the gage at Trenton is modified and used to represent all of the freshwater input for the bay (Whitney 2003).

The discharge from the river is given in ft^3/s, so it is changed to m^3/s as metric input is required by ROMS. The outflow is allowed to ramp up from the model start time for approximately 10 days before it is fully realized. All flow enters the bay at the land-water boundary at the top of the river in the grid, and salinity is set to be 0 psu. It is also set at 10 degrees Celsius to match the temperature of the model.

As usual, the forcing is entered into a NetCDF file. The river transport is applied at the same 10 *s*-levels used by the model, which is done by matching the vertical stretching information obtained from the grid. The river forcing is introduced at noon in model time, and changes every 24 hours to reflect new discharge levels.

It takes between three and four months for the salinity field in the bay to fully develop. As was stated before, the model start time is far before useful data is needed, so this bay salinity has more than enough time to be fully realized. As to be

expected the outflow varies greatly over the course of four years, and these fluctuations are illustrated in figure 2.13.

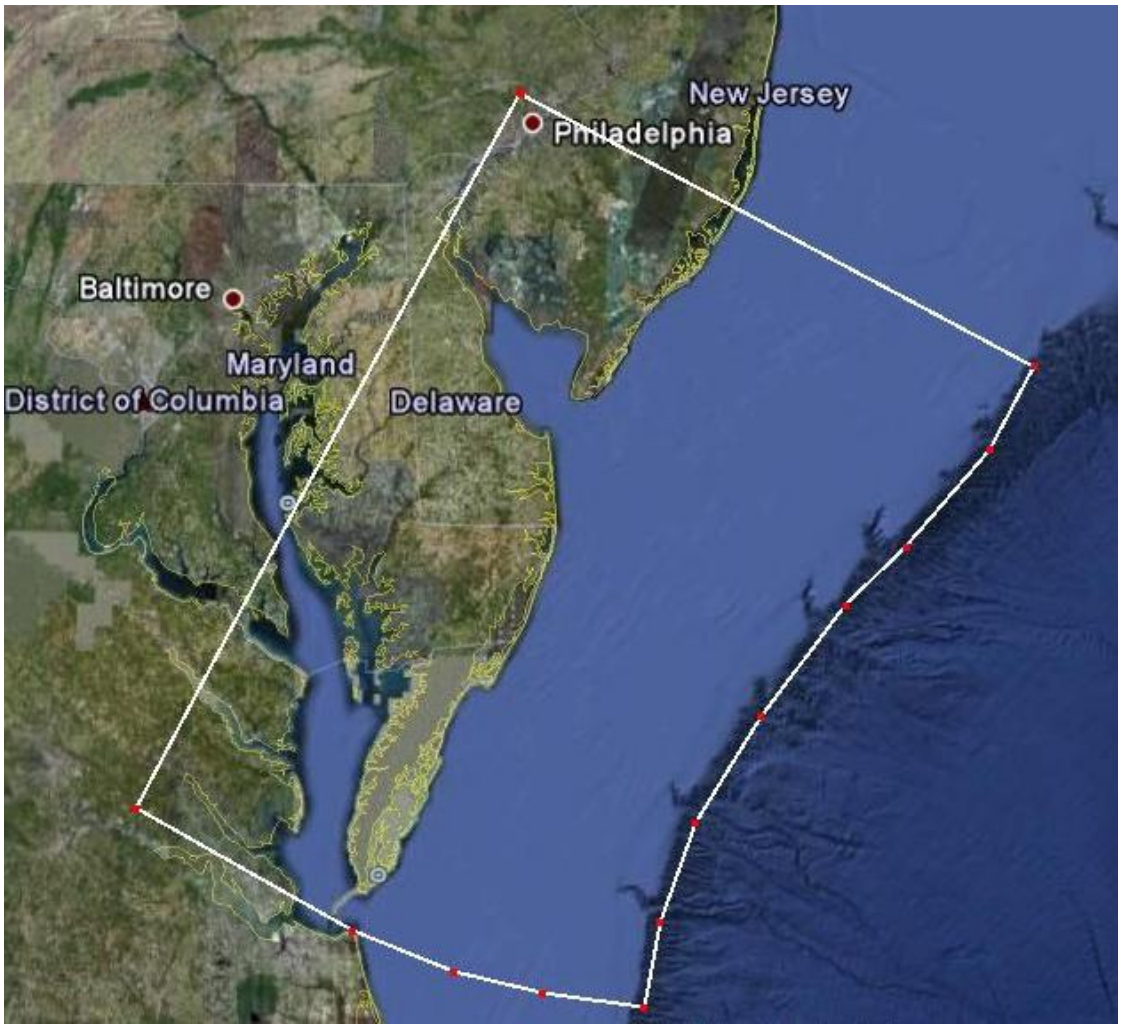

Figure 2.1 Domain of the grid, as seen from Google Earth.

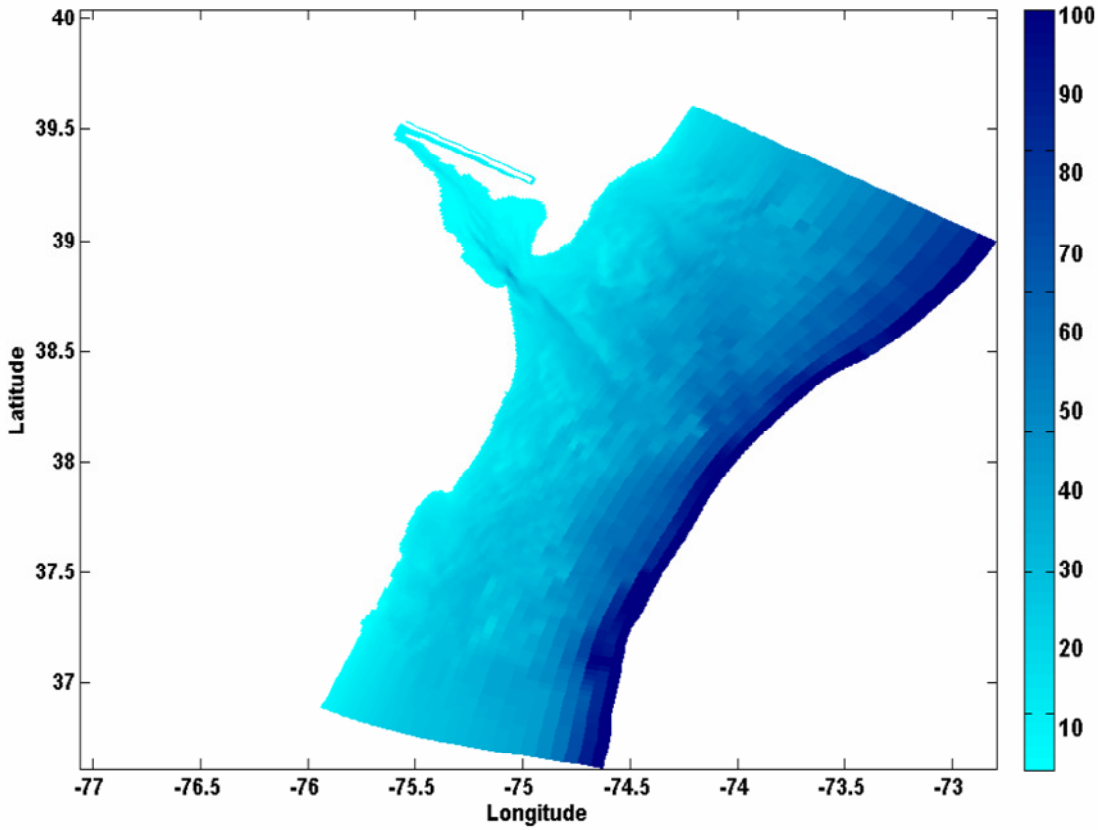

Figure 2.2 Bathymetry of the entire grid for every cell. The units of the color bar are in meters.

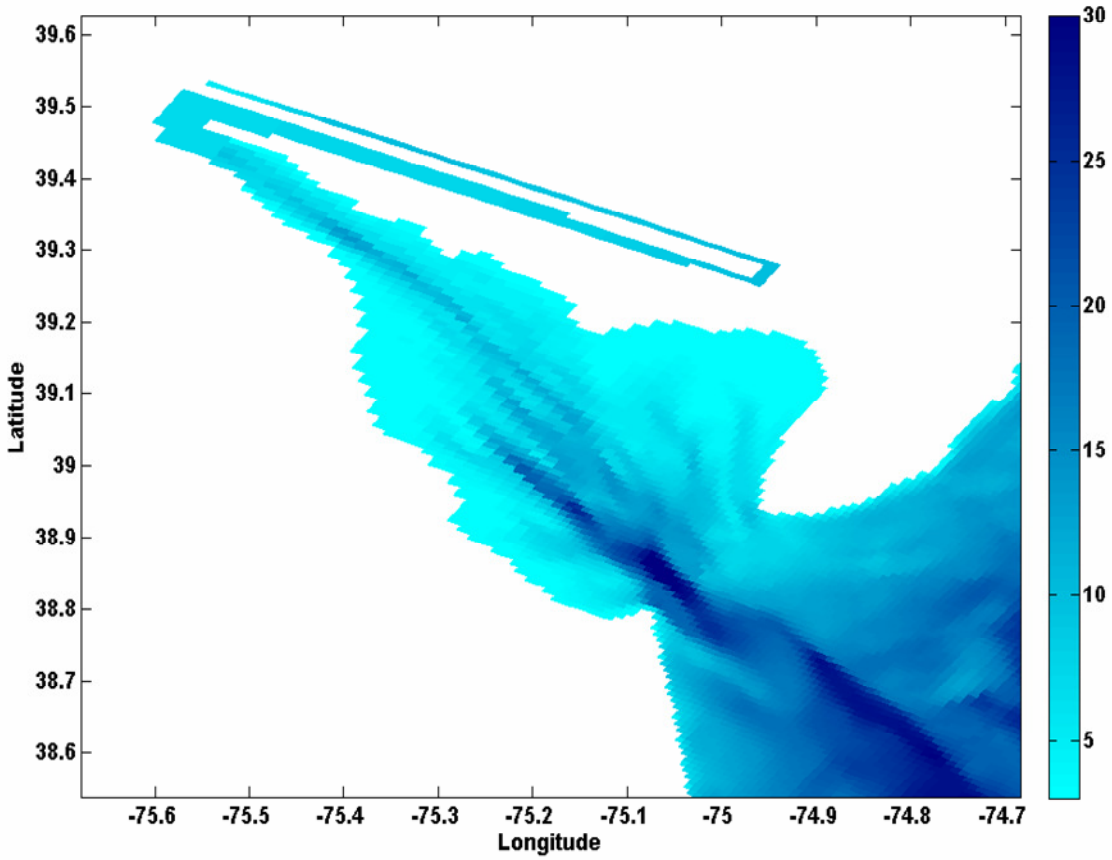

Figure 2.3 Bathymetry data for Delaware Bay. Color bar units are in meters.

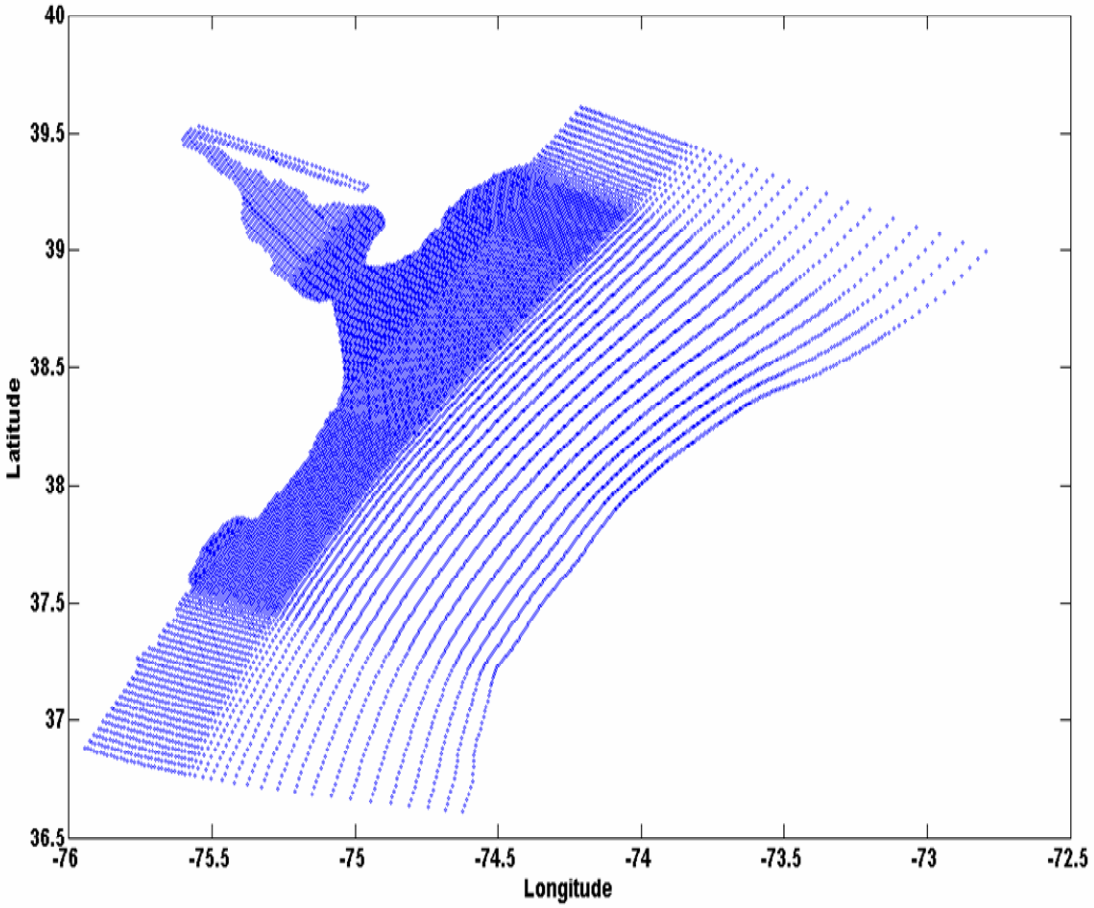

Figure 2.4 All grid points plotted to highlight the density at different locations in the domain. The Resolution is most dense around the bay mouth.

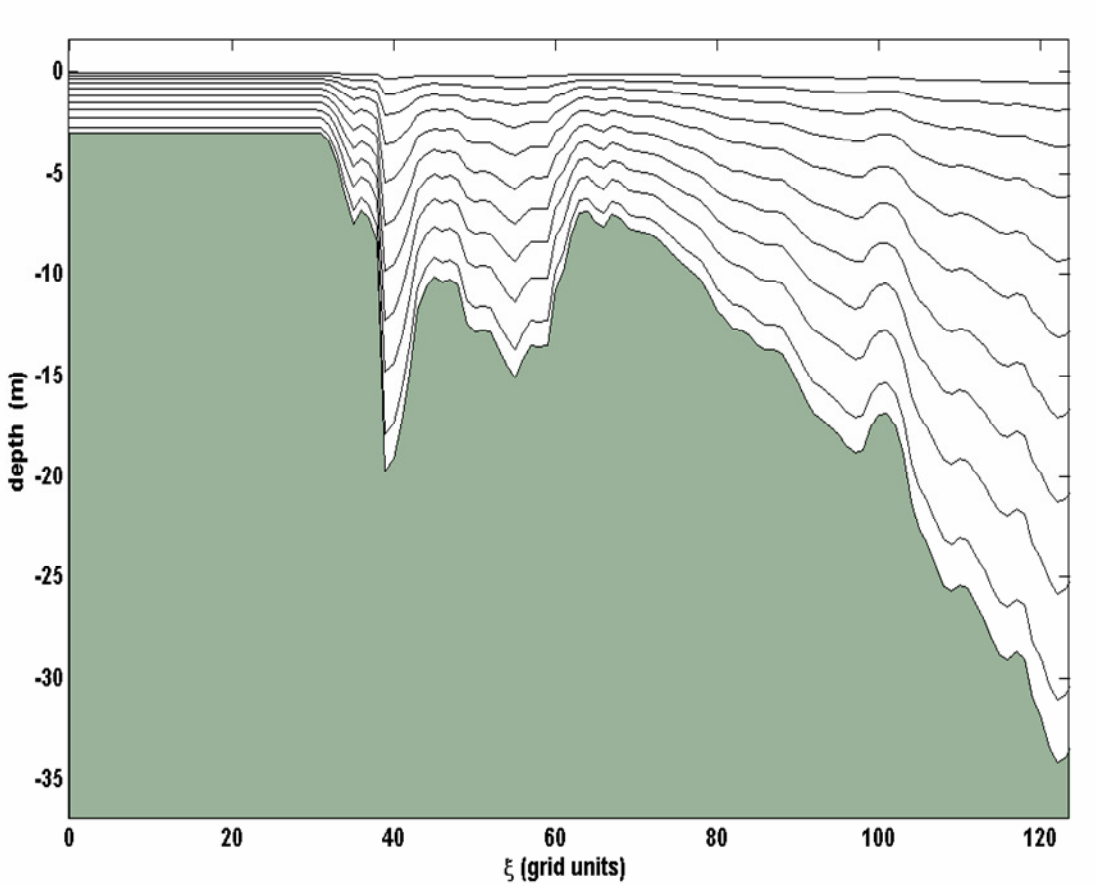

Figure 2.5 Different vertical levels for a horizontal slice through the grid at η = 205. Notice how at the top level the elevation is very close for all points, regardless of depth.

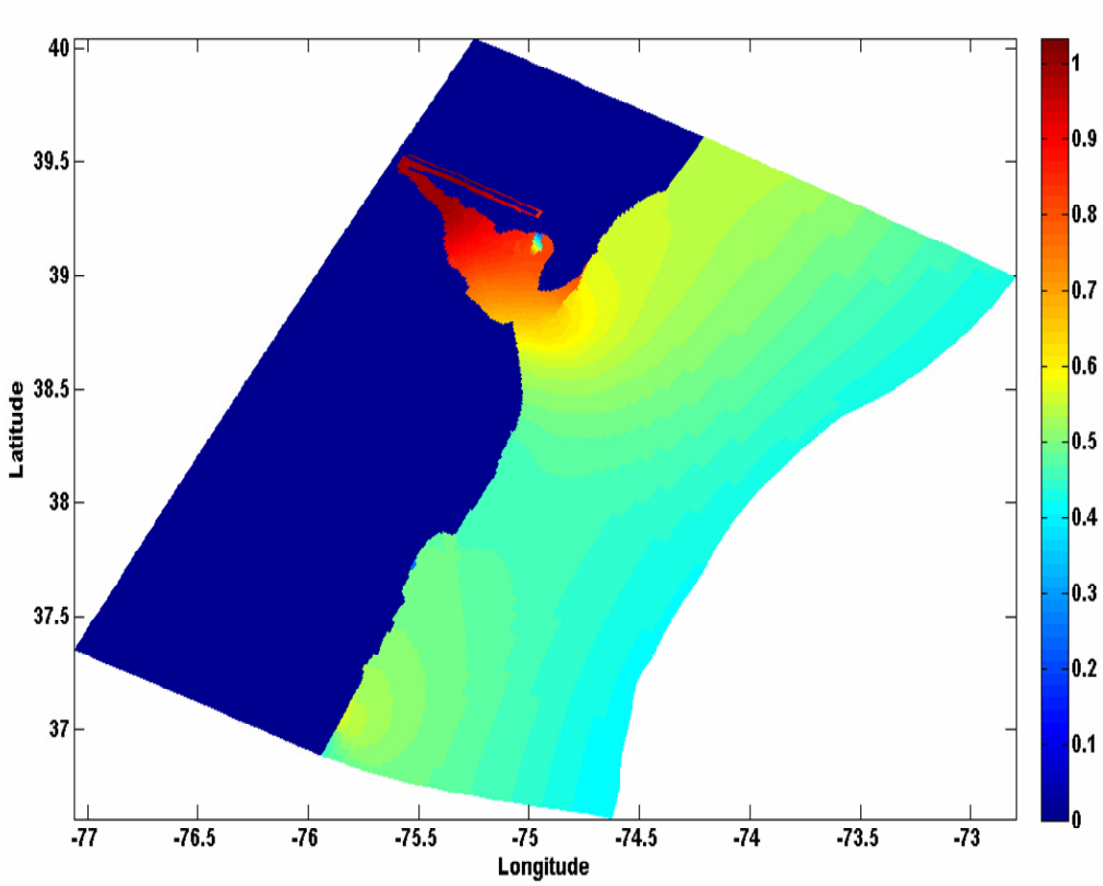

Figure 2.6 **M2 tidal amplitude as prescribed by ADCIRC. Only the values on the open boundaries are used in the model. Color bar units are in meters.**

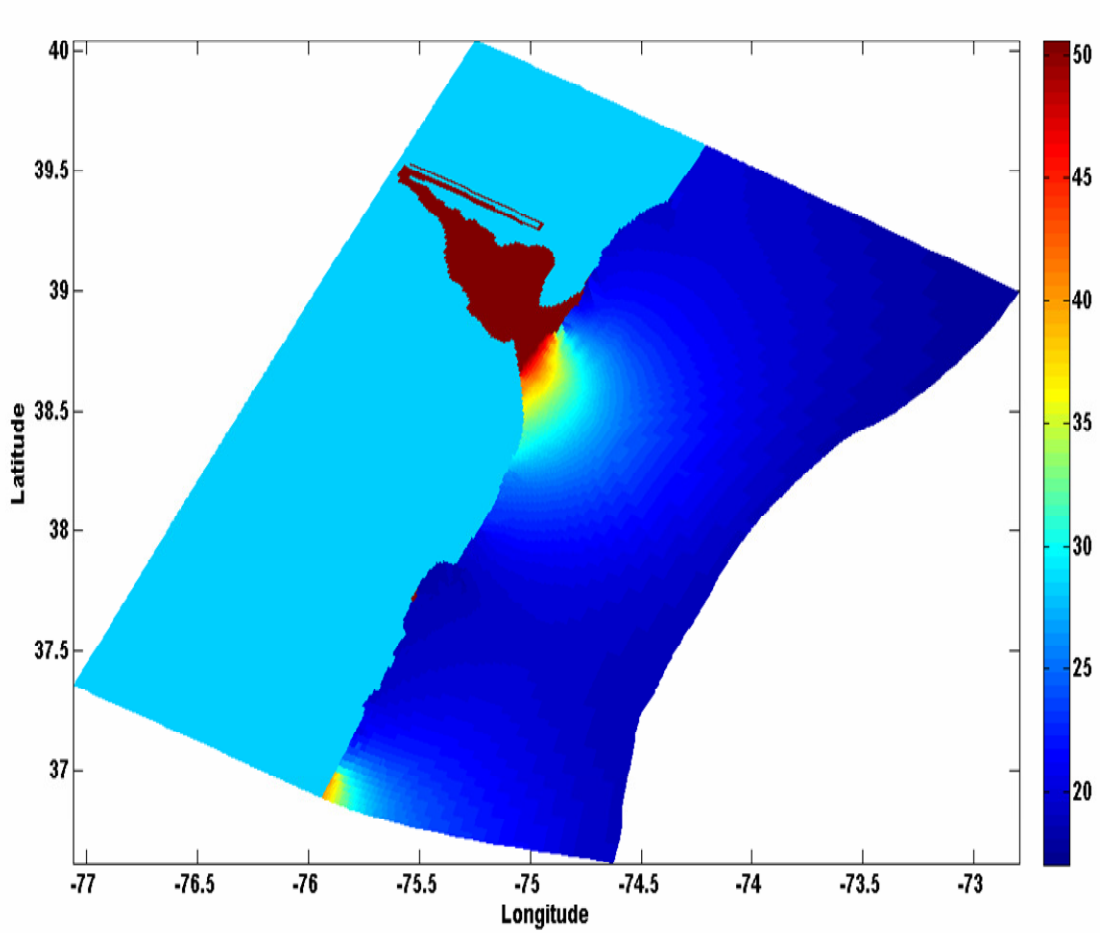

Figure 2.7 M2 tidal phase as prescribed by ADCIRC. Only the values on the open boundaries are used in the model. Color bar units are in degrees.

Figure 2.8 Locations of the three stations used to create the wind record.

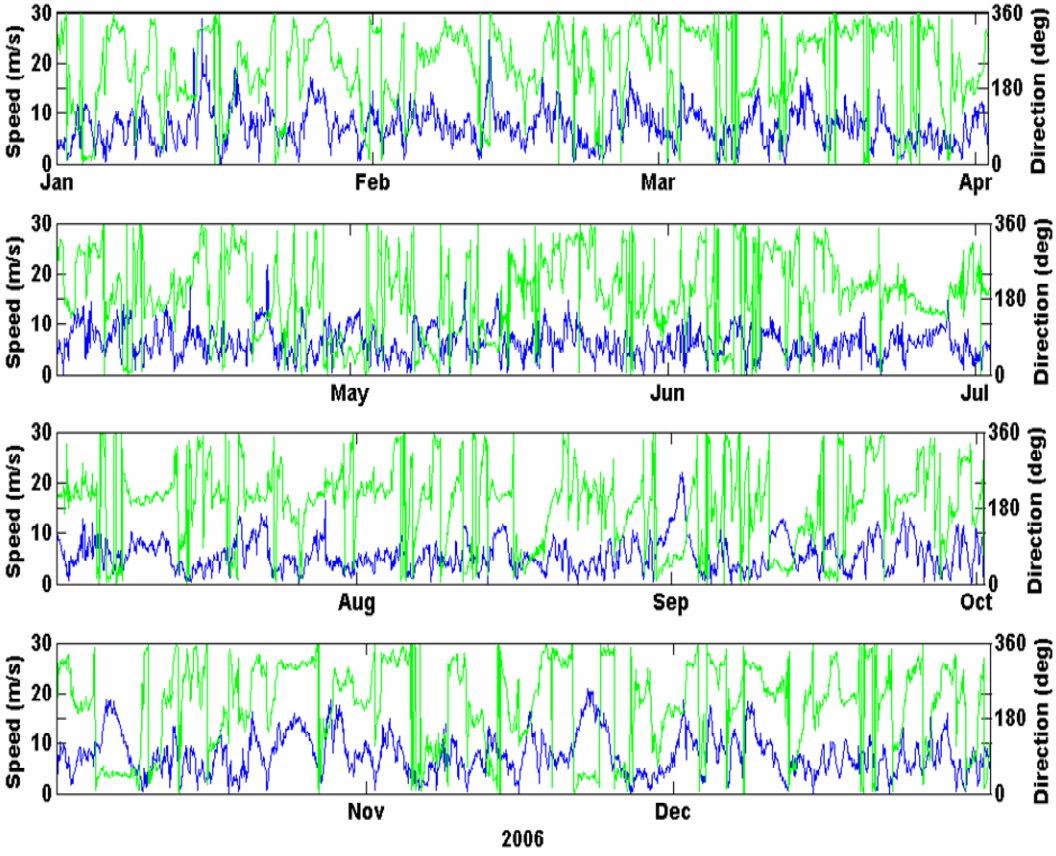

Figure 2.9 Wind magnitude and direction for 2006. Blue is wind speed, green is wind direction.

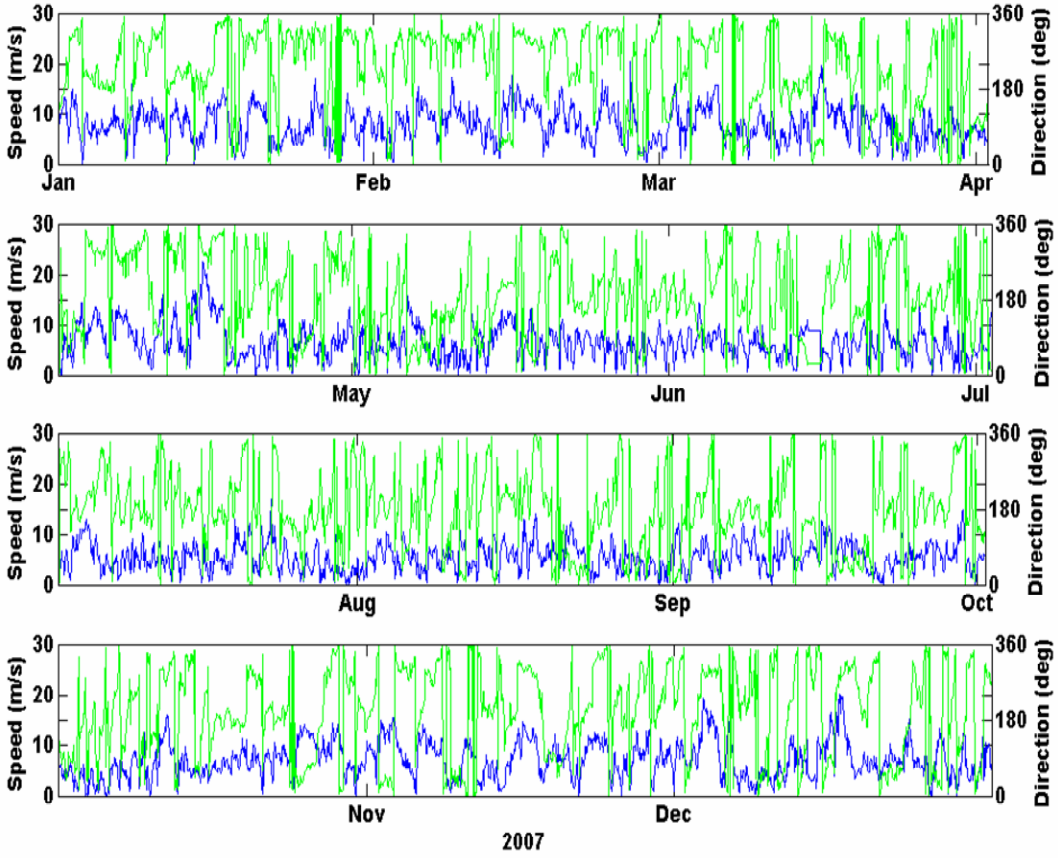

Figure 2.10 Wind magnitude and direction for 2007. Blue is wind speed, green is wind direction.

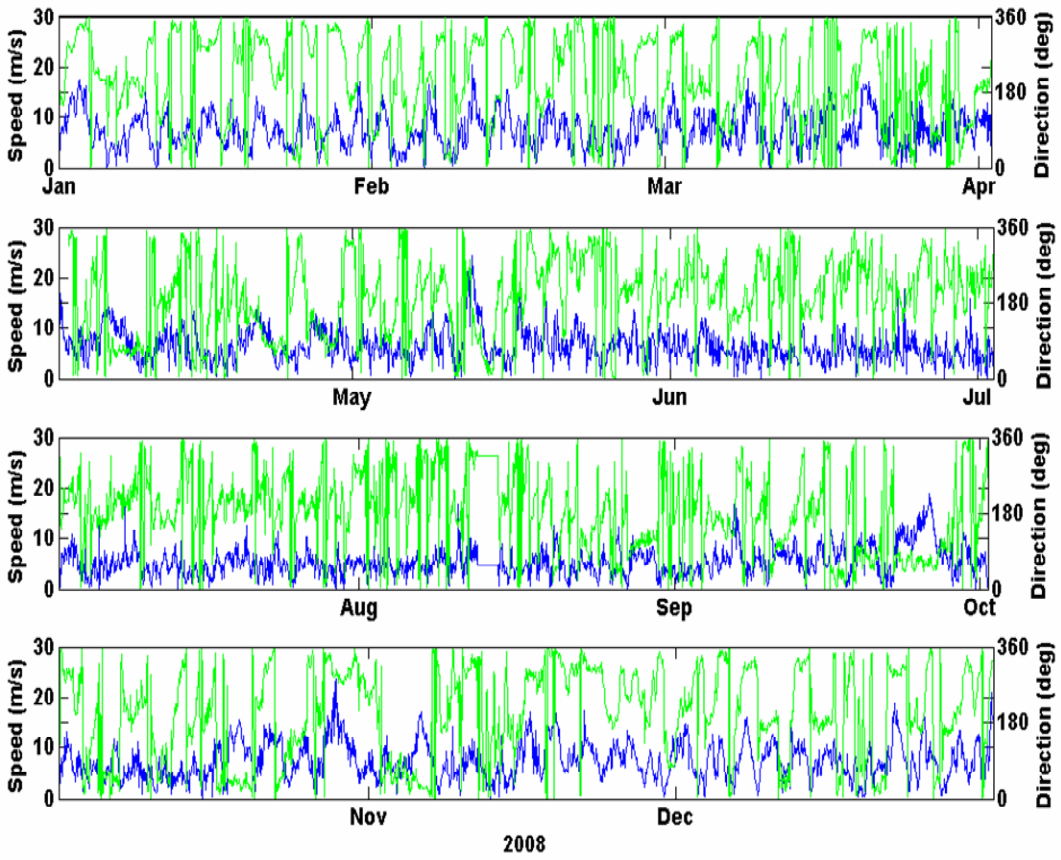

Figure 2.11 Wind magnitude and direction for 2008. Blue is wind speed, green is wind direction.

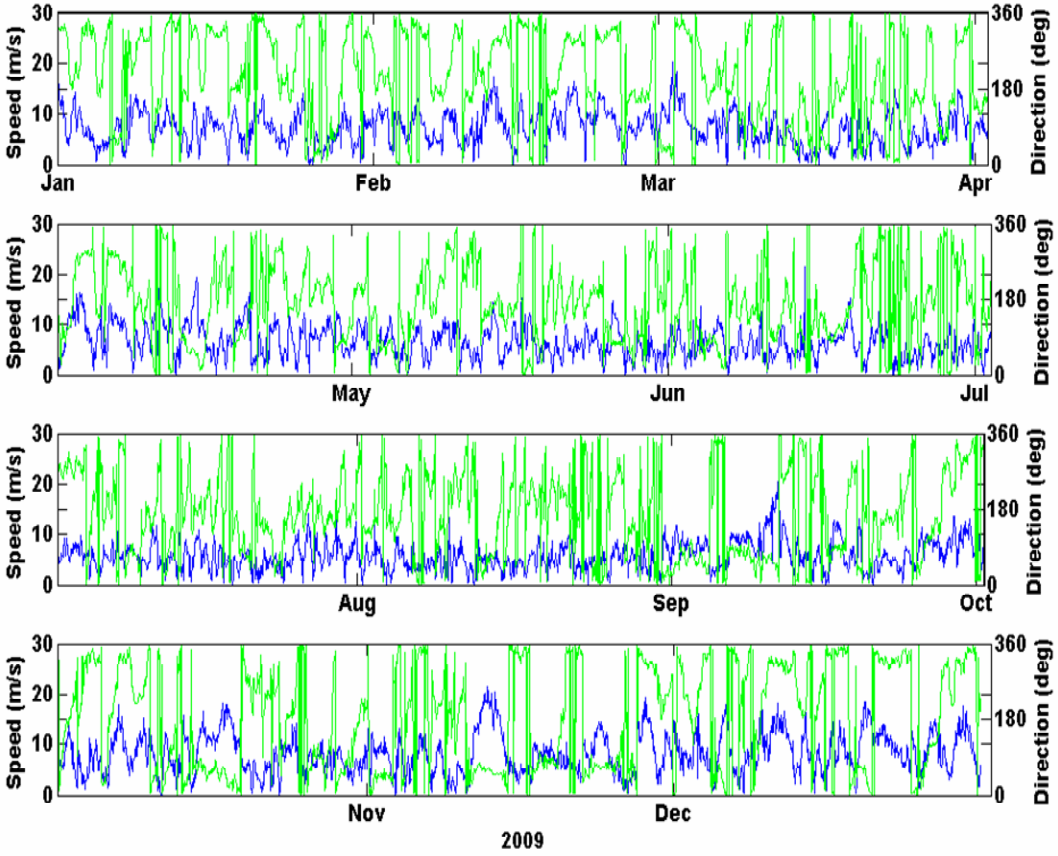

Figure 2.12 Wind magnitude and direction for 2009. Blue is wind speed, green is wind direction.

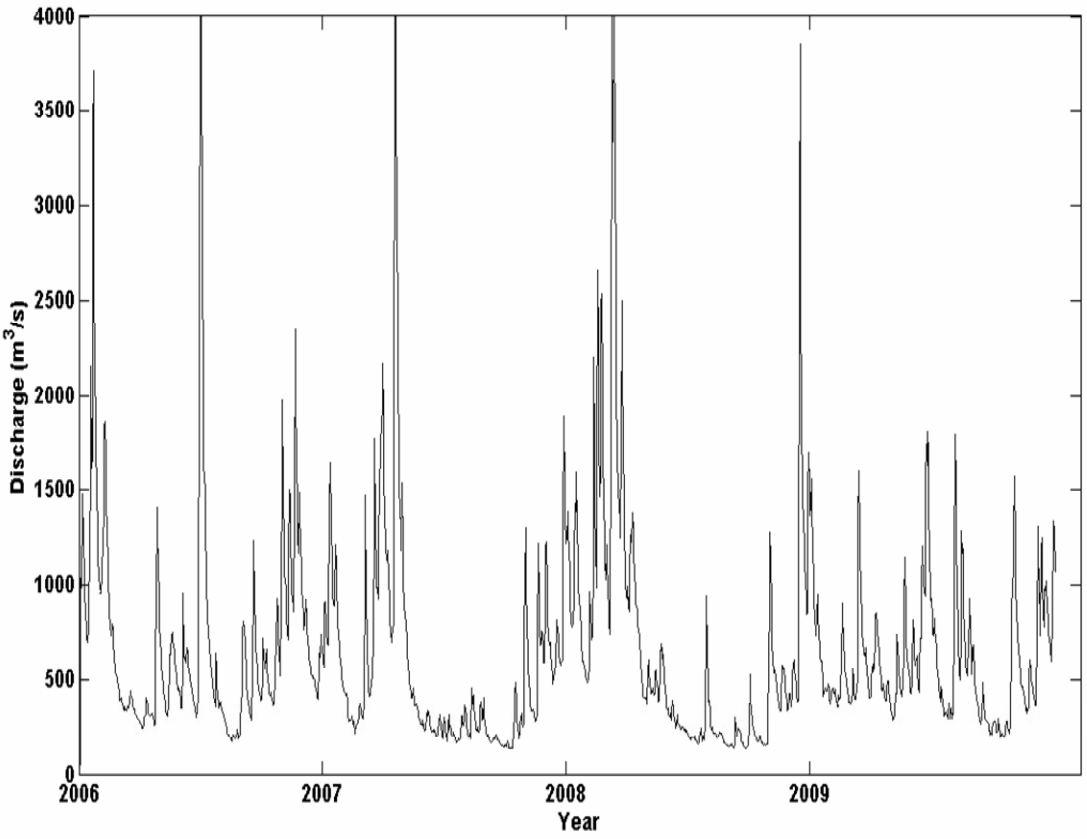

Figure 2.13 Delaware River outflow for the entire simulation.

Chapter 3

HYDROGRAPHIC DATA SOURCES AND METHOD OF MODEL/DATA COMPARISON

3.1 HF Radar

Since December 2006, the College of Earth, Ocean and Environment at the University of Delaware has maintained two high frequency radars on either side of Delaware Bay mouth. One is located at Cape Henlopen, DE (longitude -75.0890, latitude 38.7938) and the other at Cape May, NJ (longitude -74.9606, latitude 38.9313). The locations of this system can be seen in figure 3.1.

The hardware being operated are two 25 MHz SeaSonde HF radars manufactured by CODAR. The system provides good spatial coverage outside the mouth of the bay, and collects an average of surface velocity data every hour. The standard resolution of the radars is between 20-75 meters during standard operation, and may vary based on environmental conditions (http://www.codar.com/SeaSonde_gen_specs.shtml). The software provided by CODAR is used to process the data, which produces a velocity vector at each grid location (Muscarella et al. 2010).

High frequency radar is a useful tool when taking measurements of surface currents over a large area. The accuracy of these measurements has been assessed by comparisons to more conventional current measurements in numerous studies (Chapman et al. 1997, Ohlmann et al. 2007, etc.). More recently, Muscarella et al.

(2010) have done an assessment for the measurements in Delaware Bay. The evaluation of the setup by the bay mouth was done by comparing the CODAR measurements to moored and shipboard ADCPs. The agreement between ADCP measurements and CODAR data is good, but not perfect, and the RMS difference in the velocities was consistent with typical numbers. More information on this comparison can be found in Muscarella et al. (2010).

3.2 ADCP Measurements

Acoustic Doppler Current Profilers, or ADCPs, are valuable tools in collecting current data in a variety of aquatic locations. By calculating the Doppler shift caused by ocean currents accurate velocity measurements can be obtained for a multitude of vertical levels (bins) in the water column at a specific point. This proves very valuable when trying to evaluate the accuracy of 3D currents produced by a simulation.

The ADCPs used for the purposes of this study were Workhorse Sentinel ADCPs manufactured by RD Instruments. This hardware uses signals from four transducers to provide accurate measurements and compensate for tilt (RDI 2001). ADCP velocities are accurate to within an error of less than +-1cm/s.

There is one problem that makes the measurement taken closest to the surface unreliable at times. The information from the bin just below the surface is vulnerable to acoustic side lobe contamination (Teledyne 2006). This shows up as an erratic shift in magnitude of the top bin, so it is left out during the 3D data comparison done in the following chapter.

3.3 ADCP Deployment and Data

The data that will be used in the ADCP/model comparison in the next chapter came from a deployment of four ADCPs in April 2009. This deployment was assisted by Adam Skarke and Philip Muscarella, who had previous experience in placing the sensors in the bay mouth area. The ADCPs were set up prior to placing them in the water with software provided by RDI, and calibrated according to their specifications. To support the ADCPs, they were placed in heavy frames that allow them to sit comfortably on the ocean floor while keeping them steady, yet supported flexibly enough that the weight of the ADCP could self correct for minor tilt caused by sitting uneven on the ocean bottom.

The ADCP and rig supporting it was anchored by lead weights, the transducers of the hardware protected from biological material building up on them, and their locations signified by a buoy on the surface. A picture of the rig once it is set on the ocean floor can be seen in figure 3.2. They were allowed to collect data from April 9th 2009 to May 12th 2009, restricted by battery power.

Once recovered, the data was retrieved and read by the RDI software. The data can be examined using these programs, but for the purposes of the coming comparisons it needed to be exported and manipulated independently.

There were four different locations from that deployment, though unfortunately due to problems with the ADCPs not all of the data was useable which limited the assessment somewhat. A timeline of the collected data can be seen in figure 3.3. This figure also differentiates between data considered useable and not useable.

The four locations can be seen in figure 3.4. Locations A and B are around the mouth of the bay, while C and D are off the coast of Rehoboth Beach.

Each ADCP has a directional measurement error that arises from the calibration of the machines internal compass. In most cases this error is small.

The ADCP at location A is situated at latitude 38.861 N and longitude 74.964 W. The compass error in the measurements is 3.3 degrees. The records collected from the ADCP at this location seemed to be fine, but a problem arose during the analysis. During the model to measured data comparison the agreement was strong, until a point where the ADCP data shifted ahead of the ROMS data by approximately two hours. Though there is no problem when inspecting the records pulled from the ADCP, this shift started immediately after a couple of measurements that show data far above the actual surface of the water. The shift also does not appear in location B, which is in close proximity to A. To be safe it is assumed all data past the point in A where the time shift occurs to be unreliable. The occurrence of the shift can be seen in figure 3.5 in a comparison of model and measured current magnitude.

Location B's ADCP has a compass error of 1.6 degrees, and was positioned at latitude 38.840 North and longitude 74.926 West. The data retrieved from this ADCP was easily the best out of the four from this deployment. There were no problems with the data that would make it seem unreliable, the actual error on the direction was very low, and it produced a complete, reliable set of measurements for the whole time it was deployed.

The ADCP in location C is on the shoal off the coast of Rehoboth at Latitude 38.743 North by Longitude 75.052 West. The compass error for this ADCP is rather high, at 11.3 degrees. Unfortunately the ADCP at this location was wracked with problems. For the first few days of the deployment all of the data collected was no good, which certainly calls into question the seemingly acceptable data from the

rest of the deployment. A less significant problem was a difference in depth between the model and actual water column at the location. The shoal in the model grid is deeper than the portion of the shoal the ADCP was deployed on, so the scale of the profiles is very different.

Location D is situated at Latitude 38.743 North and Longitude 75.033 West, which is extremely close to Location C. A small compass error of 2.1 degrees exists in the measurements. The ADCP at D worked ostensibly well for five days, and then stopped reporting data. It was apparently an error in the programming of the ADCP makers themselves why this happened, but the data collected up until that point looks as if it is correct.

3.4 Complex Correlation

In order to compare the results of current velocity from the ROMS model run with the measured data from the CODAR sites, the method of complex correlation proposed by Kundu (1976) was used.

To use the analysis one must represent the components of the velocity vectors as complex numbers.

$$w_n = u_n + iv_n \tag{3.1}$$

The amplitude of correlation between the two sets of complex velocity vectors is calculated by first finding the 2x2 covariance matrix of the two vectors, next finding the diagonal of that matrix, then multiplying that diagonal by its transpose and dividing the covariance matrix by the square root of that number

$$C = COV(w_1, w_2) \tag{3.2}$$

$$X = \frac{C}{\sqrt{DIAG(C) \cdot DIAG(C)')}} \tag{3.3}$$

This will result in a 2x2 matrix, X in this case, with real numbers on the diagonal, and complex numbers in the other positions. The correlation amplitude is then

$$AMP = |X(2,1)| \text{ or } |X(1,2)| \tag{3.4}$$

The matrix X is also used to calculate the phase angle between the original vectors, which is now the angle of the complex portion of X

$$PHASE = \text{angle}(X(2,1)) \tag{3.5}$$

A third condition, the transfer function, is calculated by

$$TRANS = \left| \frac{C(1,2)}{C(1,1)} \right| \tag{3.6}$$

Here, the transfer function represents the difference in magnitude of the two time series. In this case, a transfer function under 1 means the ROMS data is larger than the CODAR data on average. Two time series of vectors that are exactly the same will have an amplitude of 1, phase angle of 0, and transfer function of 1.

The data from ROMS used for this correlation was that from the highest vertical level of the 3D velocity. Since the CODAR measurements are of surface velocities, it makes the most sense to use model data of the highest point of the 3D output. As was shown in figure 2.5, due to the way ROMS calculates the vertical levels, almost all top-level data is taken from a similar elevation regardless of depth. This usually turns out to be just about half a meter below the waters surface.

3.5 ROMS Output

Output from ROMS is stored in the same manner as the input used in this simulation, in NetCDF files. The storage of 3D data on a grid this size, for a

simulation this long, takes up a significant amount of disk space. For this reason the results are stored in 48 equal parts, roughly one for each month.

There are many different options for output from ROMS. For the purposes of the subsequent analysis, 3D *u*, *v*, and salinity data, along with 2D $\bar{u}$, $\bar{v}$, free surface (ζ), surface *u* stress (τ_u), and surface *v* stress (τ_v) are reported every hour. The surface stresses should be the same as they were on input since the ROMS output, as the stress inputs are using the same time step.

Careful consideration must be taken with the velocity output because the *u* and *v* reported by ROMS are the local, curvilinear values. These differ from the CODAR *u* and *v*, which positive values are true East and North respectively. Every ROMS *u* and *v* are rotated with the domain, and each individual point is different because of the curvilinear nature of the grid. The ROMS values can be rotated to match with the CODAR values as follows:

$$u(lon,lat) = u(\xi,\eta)\cos(\phi(\xi,\eta)) - v(\xi,\eta)\sin(\phi(\xi,\eta)) \tag{3.7}$$

$$v(lon,lat) = u(\xi,\eta)\sin(\phi(\xi,\eta)) + v(\xi,\eta)\cos(\phi(\xi,\eta)) \tag{3.8}$$

Where *u* and *v* are now in East and North, ξ and η are model coordinates, and ϕ is the rotation angle for each grid point

3.6 Grid Matching

The grid of CODAR data covers Delaware Bay mouth and the surrounding area. The domain of the CODAR data is completely contained within the grid used for the simulation, and is of uniform, larger spatial resolution.

In order to accurately compare the data from the model output and the CODAR measurements, the two grids must be matched. Due to the high density of

ROMS grid points in the area, this can be done relatively simply with a nearest neighbor approximation. Each location of the CODAR grid is checked for the closest ROMS grid point, and the location of these grid points are stored in a matrix the same size as the CODAR grid. These matrices of ROMS locations are stored, and ready to be called upon later to make comparing data locally a straightforward task. For each location of reported CODAR data there is a ROMS location extremely close by. Due to the close proximity of the points on the matched grid, very little would be gained by a more sophisticated interpolation scheme.

3.7 Reliable CODAR Coverage

Though the domain of the CODAR system set up for the bay covers a large region, the actual coverage of useful data is much smaller and varies over time. For a selected period of time, the data from a location on the CODAR grid is considered valid if it is being reported 80% of the time. However, this 80% coverage rule is not valid for any points within the bay, as this data is automatically considered unreliable and discounted. For the purposes of the data comparison, two of the more reliable months, October 2007 and April 2008, are used. The month of October 2007 experienced fairly calm weather, while April 2008 has much more active weather events. These two months provide a good metric to compare the ROMS data to over a fairly long time.

The information for each location is reported hourly and retrieved using a Matlab program provided by Philip Muscarella from the College of Earth, Ocean, and Environment at the University of Delaware. In order to get the coverage for each of these months, a check was made to see how often the data was reported for each location in the CODAR grid. After neglecting the points inside the bay, the remaining

points are accepted based on whether they meet the 80% coverage threshold. The actual, valid coverage footprint for each month can be seen in figures 3.6 and 3.7. As can be seen in the figures, the month of October 2007 had a greater area of valid data than April 2008. The footprint is most reliable in the middle of the valid data, a bit offshore from the bay mouth. Some of the data reported on the fringes on the applicable area are still suspect and less dependable.

3.7.1 Filling Gaps in Coverage

In order to provide a more complete time record of data at all the valid points, times of missing data were filled in when possible. With the 80% threshold, that still leaves room for over 100 missing data points, and even many of the highest coverage points have quite a few missing records. To remedy this, if a value was not reported, it was interpolated from the values immediately surrounding it that were. This was only done for points within the original coverage footprint of each month.

3.8 Splitting Tidal and Non-Tidal Data

In order to better analyze how the model is performing the output from the model, as well as the data from the CODAR, was split into tidal and non-tidal data. To do this, the time series for each month of interest from both the ROMS data and the CODAR measurements were fed through t_tide (Xu, 2000; Pawlowicz et al. 2002).

The product of the analysis done by t_tide results in the harmonic portion of the data time series (representing the tidal components) separated out from the original. Using this information it is simple to find the non-tidal data by subtracting this harmonic portion from the unfiltered time series. This non-tidal component

comprises mainly of currents forced by the wind in the area of the comparison, but other factors such as non-tidal circulation and the river forcing come into play as well.

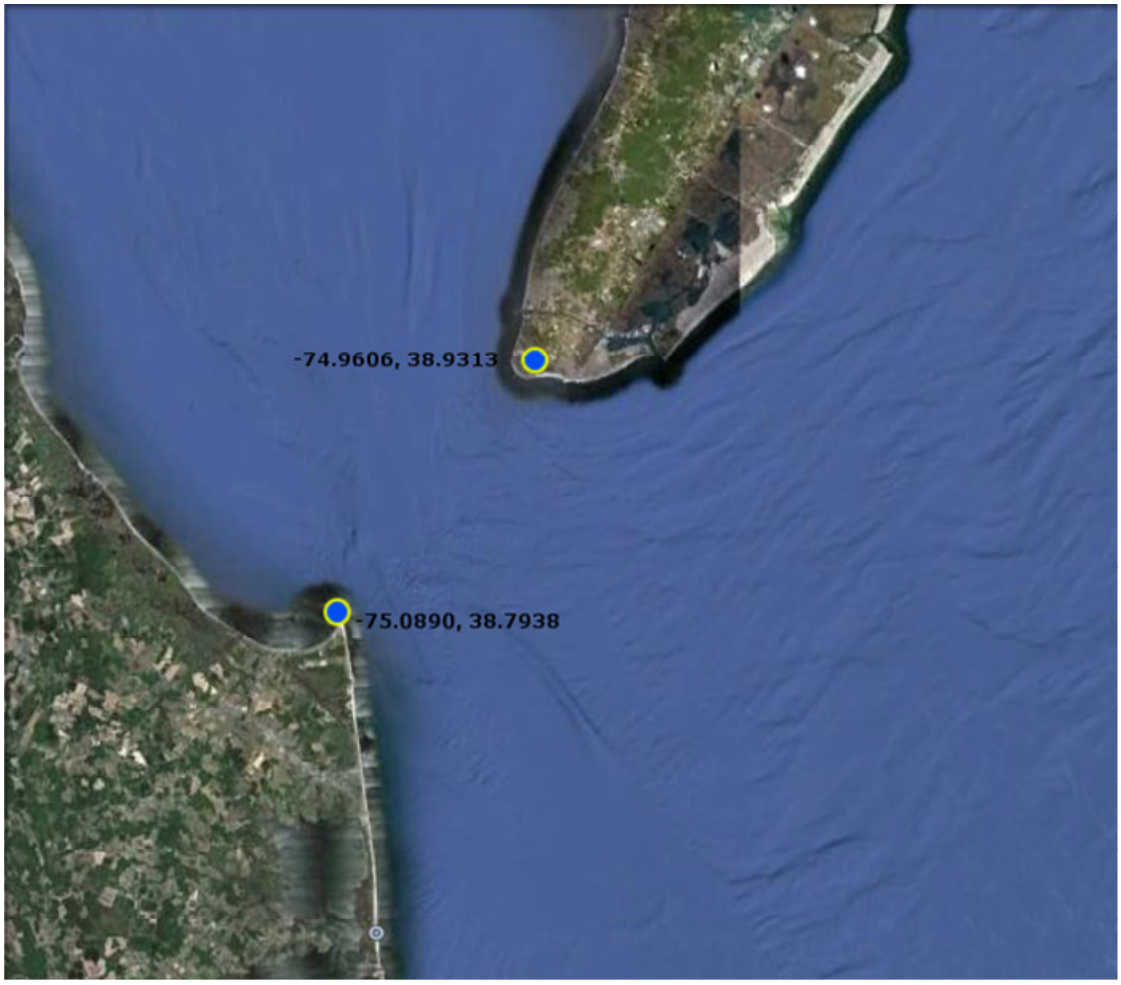

Figure 3.1 **HF Radar locations at the mouth of Delaware Bay. Cape Henlopen is the DE side, and Cape May is the NJ side.**

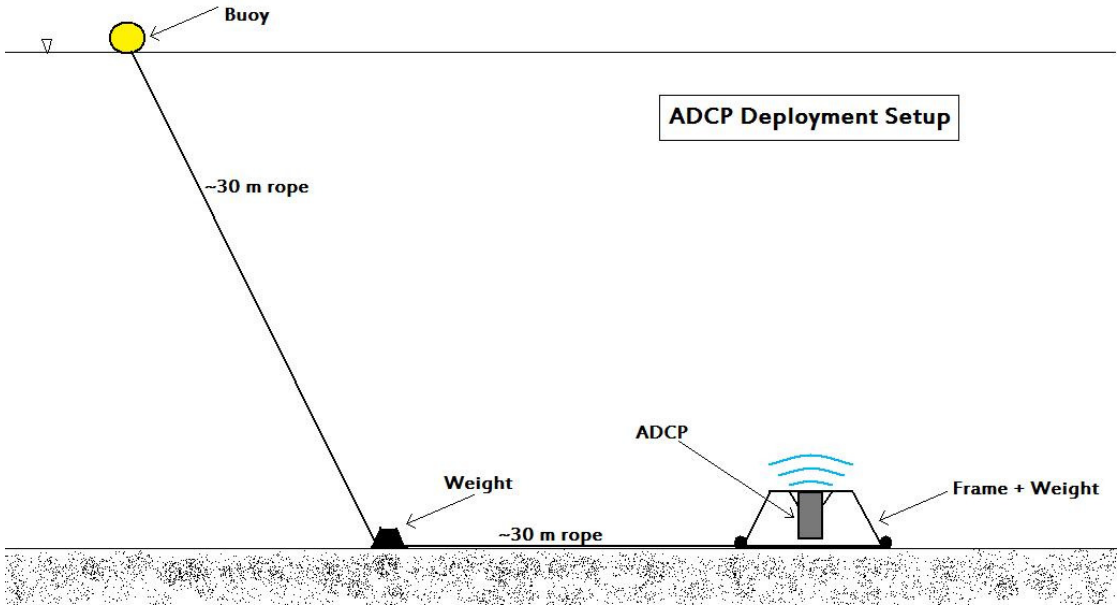

Figure 3.2 Sketch of the system used for ADCP deployments in Delaware Bay.

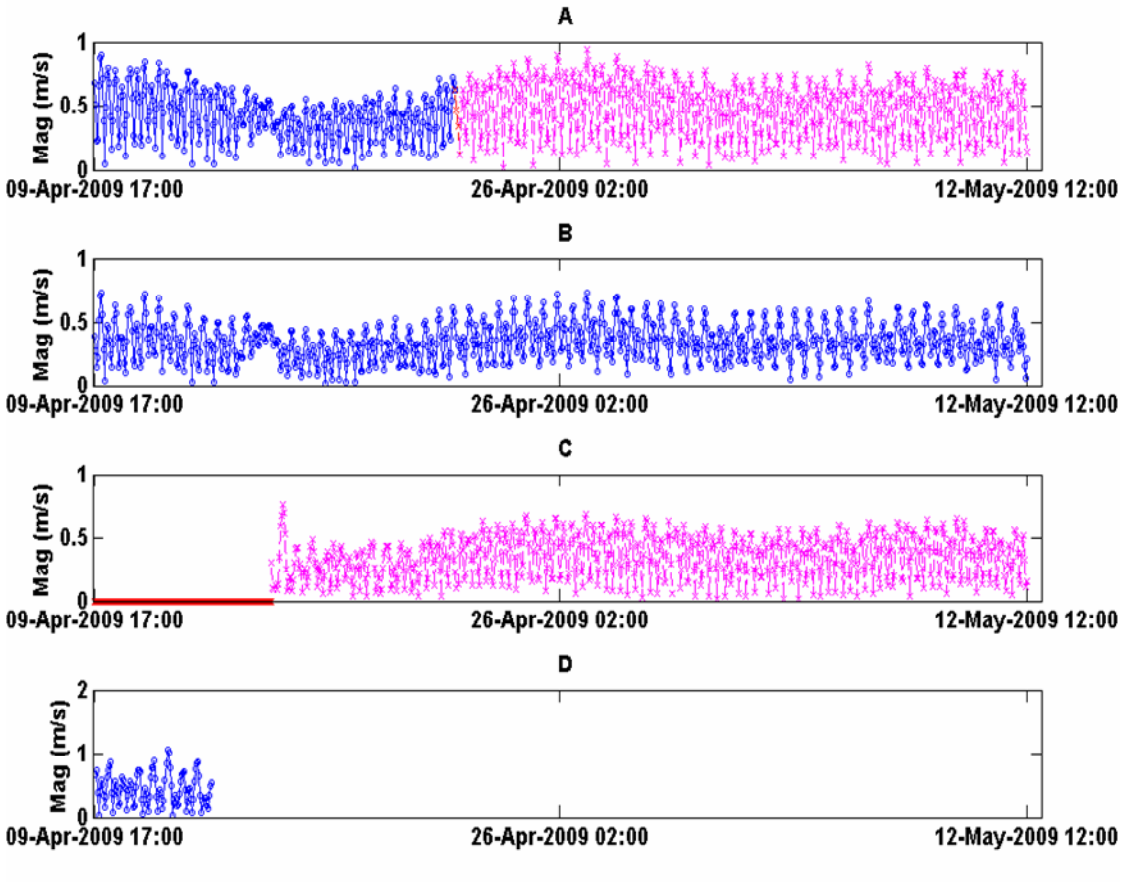

Figure 3.3 **Range of collected data for each of the ADCPs. Blue markers indicate data there was no problem with, red markers indicate an error in data collection by the ADCP, and pink markers indicate suspect data that shows no problem in the ADCP record but do show signs of being inaccurate during a data comparison. The record at D stops after about four days due to the ADCP at D shutting itself down prematurely.**

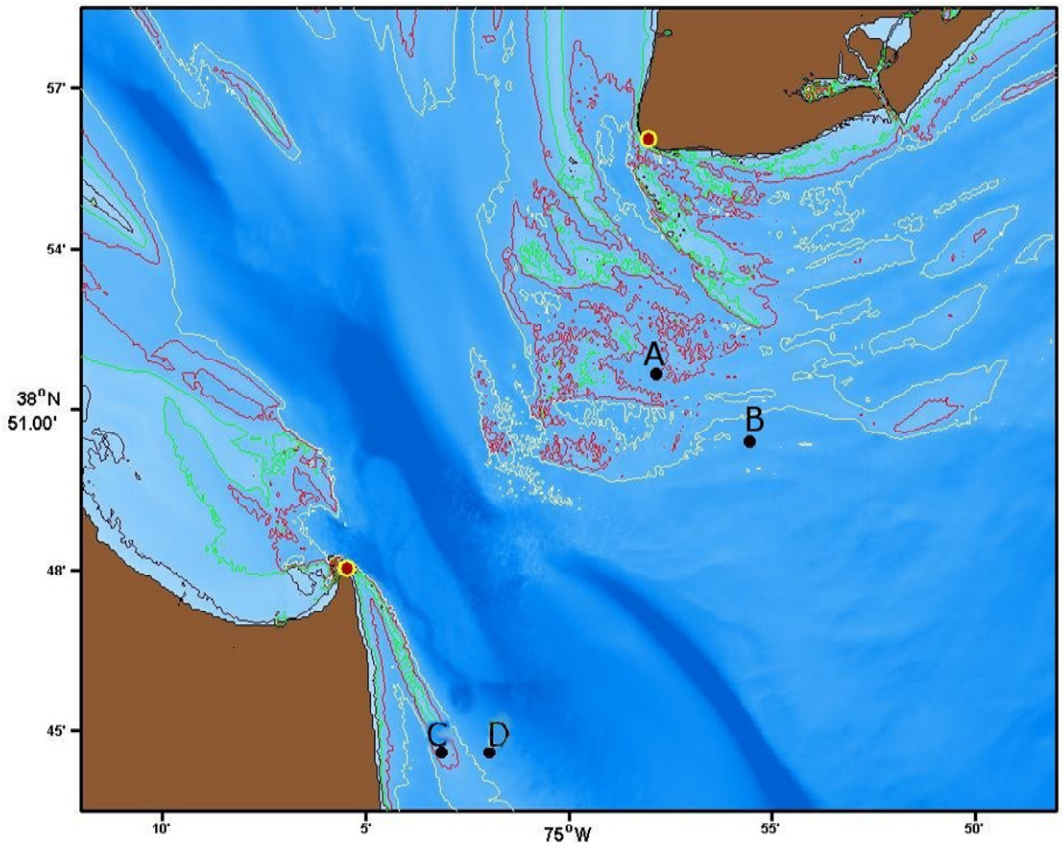

Figure 3.4 ADCP locations for the May 2009 deployment.

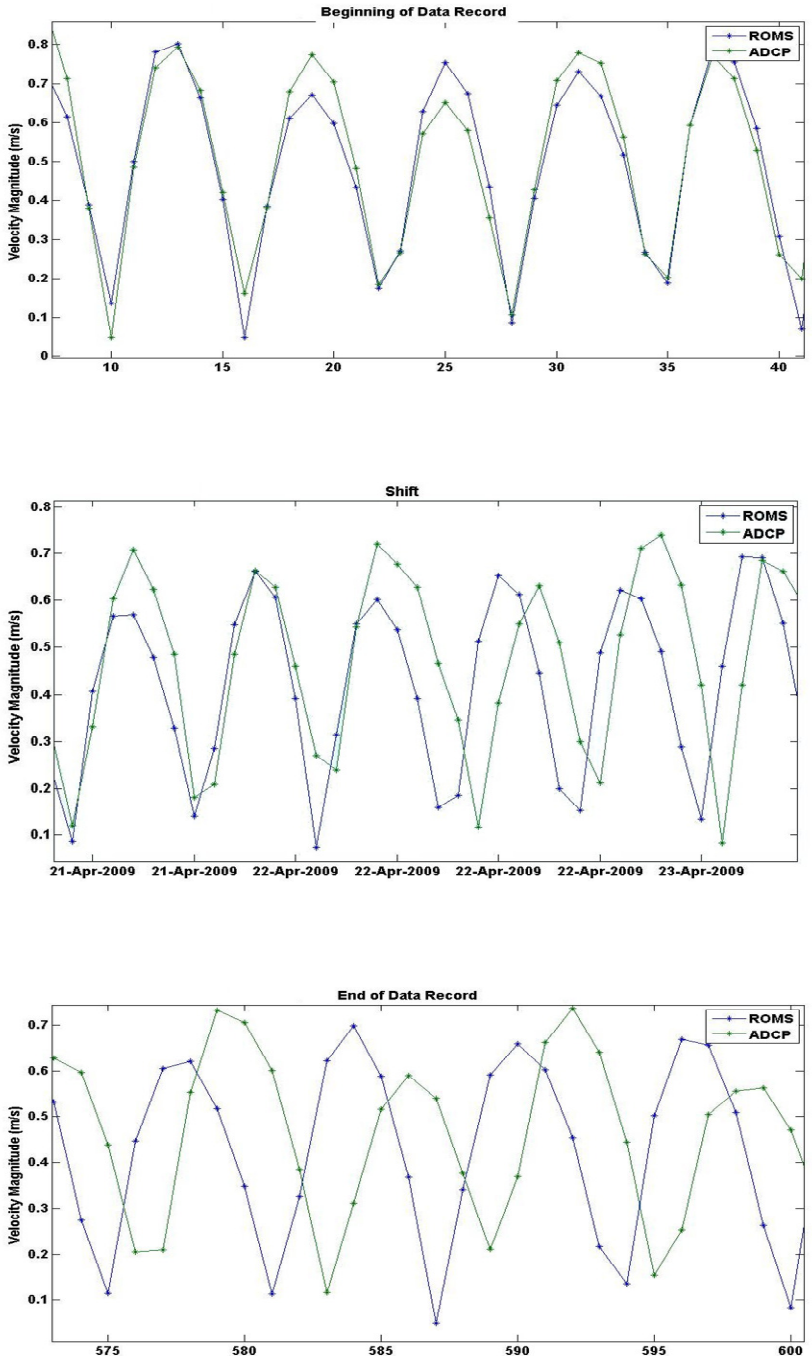

Figure 3.5 **Illustration of the shift that happens in the location A ADCP data. Includes contrast of how the data looks at the beginning and towards the end of the comparison as well. Blue is ROMS data and green is ADCP.**

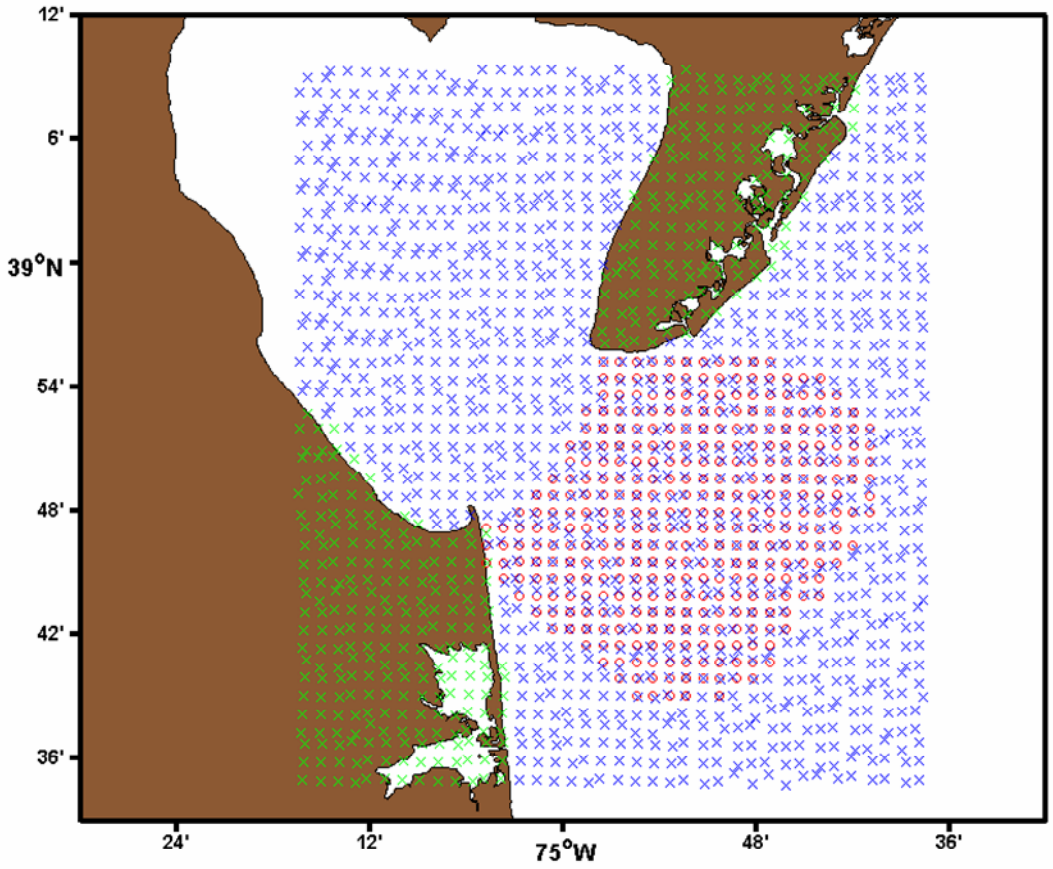

Figure 3.6 **There are 349 valid CODAR points (80% coverage) for October 2007. Blue and green x's are ROMS water and land points. Red circles are the CODAR points that meet the 80% coverage threshold for October 2007.**

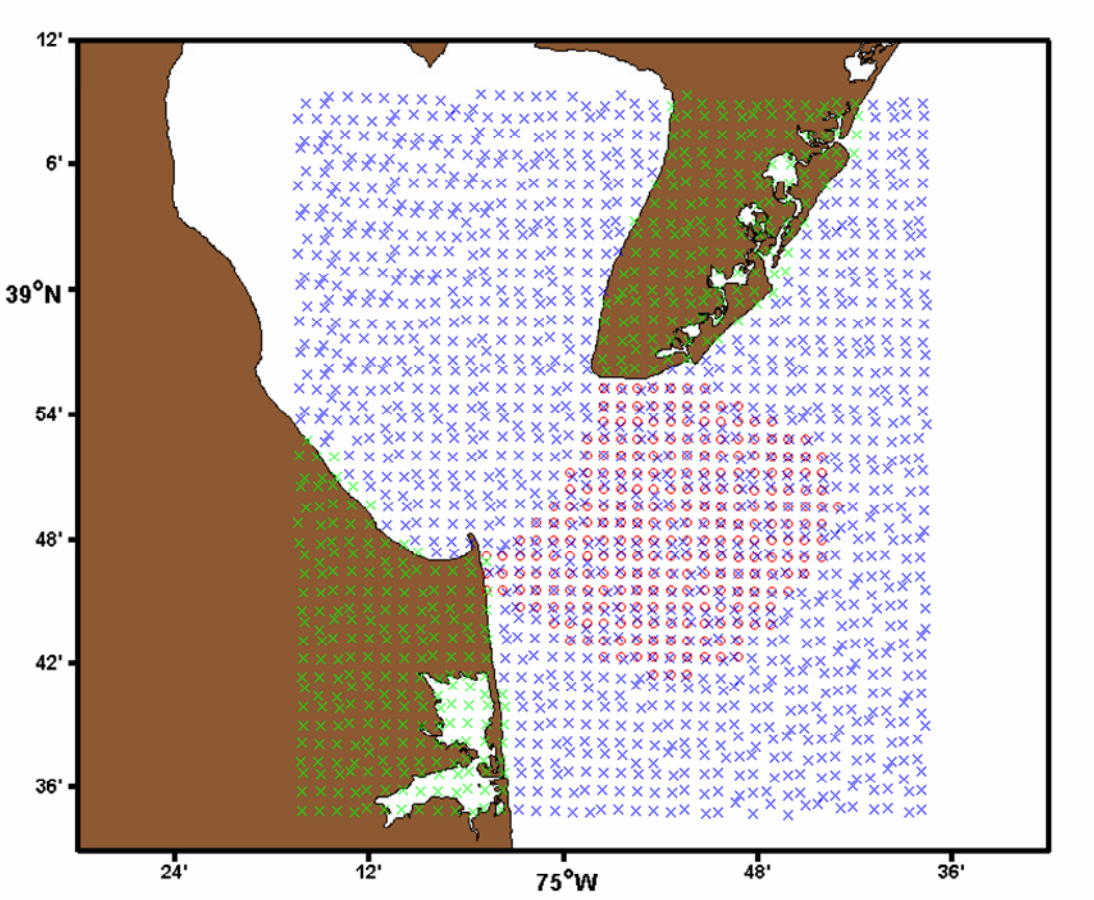

Figure 3.7 **There are 256 valid CODAR points (80% coverage) for April 2008. Blue and green x's are ROMS water and land points. Red circles are the CODAR points that meet the 80% coverage threshold for April 2008.**

Chapter 4

MODEL DATA COMPARISON

4.1 October 2007 Comparison

The month of October 2007 experienced fairly calm weather conditions, which can be seen in figures 4.1 and 4.2. There was not much outflow from the Delaware River until it started to increase a little at the end of the month, and the wind was mostly weak, with the *u* and *v* components staying under 10 m/s the majority of the time.

After the harmonic portion of the time series data from the ROMS output and CODAR measurements were separated out, the complex correlation was run to see how the model is performing. The correlation amplitude is very high throughout the entire footprint of valid CODAR data, with the majority of points comfortably above a 0.9 correlation. This can be seen in figure 4.3. The amplitude only starts to decrease slightly along the fringes of the coverage, where the confidence of the CODAR measurements is much less than the "sweet spot" just offshore of the middle of the bay mouth. The phase angle, figure 4.4, also shows the majority of locations reporting under a 10 degree difference, again only decreasing in accuracy on the outskirts. Lastly is figure 4.5, the transfer function. The correlation here is close to 1.0, which is a perfect match, over the majority of the coverage footprint. To better illustrate how the tidal portion of the two time series match up with each other, a plot of the tidal

current *u* and *v* velocities at a specific point located at [longitude -74.8726, latitude 38.8131] is shown in figure 4.6.

The complex correlation was also run on the non-tidal data that resulted from running the time series through t_tide. As to be expected, the correlation is not quite as high as it was for just the tidal data, though it still remains reasonably accurate. The amplitude is still close to 1.0 in most locations, decreasing south of the bay mouth, as illustrated in figure 4.7. Phase angle error is within 10 degrees of 0 for much of the coverage area, only getting larger around the fringes of the coverage (figure 4.8). The transfer function shows agreement close to 1.0 for the majority of the points, and by looking at figure 4.9 it can be seen the accuracy of the comparison follows a similar pattern to the amplitude. Figure 4.10 shows a plot of the non-tidal *u* and *v* at the same location as was show for the tidal current.

4.2 April 2008 Comparison

For April 2008 the same analysis from the previous section was repeated. This was a much more active month regarding the weather. The discharge in figure 4.11, though not astronomical, is much higher than it was in October 2007. It can also be seen in figure 4.12 that the wind is much higher this month as well. This makes for more challenging conditions to evaluate model performance.

Like before, the first thing examined was the tidal component. The complex correlation amplitude is again extremely close to 1.0 for the tidal data almost everywhere (figure 4.13). The phase angle still remains near 0 throughout most of the footprint, as seen in figure 4.14. It only increasing on the boundary locations like before. Though not as strong as in October, the transfer function still shows agreement around 1.0, which is shown in figure 4.15. As before, a plot of the time series at an

individual location is presented in figure 4.16. The same location from the previous section was chosen for consistency. The curves closes resemble one another, though ROMS over predicts the oscillation amplitude at times.

The correlation on the non-tidal data, while still showing a strong correlation, provides the weakest agreement out of all the comparisons. The amplitude in figure 4.17 is more in the 0.6-0.7 range, which isn't bad, but a little on the low side. The phase angle agreement performs the weakest. While it is still with 20 degrees of 0 for the middle section of the footprint, it reaches above 30 as it moves towards the edges (figure 4.18). The transfer function is similar to what it was in October 2007, though slightly lower this time (figure 4.19). The weaker correlation from this non-tidal data is likely due to the more active conditions of this month being tougher for the model to properly emulate. That said, in figure 4.20 the plot of the model and measured data from the same location in the coverage as before still follows the trend of the non-tidal measurements.

4.3 ADCP Data Comparison

Along with the more sweeping analysis based on the CODAR data, a more local assessment was done with the ADCP data recovered from the Spring 2009 deployment. A comparison of the free surface measured by the ADCP to the free surface calculated by ROMS is show in figure 4.21 for each of the four ADCP locations. Some older ADCP data collected by the College of Earth, Ocean, and Environment at the University of Delaware during previous deployments in the Fall of 2007 and the Summer of 2008 are used for comparison as well.

The benefit to having ADCP data to compare to is that it is taken at multiple vertical levels, so a comparison of the profile of ROMS velocities can be

made with that of the ADCP. In order to do this a movie was made showing the profile of the magnitudes of both ROMS and ADCP velocities at each time step. This provided an appropriate platform to see how well the ROMS data matched the measured data in real time.

4.3.1 Location A

The velocity profile produced by the model follows the profile constructed from the ADCP data with reasonable accuracy before the previously mentioned time-shift. The slope from lowest to highest elevation for the ROMS data matches with that of the measured data most of the time, and it adjusts to deviations as well. Figure 4.22 shows a sequence of 15 time steps of the 3D velocity. It is clear from the figure that the ROMS and ADCP data exhibit similar profiles. The complex correlation is not calculated due to the shift mentioned in the last chapter.

4.3.2 Location B

The comparison from this location showcased a high degree of precision throughout. For almost the entire month of the deployment the model results match nearly perfectly to the measurements. The slope of the 3D velocity along with the fluctuations from the typical velocity profile are both followed closely. An example of this can be seen in figure 4.23, which, as before, shows a sequence of comparisons. The complex correlation of the vertical average of the 3D data presented in the figure's caption is, predictably, close to an exact match to the measured data.

4.3.3 Location C

No meaningful assessment was able to be made here due to the likelihood that the data collected from this ADCP was unreliable.

4.3.4 Location D

By examining figure 4.24 it can be seen that the model and measured data closely mirror one another. In the profiles shown, ROMS moves with the variations in the data well, and displays an accurate current projection. However, at times the variations from the measured data become very prevalent due to high non-tidal flow in the area, and the model does not always keep up with the magnitude of these changes. This can be seen in the complex correlation listed in the caption of the figure. The amplitude is very high, but the transfer function is actually above one, atypical of the majority of data compared so far. Regardless of that, the model performs well at reproducing the flow in the area, albeit for the brief time data was able to be collected.

4.3.5 Older Data

The ADCP deployments used here from the Fall of 2007 and the Summer of 2008 are both located at latitude 38.96959, longitude -075.06480. The data was collected with the same method used for the 2009 deployments.

Figure 4.25 shows the comparison for the Summer 2008 data. The data from the ADCP and that produced by ROMS resemble each other. A complex correlation analysis yields an amplitude and transfer function near 1.0, but curiously the comparison is very out of phase. The assessment of the Fall 2007 measurements can be found in figure 4.26. The results are similar to the Summer 2008 comparison, however the correlation shows almost no phase difference as opposed to the very high difference from before. Both comparisons were done at the same location, so the reason for the high phase error in the Summer 2008 data is unknown. It is possible the ADCP used in the Summer 2008 deployment reported the velocity data at the wrong angles due to compass error.

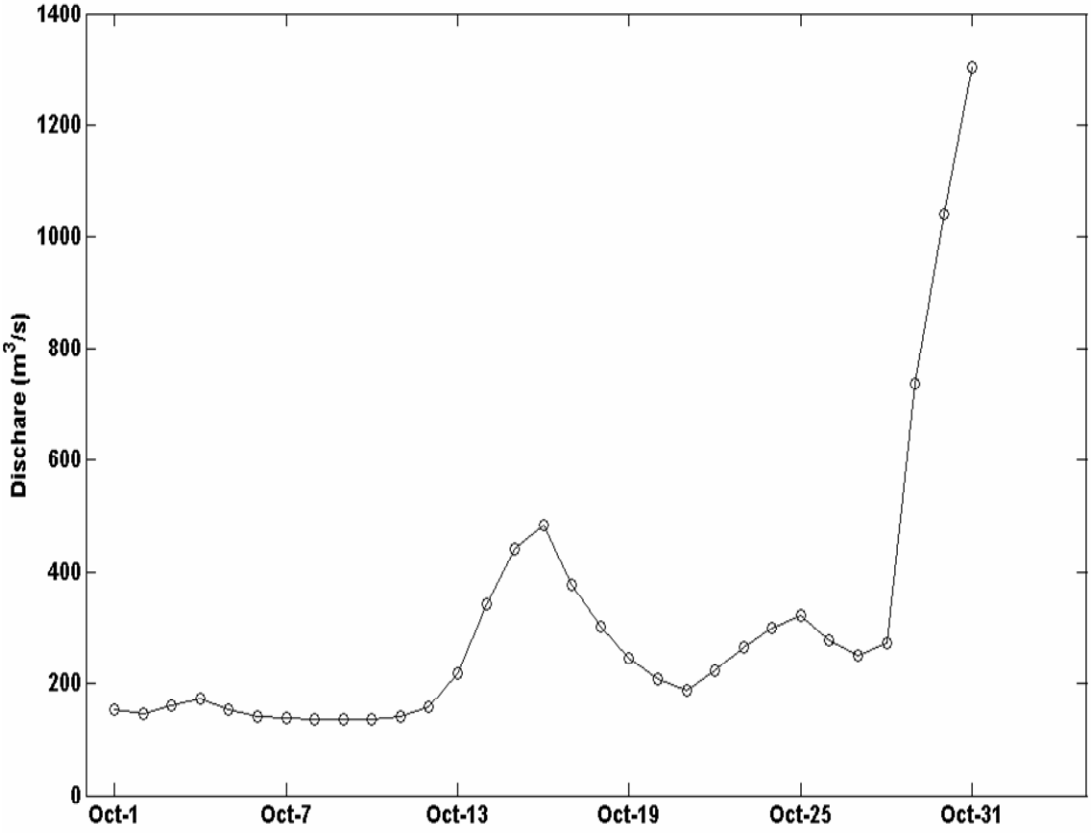

Figure 4.1 River discharge during October 2007.

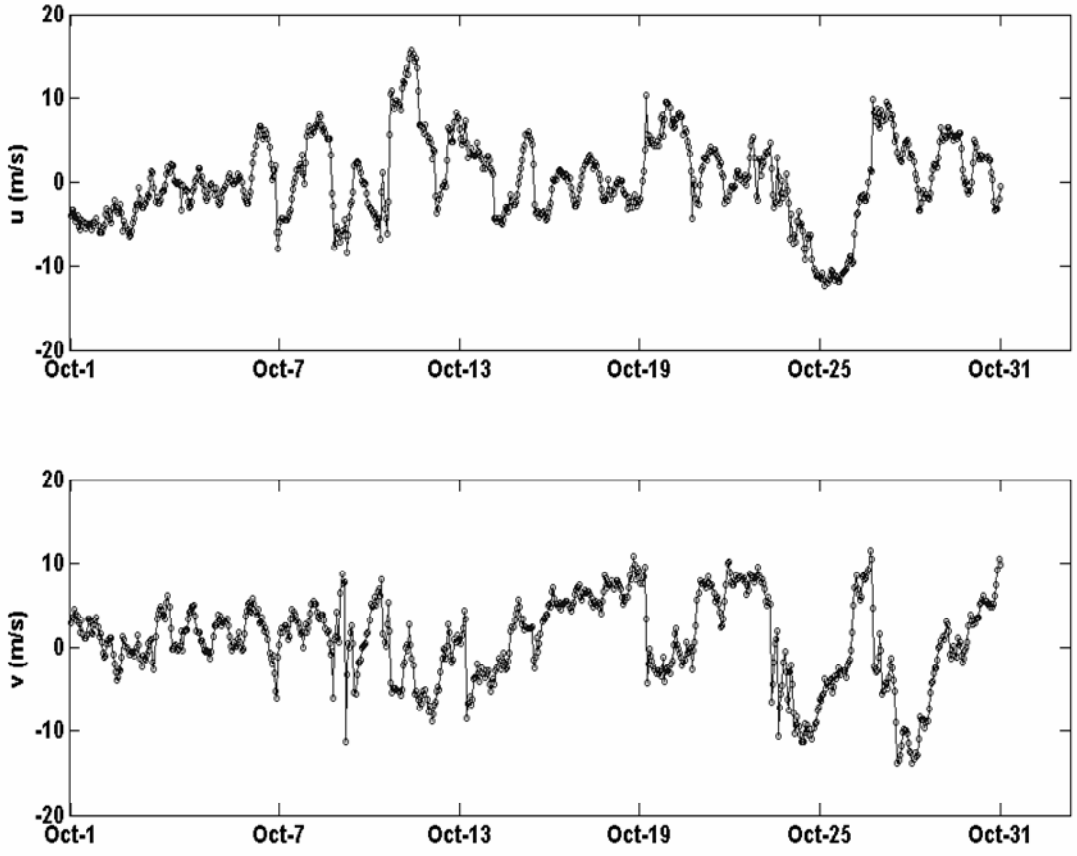

Figure 4.2 East-West and North-South wind speeds for October 2007.

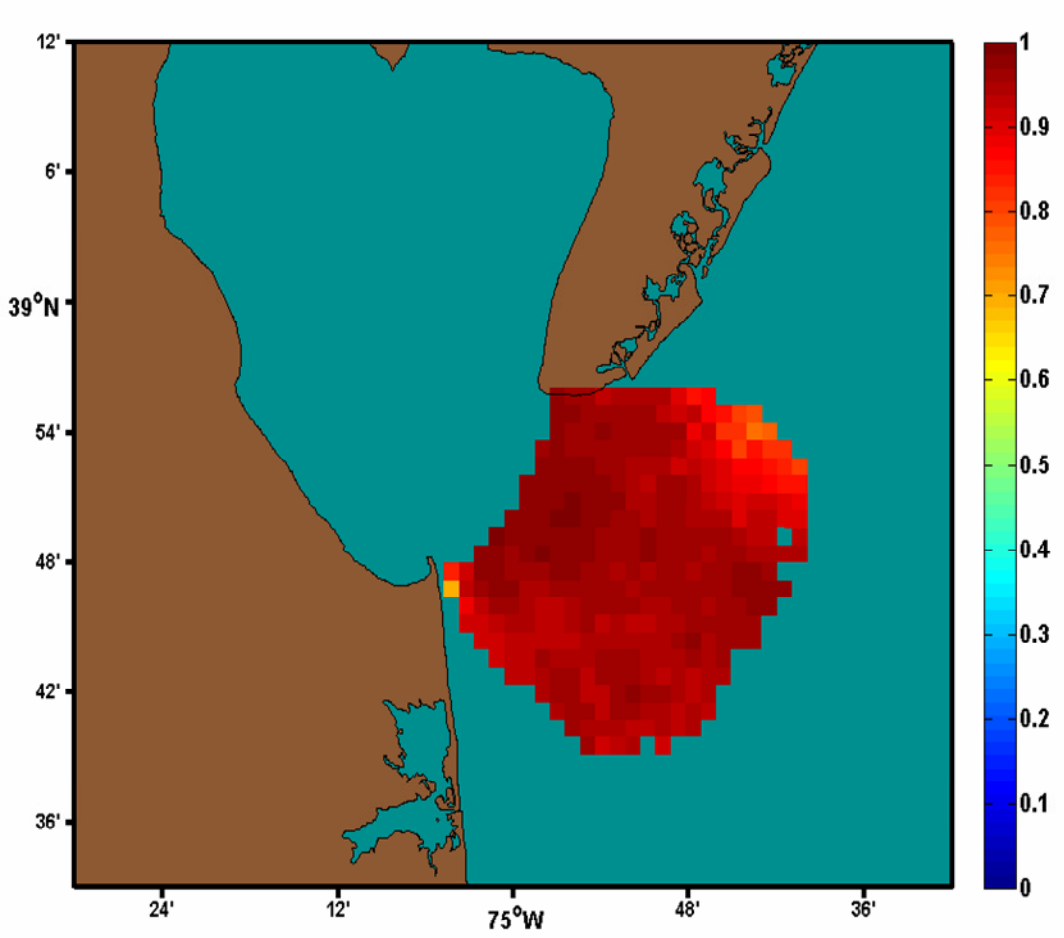

Figure 4.3 **Complex vector correlation amplitude of the ROMS and CODAR tidal velocity for October 2007. An amplitude of 1 is perfectly correlated.**

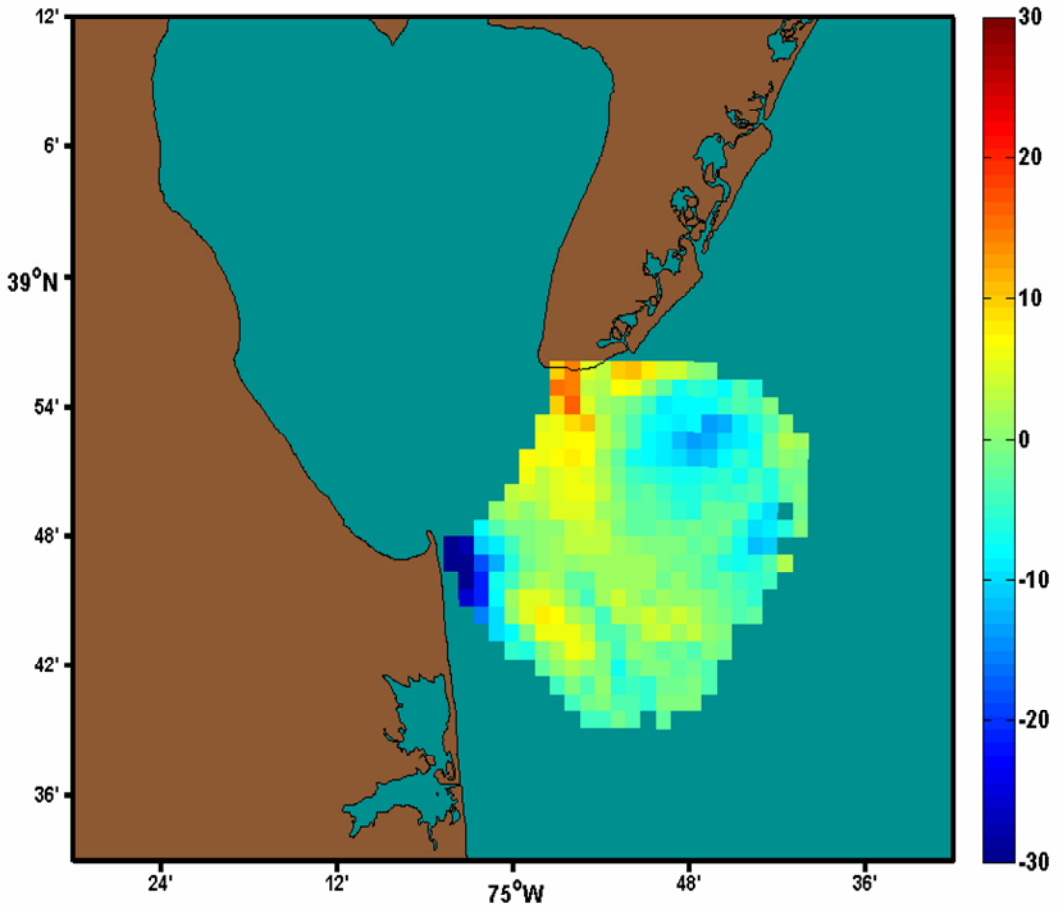

Figure 4.4 **Complex vector correlation phase angle of the ROMS and CODAR tidal velocity for October 2007. Colorbar unit's in degrees. A zero degree phase difference is perfectly correlated.**

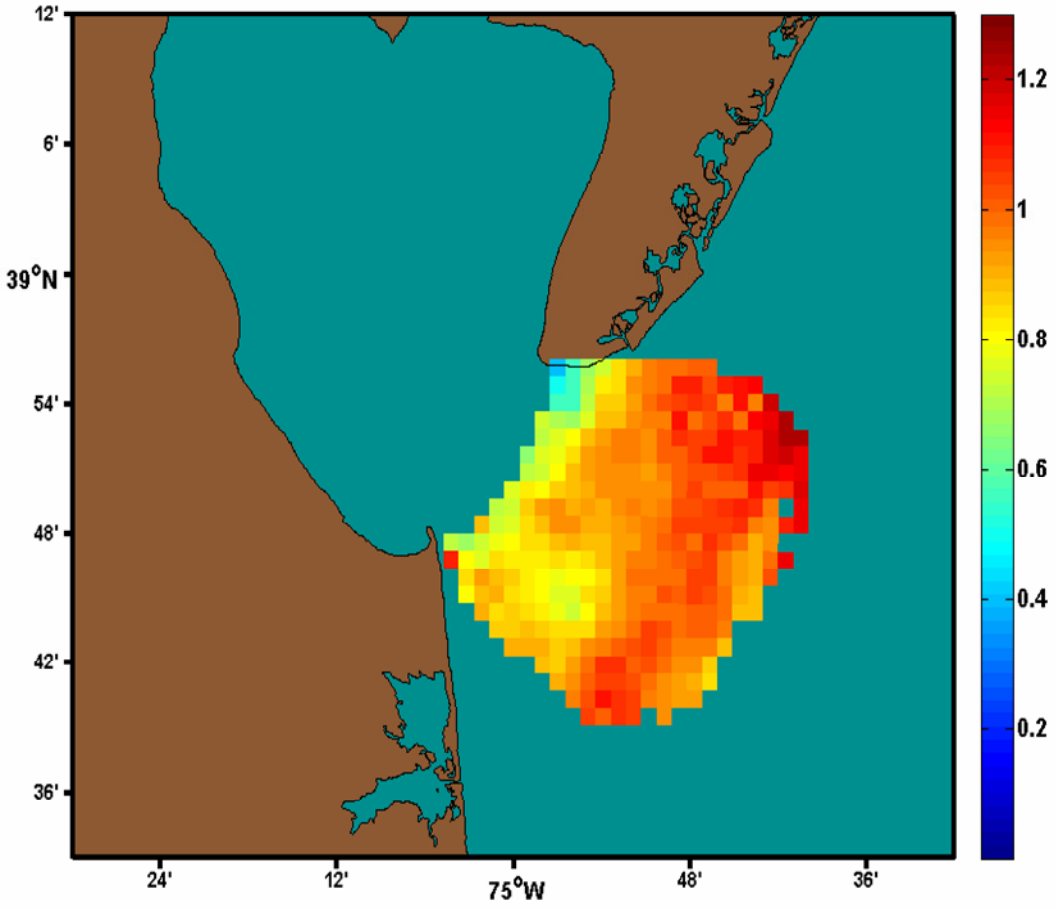

Figure 4.5 **Complex vector correlation transfer function of the ROMS and CODAR tidal velocity for October 2007. A transfer function of 1 is perfectly correlated.**

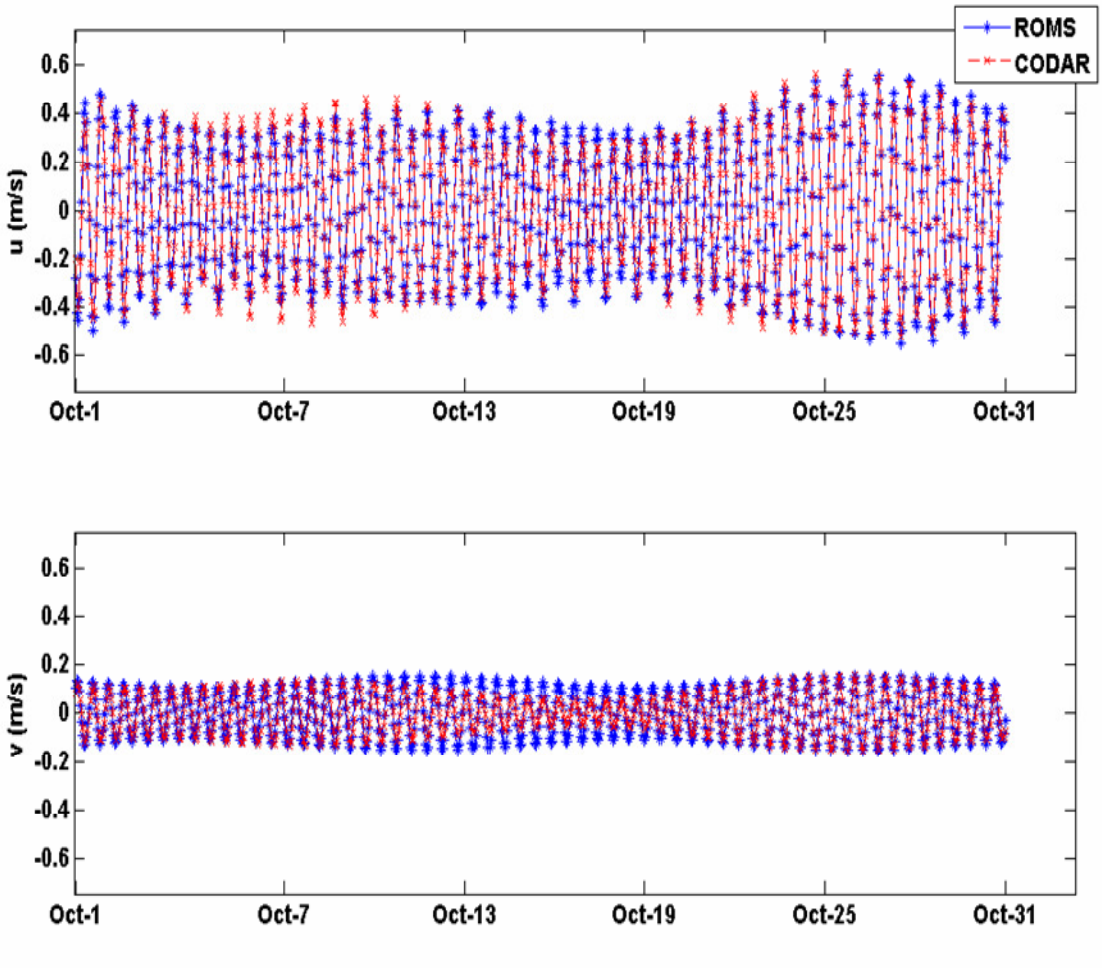

Figure 4.6 **Point comparison of ROMS and CODAR tidal velocity for October 2007 at a location (-74.8726 lon, 38.8131 lat) in the middle of the CODAR coverage footprint. Correlation amplitude 0.97785, phase angle -2.1324, transfer function 0.96557.**

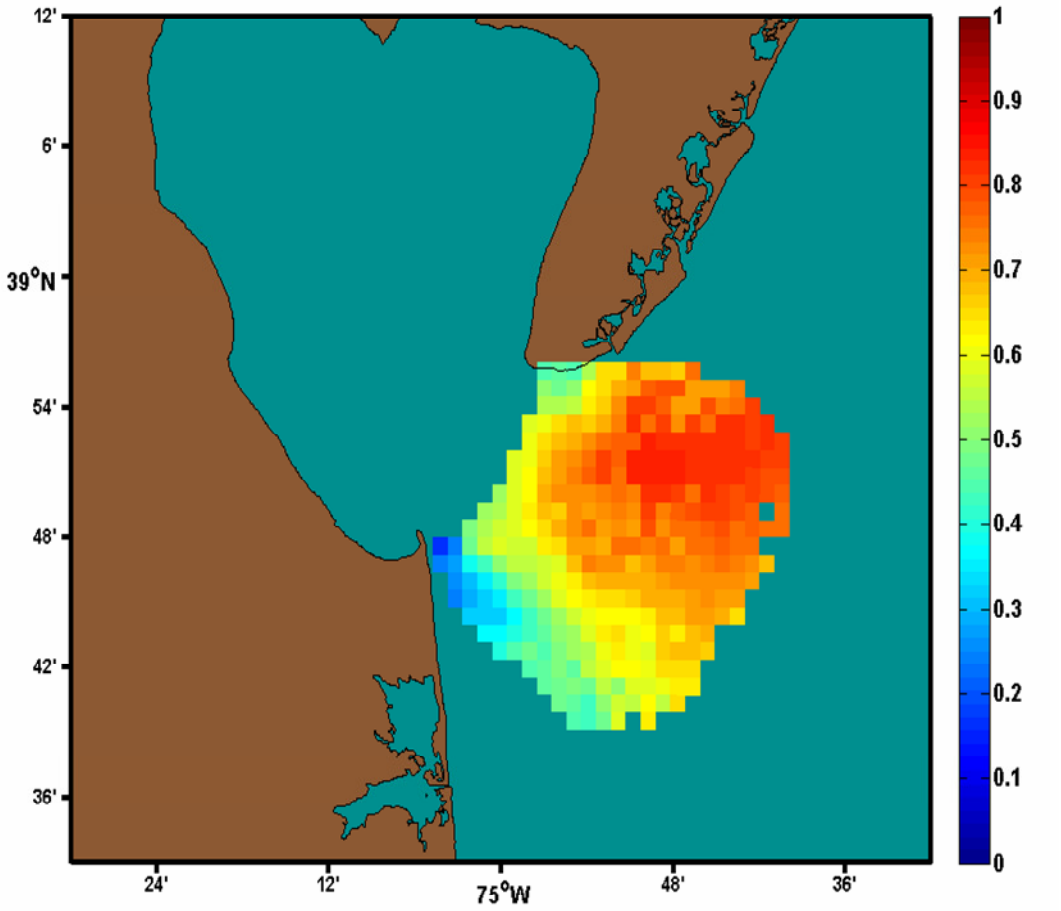

Figure 4.7 **Complex vector correlation amplitude of the ROMS and CODAR non-tidal velocity for October 2007. An amplitude of 1 is perfectly correlated.**

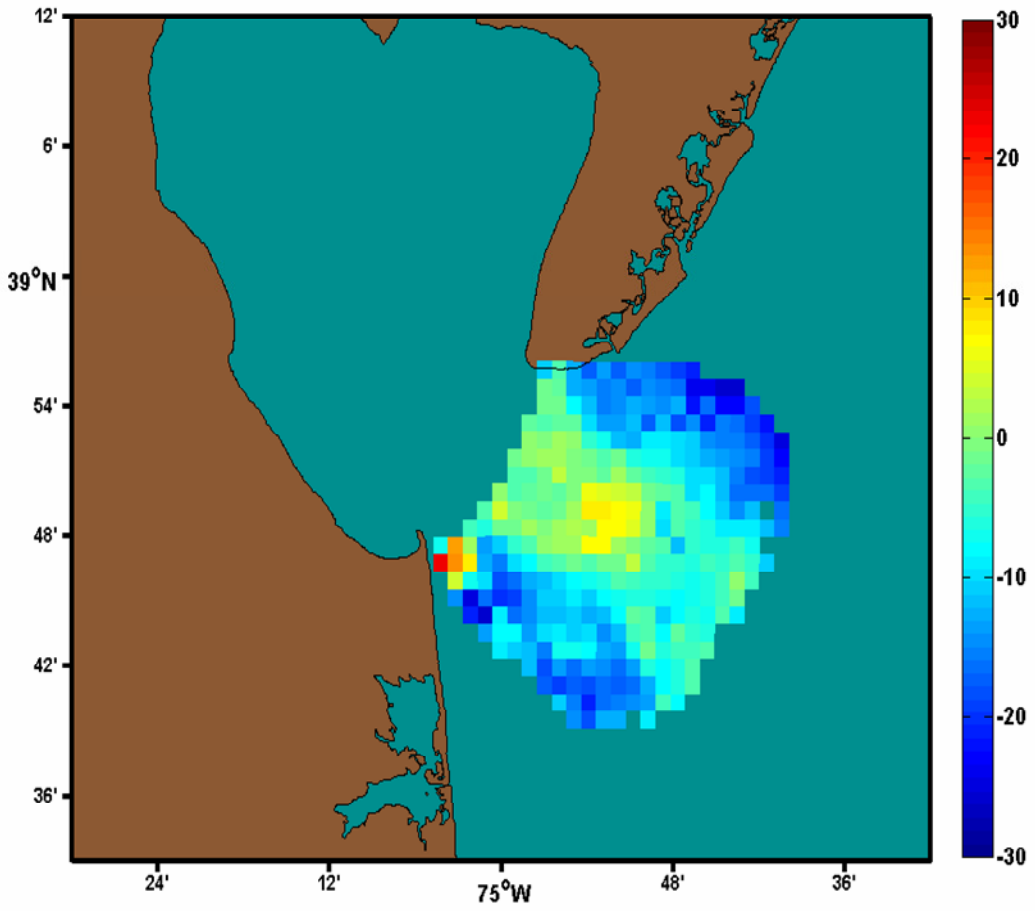

Figure 4.8 **Complex vector correlation phase angle of the ROMS and CODAR non-tidal velocity for October 2007. Colorbar units in degrees. A zero degree phase difference is perfectly correlated.**

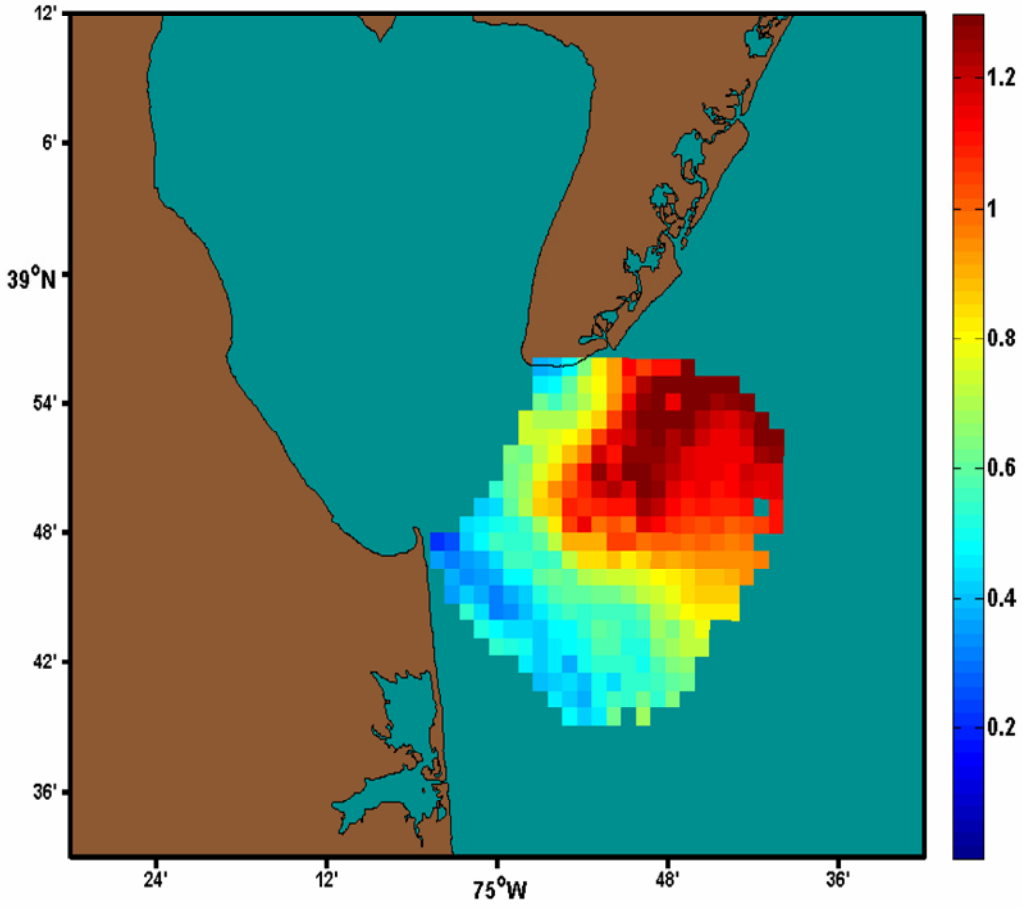

Figure 4.9 **Complex vector correlation transfer function of the ROMS and CODAR non-tidal velocity for October 2007. A transfer function of 1 is perfectly correlated.**

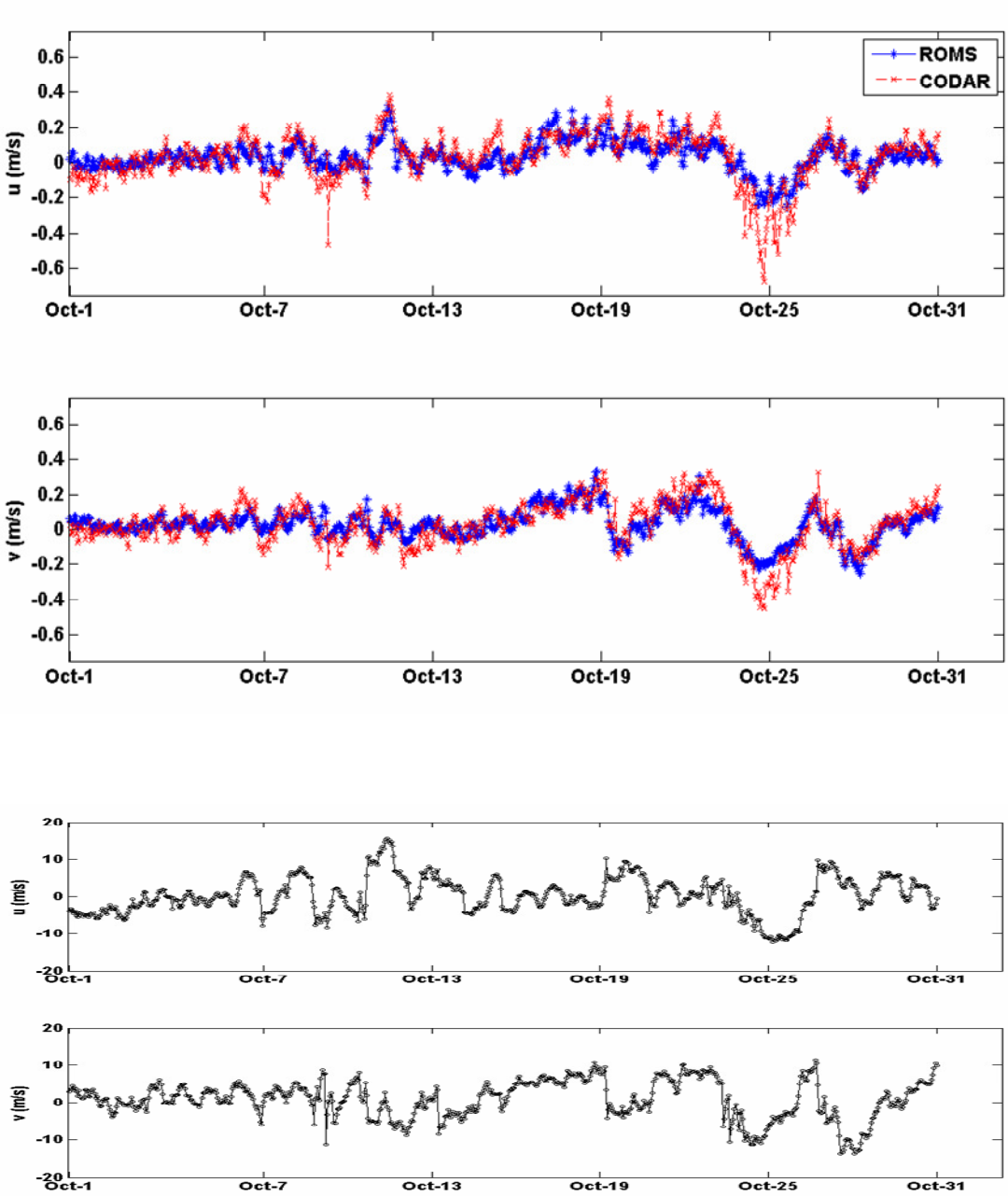

Figure 4.10 Point comparison of ROMS and CODAR non-tidal velocity for October 2007 at a location (-74.8726 lon, 38.8131 lat) in the middle of the CODAR coverage footprint. Correlation amplitude 0.81016, phase angle -0.36100, transfer function 1.2116. Wind speed for the same time is also included.

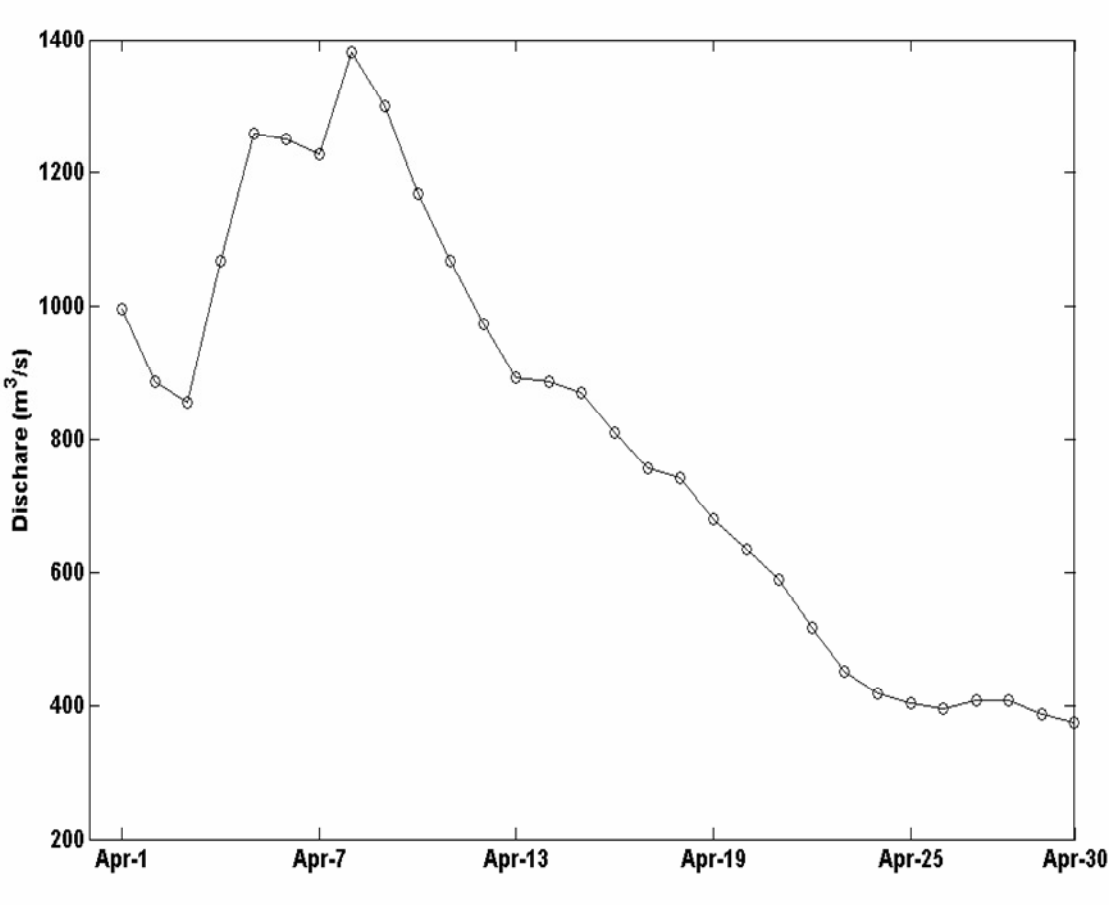

Figure 4.11 River discharge during April 2008.

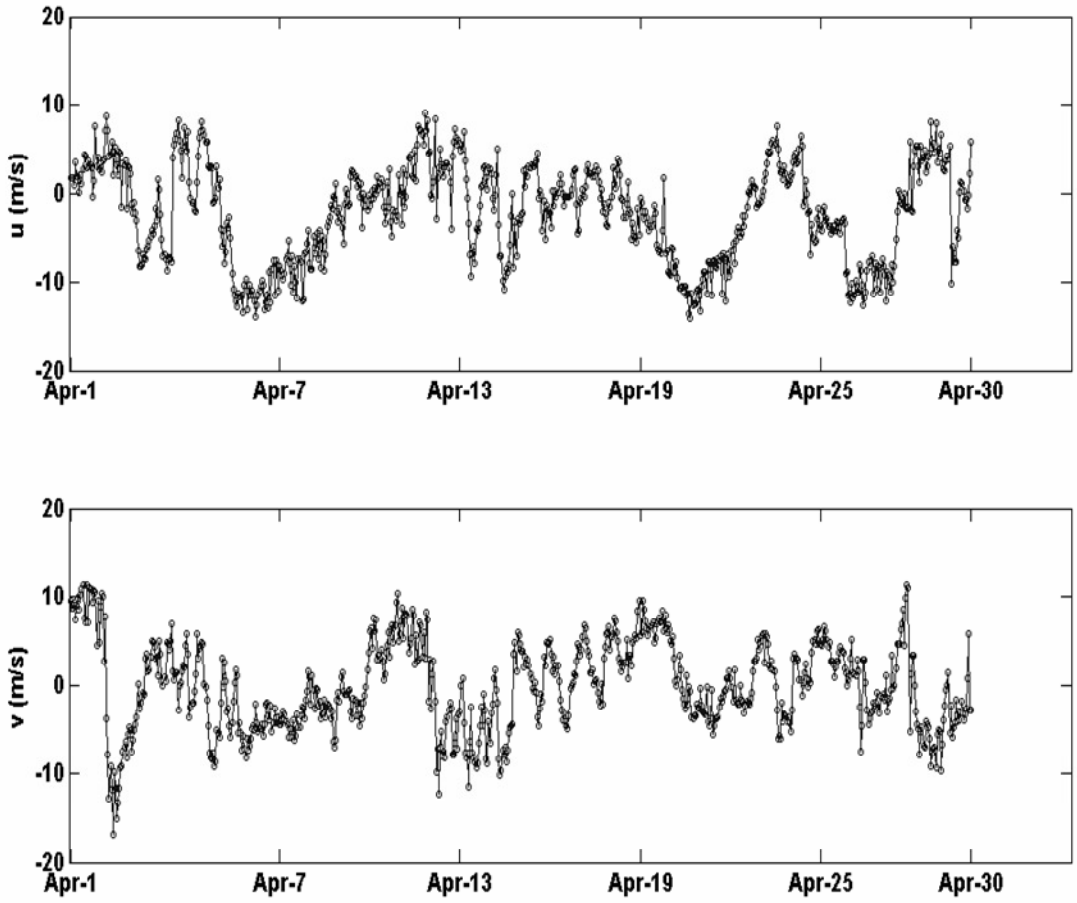

Figure 4.12 East-West and North-South wind speed for April 2008.

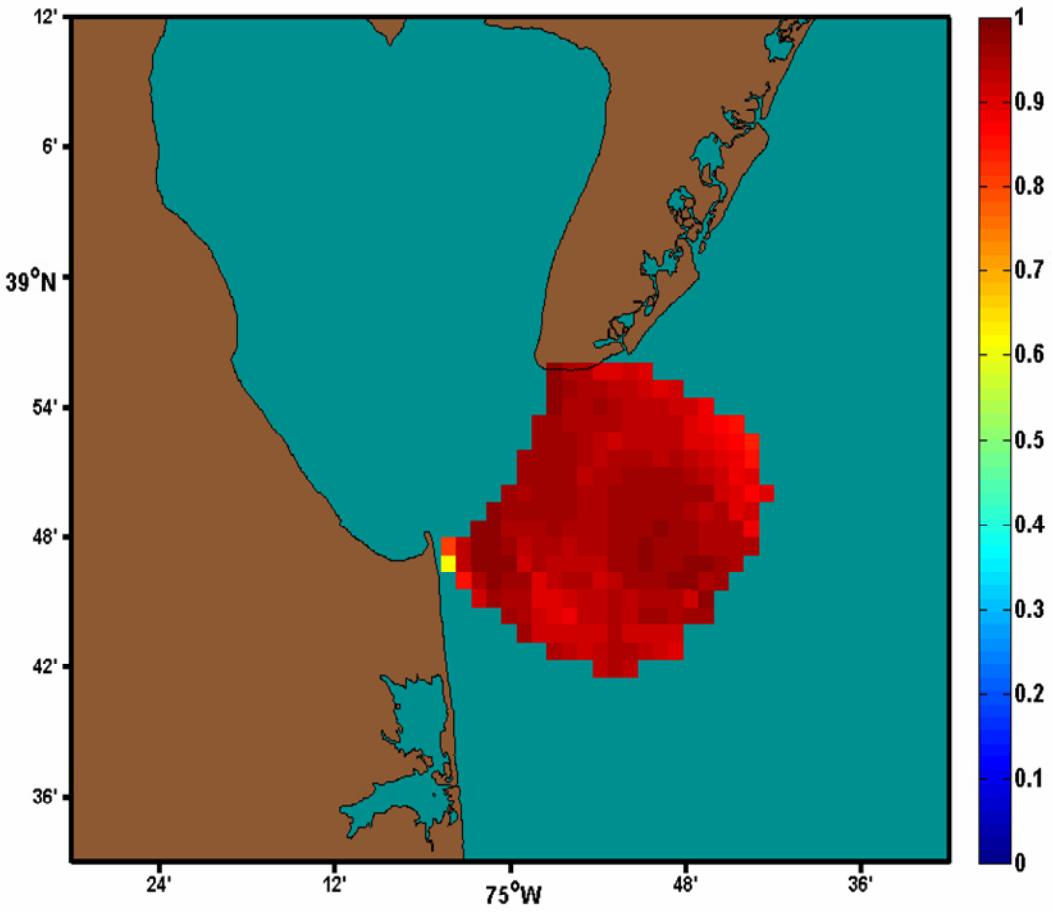

Figure 4.13 Complex vector correlation amplitude of the ROMS and CODAR tidal velocity for April 2008. An amplitude of 1 is perfectly correlated.

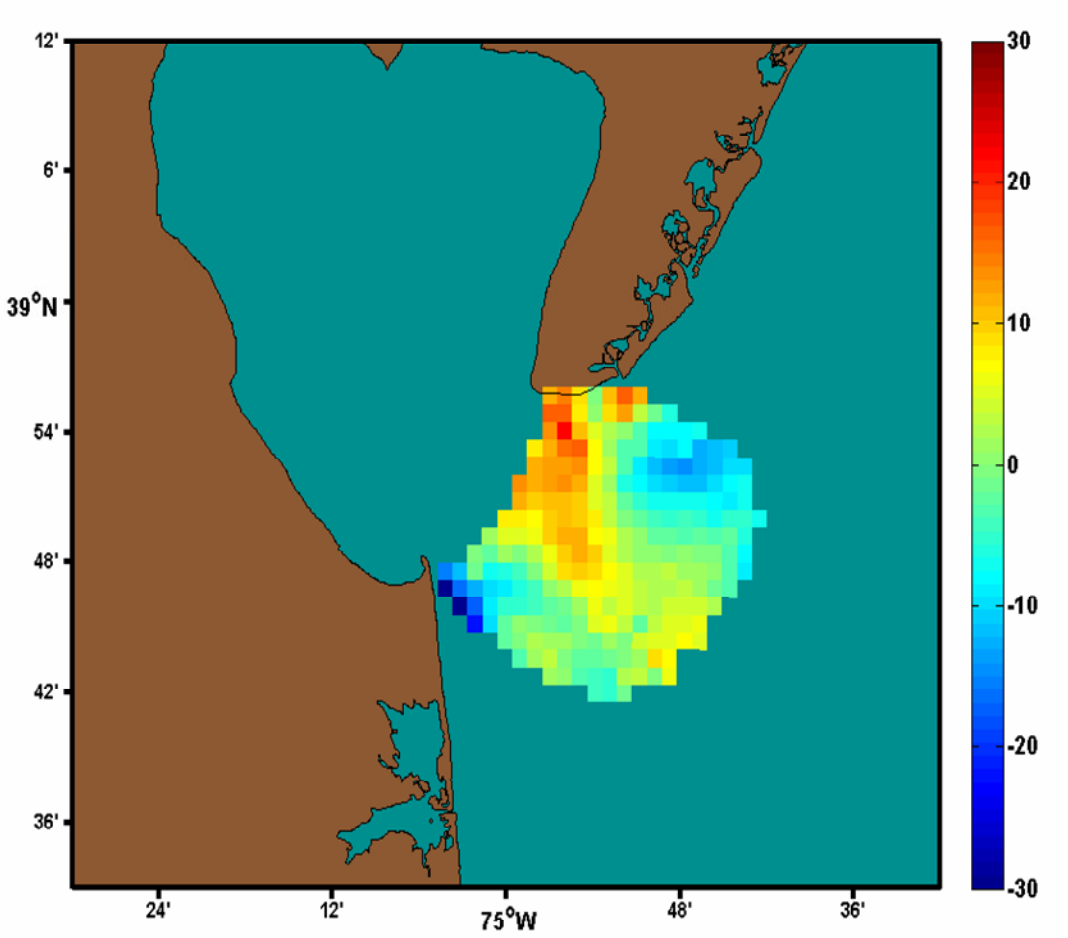

Figure 4.14 Complex vector correlation phase angle of the ROMS and CODAR tidal velocity for April 2008. Colorbar units in degrees. A zero degree phase difference is perfectly correlated.

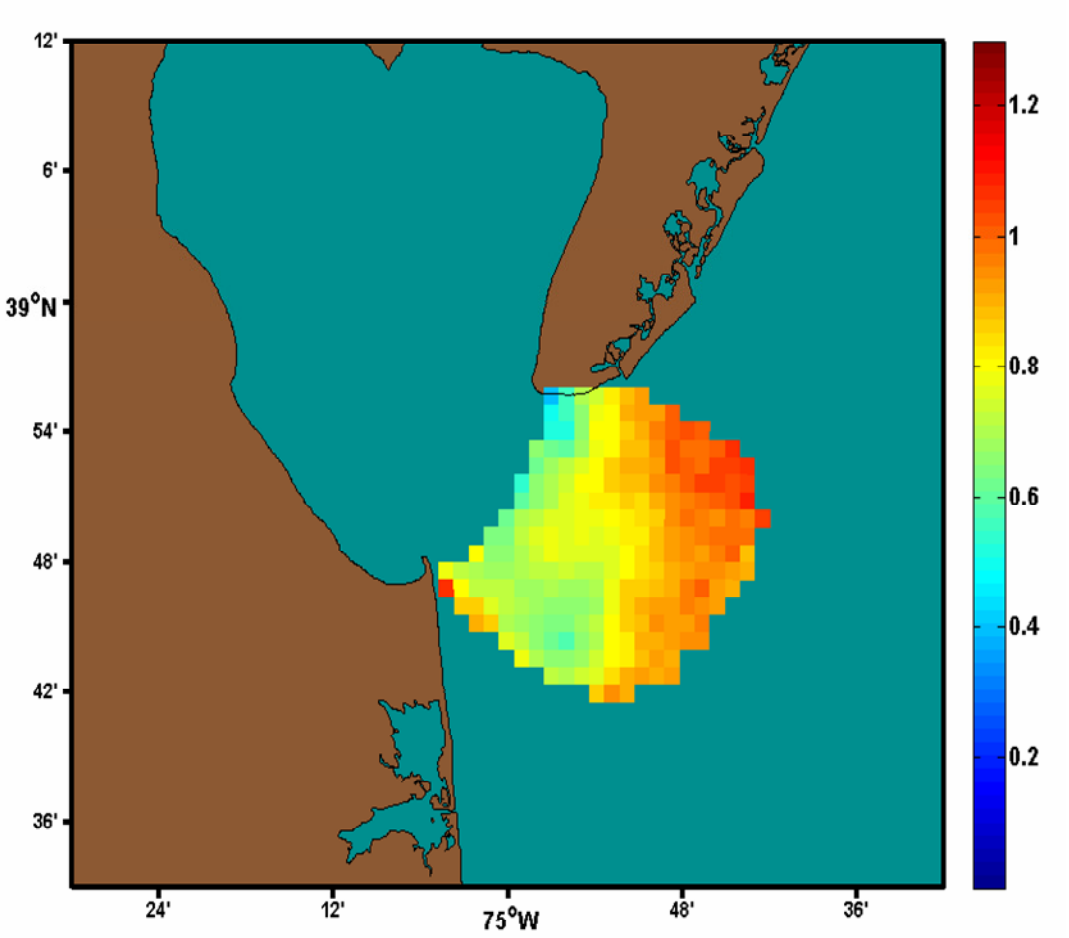

Figure 4.15 Complex vector correlation transfer function of the ROMS and CODAR tidal velocity for April 2008. A transfer function of 1 is perfectly correlated.

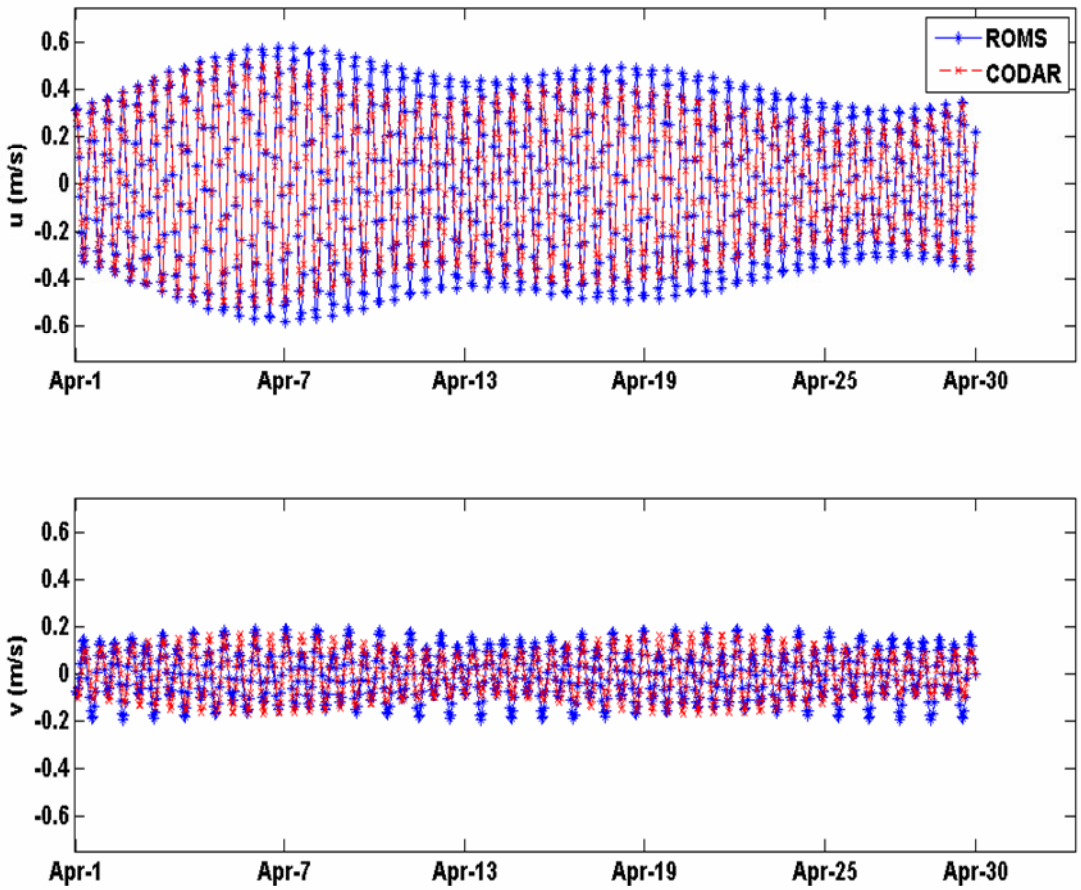

Figure 4.16 Point comparison of ROMS and CODAR tidal velocity for April 2008 at a location (-74.8726 lon, 38.8131 lat) in the middle of the CODAR coverage footprint. Correlation amplitude 0.97541, phase angle 1.8801, transfer function 0.83468.

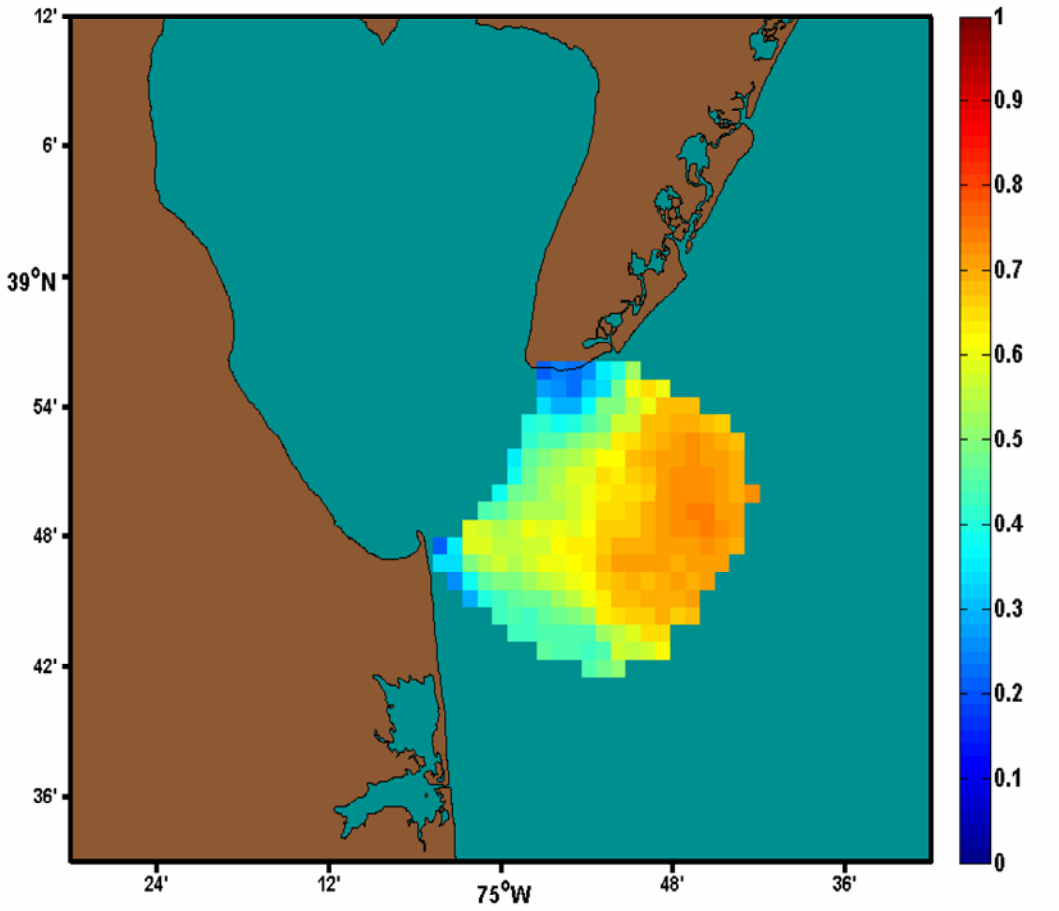

Figure 4.17 Complex vector correlation amplitude of the ROMS and CODAR non-tidal velocity for April 2008. An amplitude of 1 is perfectly correlated.

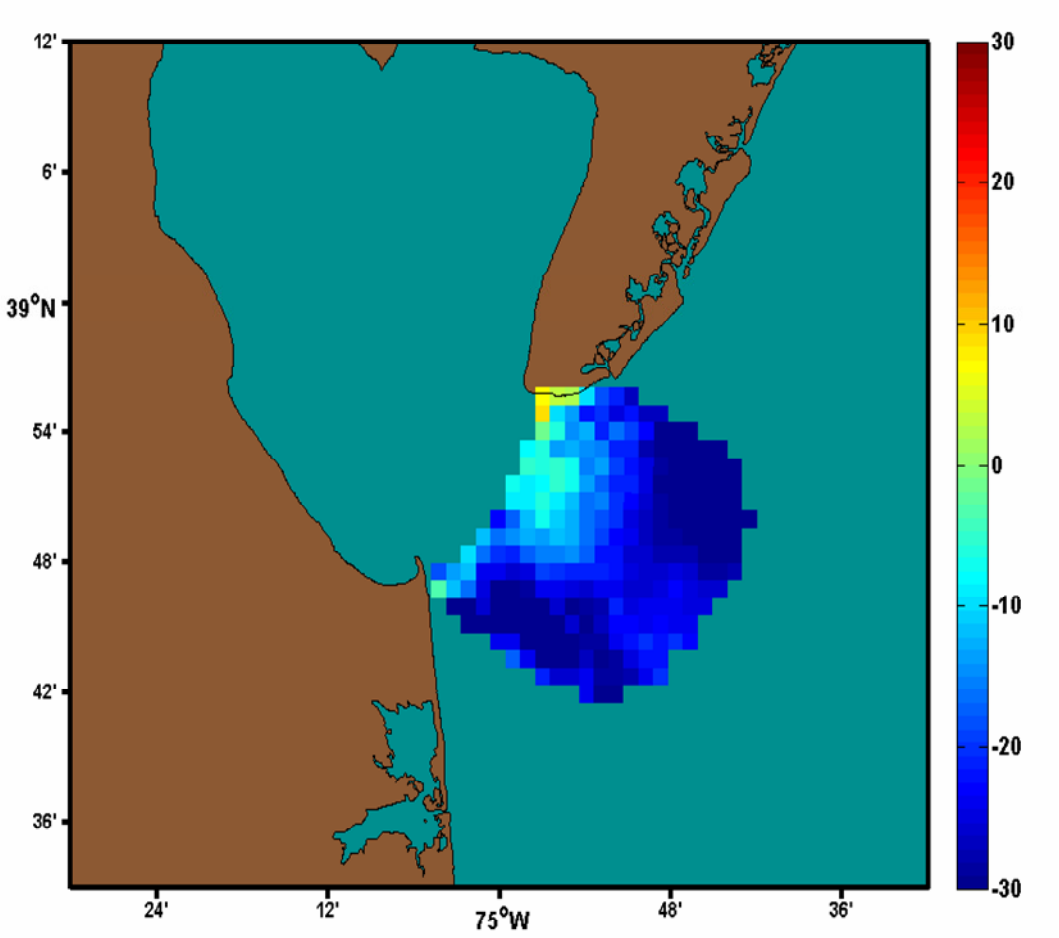

Figure 4.18 Complex vector correlation phase angle of the ROMS and CODAR non-tidal velocity for April 2008. Colorbar units in degrees. A zero degree phase difference is perfectly correlated.

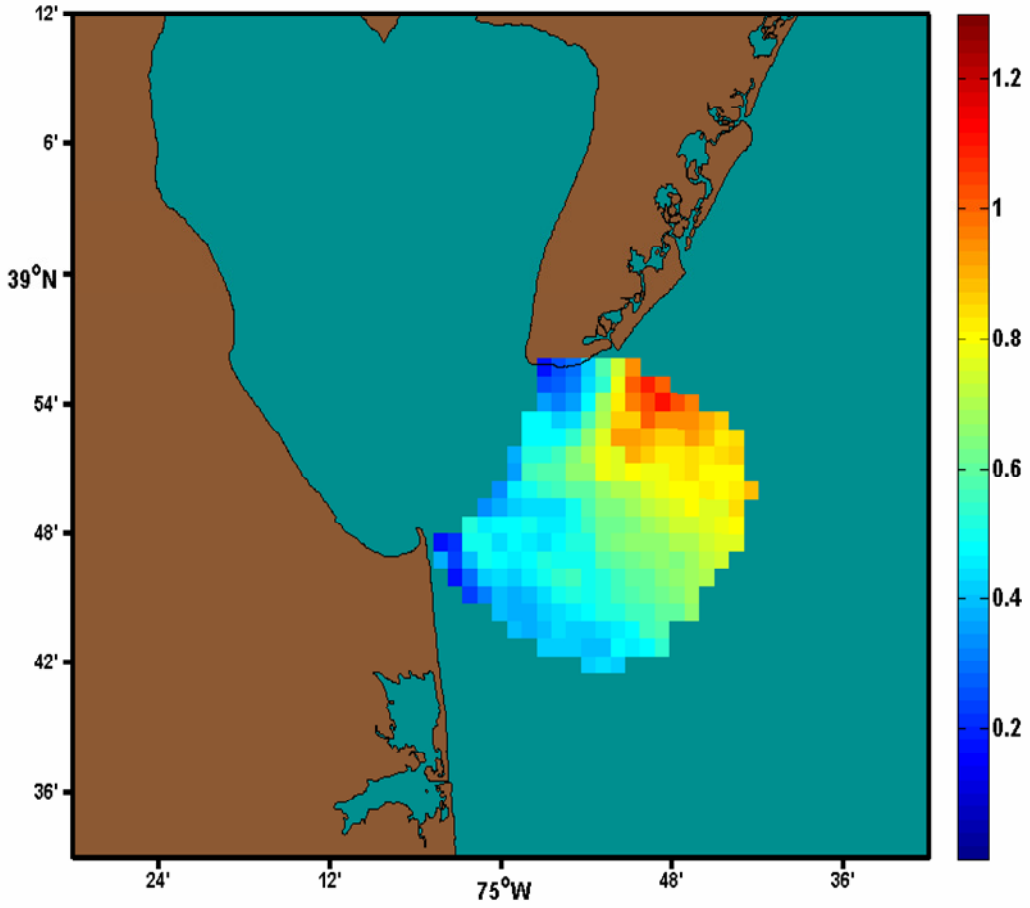

Figure 4.19 Complex vector correlation transfer function of the ROMS and CODAR non-tidal velocity for April 2008. A transfer function of 1 is perfectly correlated.

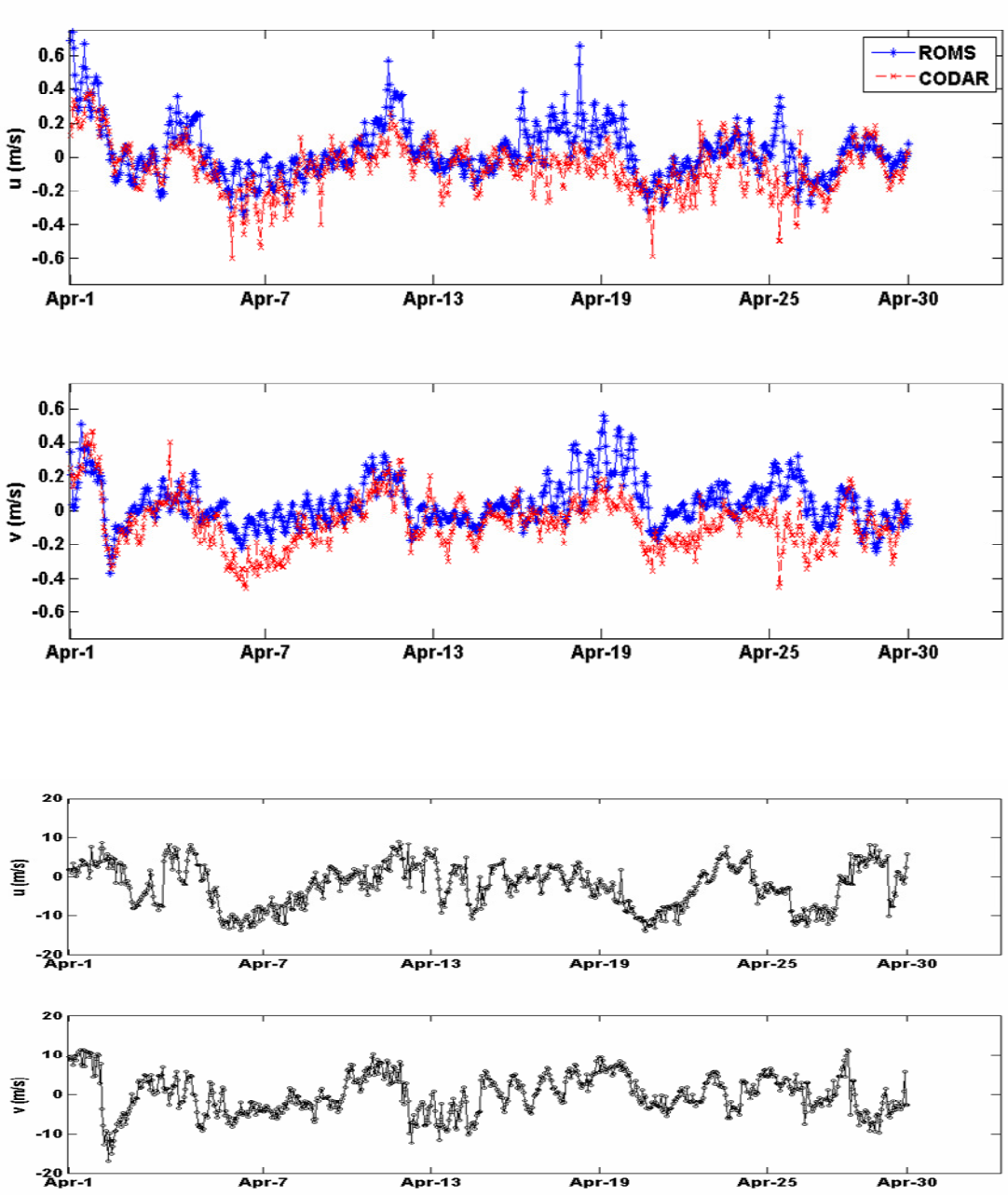

Figure 4.20 Point comparison of ROMS and CODAR non-tidal velocity for April 2008 at a location (-74.8726 lon, 38.8131 lat) in the middle of the CODAR coverage footprint. Correlation amplitude 0.66132, phase angle -23.2102, transfer function 0.65615. Wind speed for the same time is also included.

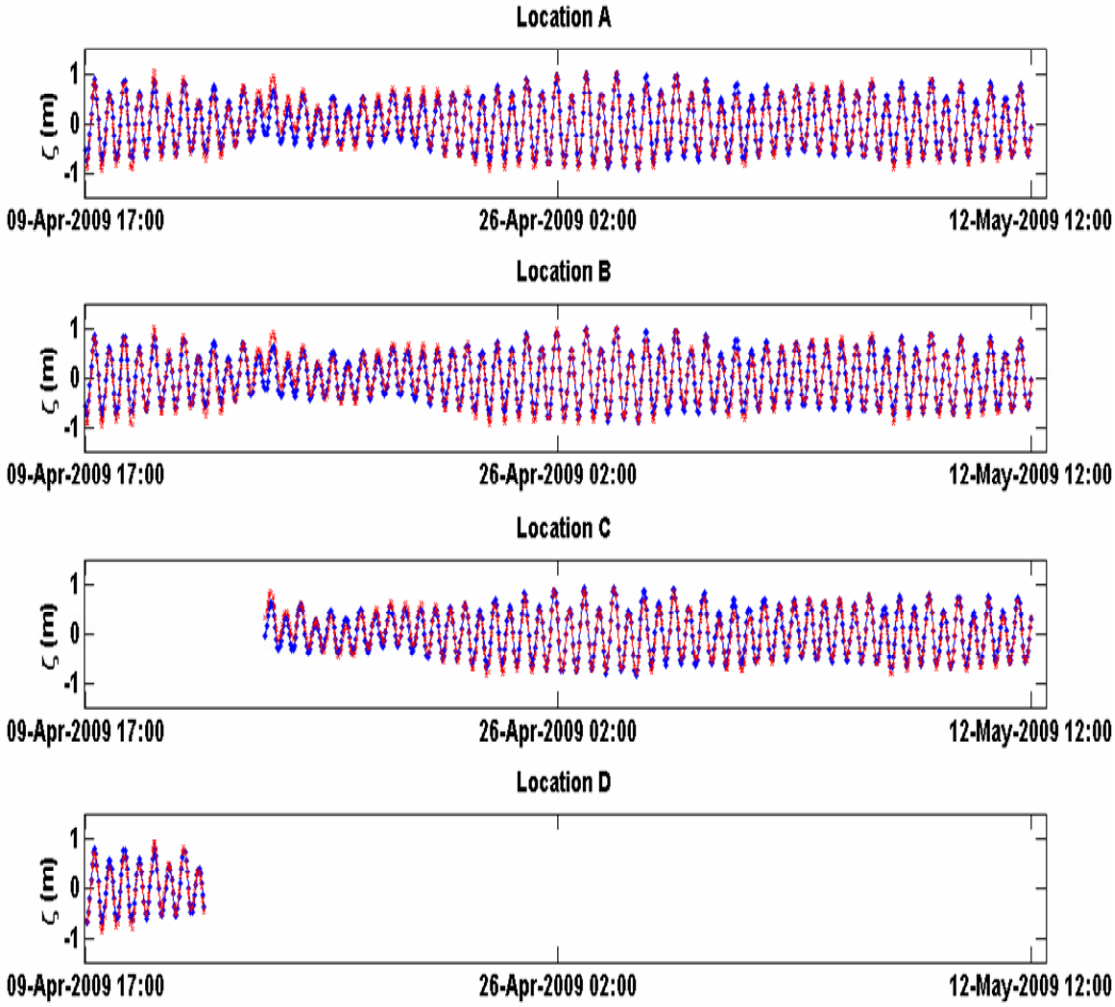

Figure 4.21 Comparison of the measured free surface data from the ADCP, and the free surface calculated by ROMS. ROMS data is blue and ADCP data is red.

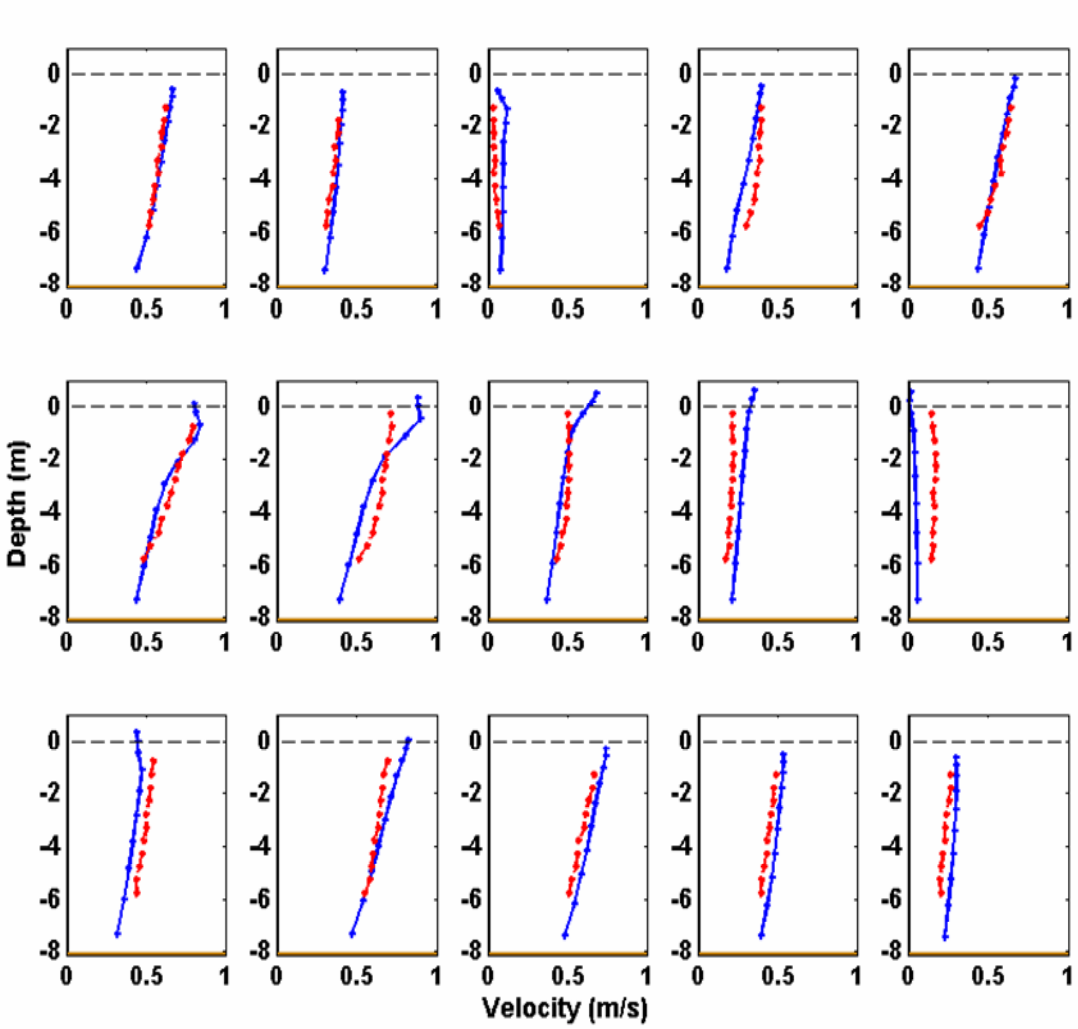

Figure 4.22 Sequence of ROMS/ADCP velocity profile comparisons at location A, 13-Apr-2009 20:00:00 to 14-Apr-2009 11:00:00. ROMS data is the blue curve and the ADCP data is the red curve.

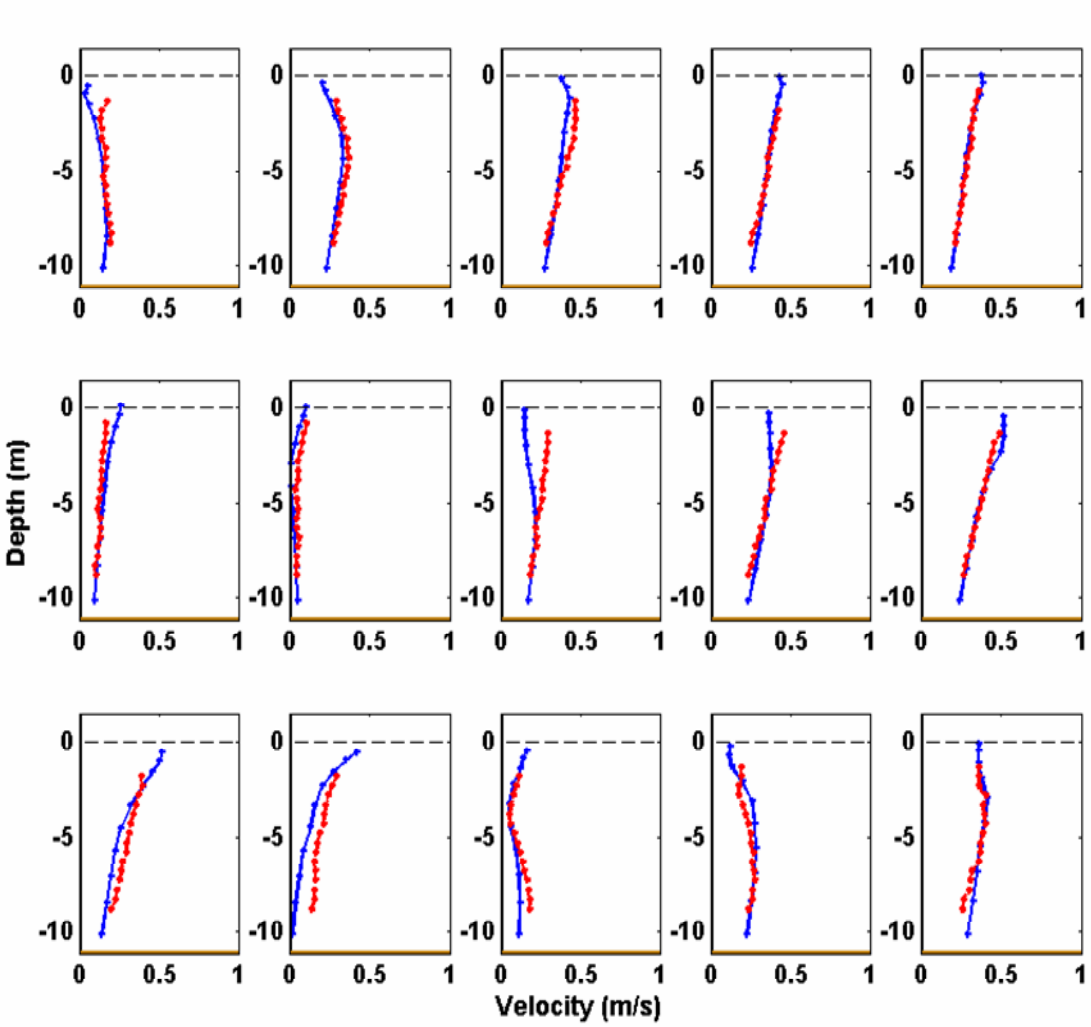

Figure 4.23 **Sequence of ROMS/ADCP velocity profile comparisons at location B, 17-Apr-2009 14:00:00 to 18-Apr-2009 05:00:00. ROMS is the blue curve and the ADCP data is the red curve. Complex correlation information: Amplitude 0.97311 | Phase Angle 11.8917 | Transfer Fn 1.0436.**

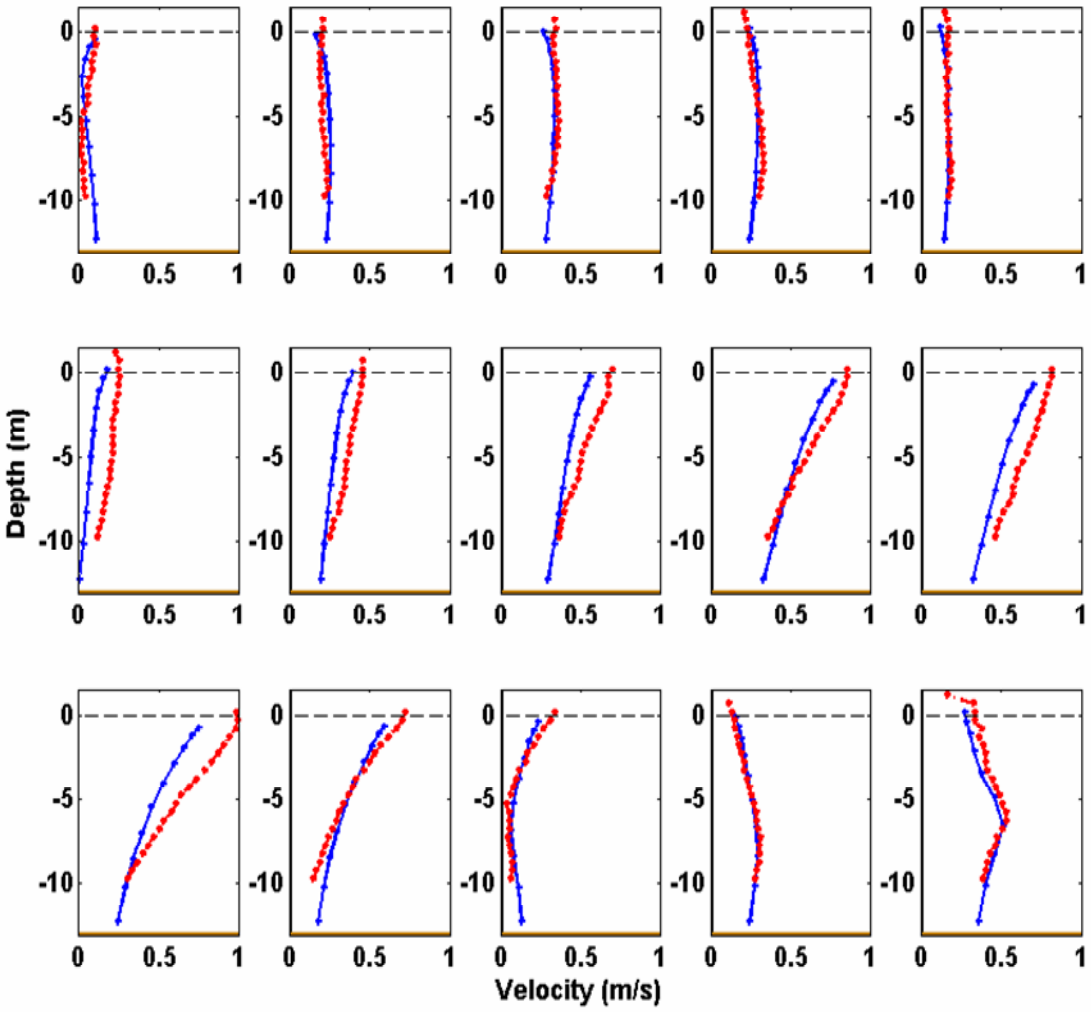

Figure 4.24 **Sequence of ROMS/ADCP velocity profile comparisons at location D, 12-Apr-2009 11:00:00 to 13-Apr-2009 02:00:00. ROMS is the blue curve and the ADCP data is the red curve. Complex correlation information: Amplitude 0.97074 | Phase Angle 9.5595 | Transfer Fn 1.2777.**

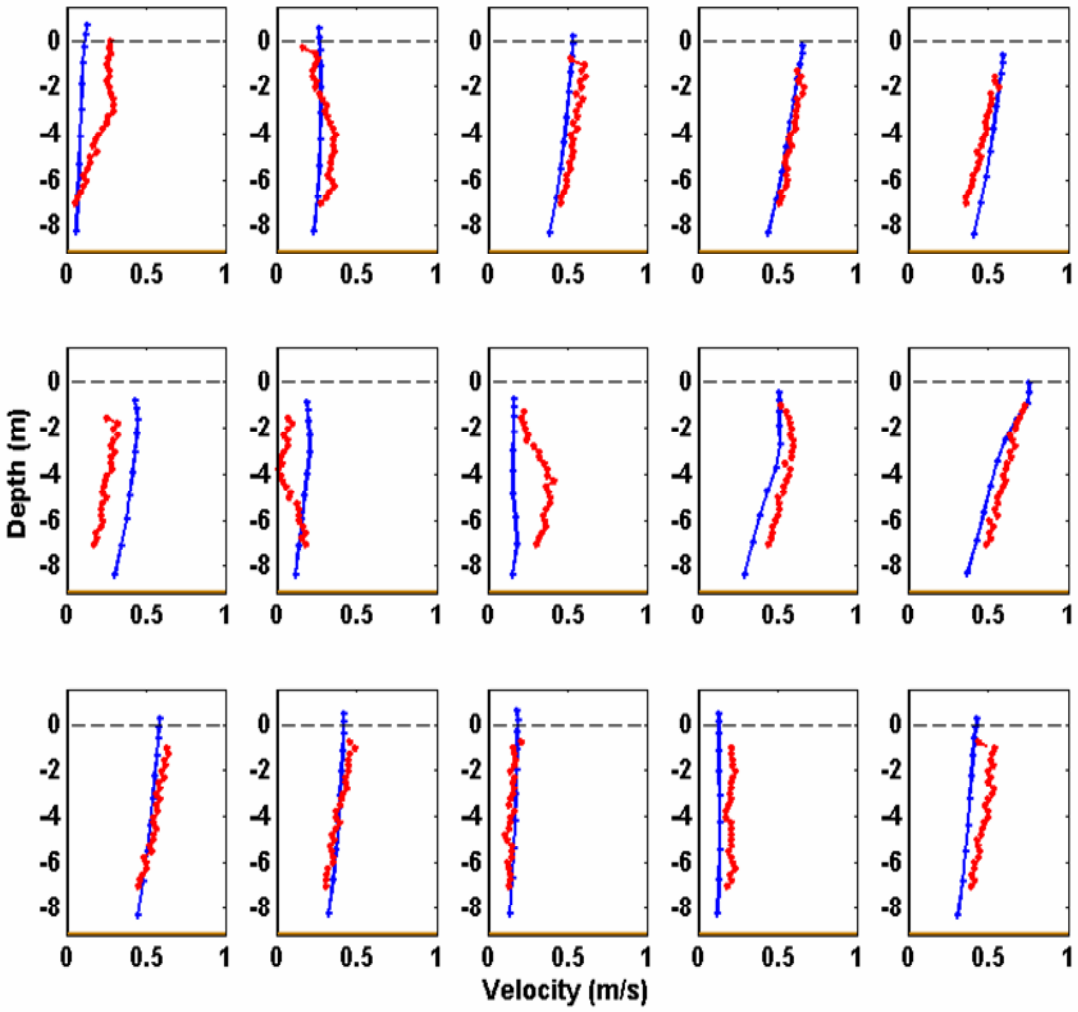

Figure 4.25 Sequence of ROMS/ADCP velocity profile comparisons at old deployment location during Spring 2008, 18-Aug-2008 02:00:00 to 18-Aug-2008 17:00:00. ROMS is the blue curve and the ADCP data is the red curve. Complex correlation information: Amplitude 0.94037 | Phase Angle -59.6004 | Transfer Fn 1.0229.

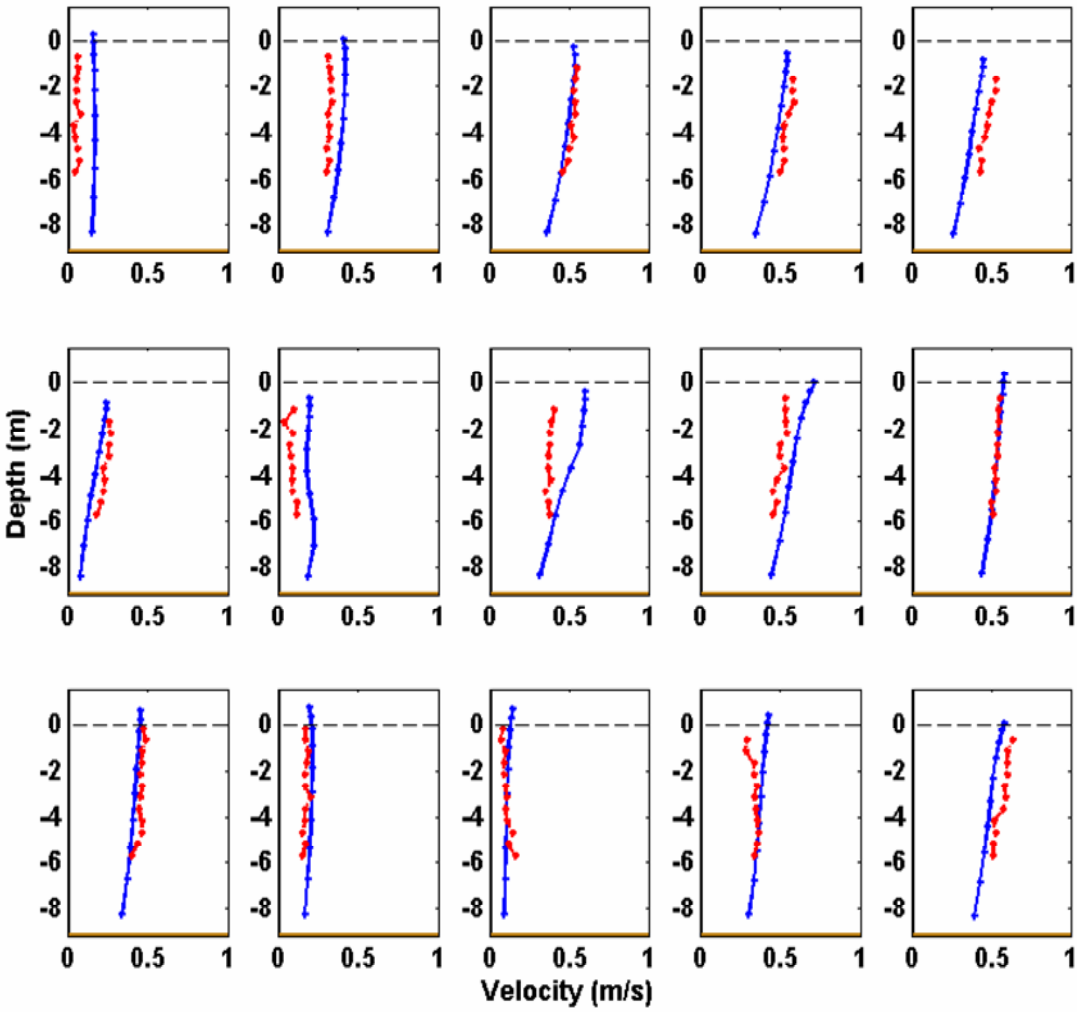

Figure 4.26 Sequence of ROMS/ADCP velocity profile comparisons at the old deployment location during Fall 2007, 13-Nov-2007 04:00:00 to 13-Nov-2007 19:00:00. ROMS is the blue curve and the ADCP data is the red curve. Complex correlation information: Amplitude 0.94813 | Phase Angle -0.37166 | Transfer Fn 1.1238.

Chapter 5

SALINITY AND BOUYANT PLUME

5.1 Bay Salinity Conditions

After the initial spin up period the simulation produces a realistic salinity field. The salinity in the bay is highly variable over both short and long time scales, and for this simulation in particular it changes with the tides, wind conditions, and discharge coming in from Delaware River. There is not a large amount of measured data on the salinity in the bay, but there are scattered salinity measurements over the course of 50 years available in the National Oceanographic Data Center database. The coverage of the bay from these measurements was good, and the observations were averaged together to produce a mean field in Whitney (2003). The resulting salinity structure of the bay can be seen in Figure 3.8 of the same work.

The resulting salinity field developed by the model matches well with the observed conditions. A typical picture of the depth-averaged salinity, post spin up, can be seen in figure 5.1. This is the average over the life of the simulation, except for 2006. The salinity from 2006 was not used in the averaging because of the initial spin up period, and using the rest of the year after the spin up may create a season bias. As mentioned before the salinity is highly variable due to a number of outside factors, but the structure remains very similar regardless. Since the tidal flux is much stronger than river outflow the waters are likely to be vertically well mixed (Hansen and Rattray, 1966). Figure 5.1 shows that more fresh water travels down the flanks of the

bay than in the middle, with a large amount situating itself around the Cape May area. This is consistent with the measured values in Figure 3.8 of Whitney (2003), and this structure is explained in Wong (1994). More detailed information about the bay salinity can be found in Garvine (1992) and Whitney (2003).

5.2 Buoyant Plume Investigation

Though not the main focus of this modeling effort, an accurate model of Delaware Bay offers a good opportunity to examine the plume of freshwater that is known to travel out of the bay under the right conditions. Due to the coriolis effect the tendency is for this plume to move in a southern direction down the coast towards the Chesapeake Bay, but this may be slowed or reversed due to the atmospheric conditions at the time.

In order to properly investigate this phenomenon, a video was created to examine the surface salinity in the bay and along the coast for the entire time of the simulation. Each frame of the video progresses the time of the output by only two hours, so a fairly complete picture of how the salinity in the model is behaving can be seen. This video has been posted online, and can be downloaded here (http://chinacat.coastal.udel.edu/~kirby/). Though the video is used here as a tool to see when a significant plume escapes from the bay, it cannot be shown here in this document. In its place, figures will be used showing a snapshot of the surface salinity at a prescribed time, the discharge from the Delaware River over the prior two weeks, and the magnitude and direction of the wind for the past 2 days. The 14 days of river discharge is presented because of the lag in response at the bay mouth to the outflow (Garvine et al. 1992, Whitney 2003).

5.3 Significant Discharge Events

Over the course of the four years of time simulated there were five times of very significant outflow from Delaware Bay, though the first high-discharge event happened very early in the simulation, and cannot be used because the model had not had time to spin up yet. These events can be seen in figure 2.13 of this document. There is usually fresh water flowing out of the bay in some quantity under typical conditions, but these are times that would produce a significant plume under a no-wind state. These times will be used to examine plume behavior.

5.3.1 Early July 2006 Event

This period of high outflow occurred in late June and early July of 2006. The model had been running for six months at that point, and the salinity conditions in the bay were properly well mixed by then.

Figure 5.2 shows a plume that has developed in response to the very high outflow of days before. As you can see from the picture, the large amount of fresh water flux makes its way out of the bay and begins to head down the coast. The recent wind behavior is slightly to the South-West, providing favorable conditions for the plume to form and travel. The tendency is for surface water to remain contained near the coast during these wind conditions, as the surface water will have a net movement at a 90 degree angle to the right of the wind direction (in the northern hemisphere). This is known as Ekman transport. Figure 5.3 shows the conditions in the same area only approximately two days later. There has been a swift change in the behavior of the fresh water brought about by the shifting of the winds. The Ekman transport created from these upwelling-favorable winds, which in this case is wind blowing to the North-East, dispersed the plume. The fresher water near the surface is moved out

further into the ocean, and higher salinity water moves in to take its place. Discharge also returned back to more reasonable levels.

5.3.2 Late April 2007 Event

The next big discharge event happened in Spring 2007, at the end of April and beginning of May. It was a fairly wet time in general, but had one very large spike in river discharge for a couple of days.

A good portion of the previous month had been experiencing higher discharge, as is typical of Spring, but a noteworthy plume did not form until after the large influx of freshwater at the end of April. The wind conditions had kept most of the freshwater contained within the bay up until that point. In figure 5.4 the plume can be seen, and at that point the wind conditions had recently been slightly offshore yet still fairly weak. It was short-lived, however, as the wind picked up shortly after that and began to blow much more significantly offshore. The widening and dispersal of the plume caused by this is shown in figure 5.5. This was similar to what happened to the plume from the last event, though because of the different wind conditions it did not destruct in the same way as before.

5.3.3 Early March 2008 Event

The river outflow was fairly high throughout much of early 2008, but around mid March was the greatest spike. The discharge remained low for a considerable period of time after the Spring months.

Though conditions were very favorable, a substantial plume did not form during this time. Instead, many smaller plumes formed, though due to the high discharge freshwater was constantly exiting the bay in significant amounts. The fact

no continuous plume traveling down the shoreline was formed was most likely due to the sporadic atmospheric forcing during that time. After the highest freshwater event and some constructive wind conditions, a short, thick plume was seen (figure 5.6), though it did not last for a long time. It began to disperse almost immediately after, and less than two days later it was all but gone (figure 5.7).

5.3.4 Mid December 2008 Event

The last big spike in discharge during the simulation was at the very end of 2008, and was fairly isolated. Throughout 2009 there were many times of higher discharge and it was much more consistent than the previous years, but late December 2008 saw the last major event.

Around the time a plume would be expected, there is not much activity around the bay mouth compared to the other large events (figure 5.8). This is most probably a combination of this spike being shorter and less noteworthy than the others, and the small amount of outflow preceding it for a long time causing higher salinity conditions in the bay. The decrease in bay salinity caused by this time did, however, set the stage for a plume to develop a couple weeks later, seen in figure 5.9. It is higher salinity than the last few pictured in previous figures, but still sends a large amount of fresh water down the coast.

5.4 Wind Driven Events

There were many reactions to differing outflow and salinity conditions around the bay mouth over the course of four years of simulation outside of the few obvious ones highlighted above. Attention will be given to a couple of the more interesting events below.

5.4.1 Coastal Jets

Under specific conditions a coastal jet can develop in the form of a long, skinny plume and sustain for quite a few days. This typically happens during light to heavy periods of downwelling-favorable wind. A prime example of this was the end of November 2006. Figure 5.10 shows just after the beginning of this formation, which is characterized by fairly high, sustained discharge and very strong winds blowing down the coast. Figure 5.11 displays the plume a few days later, after the winds had shifted a bit yet still remained strong. It had grown larger by that instance and still extended far outside of the bay. After that point, the winds calmed down significantly and began weak upwelling-favorable tendencies. This dispersed the freshwater that had amassed along the coast over the last week creating a fatter plume, but its progress had been halted. This can be seen in figure 5.12. It will eventually dissolve to the point of normal conditions a couple days later.

Another example of this type of plume forming can be seen in figure 5.13. This happened in early September of 2009. Though the discharge conditions had been very low for this time, the wind velocity was blowing in a downwelling-favorable manner for a sustained period of time, and a long skinny plume existed for over a week.

There were certainly other times that this type of plume came into play, but these two examples were the most prominent.

5.4.2 Reverse Plumes

If the wind velocity is high enough in an Easterly direction a plume can actually be created exiting out of the top of the bay and head up the coast. This behavior is exhibited in late October 2006. Figure 5.14 depicts a time when the

atmospheric forcing had been strong enough in the appropriate direction, and this phenomenon occurred. Notice that the discharge had not been very high the majority of the time preceding this event, but because the wind forcing was so strong it created this reverse plume.

This happens again at the same time of year in late October 2008. Figure 5.15 shows a much similar situation to before. The wind velocity is very high, and the outflow is very low.

It may just be coincidence that two of the most significant instances of this happening happened to be at the very end of October, as it did not occur to any significant degree in 2007 and 2009. What does seem clear is that the conditions for this reverse plume are low discharge and high Easterly winds.

5.5 Summary

The analysis from this chapter has painted an interesting picture of the salinity behavior in the bay and around the bay mouth according to the model. A buoyant plume will certainly escape the confines of the bay and develop under high discharge conditions as would be expected, but the wind can also play a role that is just as important if not greater than the introduction of high freshwater flux.

Without favorable wind conditions a plume will not be sustained, and can even be prevented from developing. On the other hand, the wind by itself can create some unique circumstances if it is strong enough.

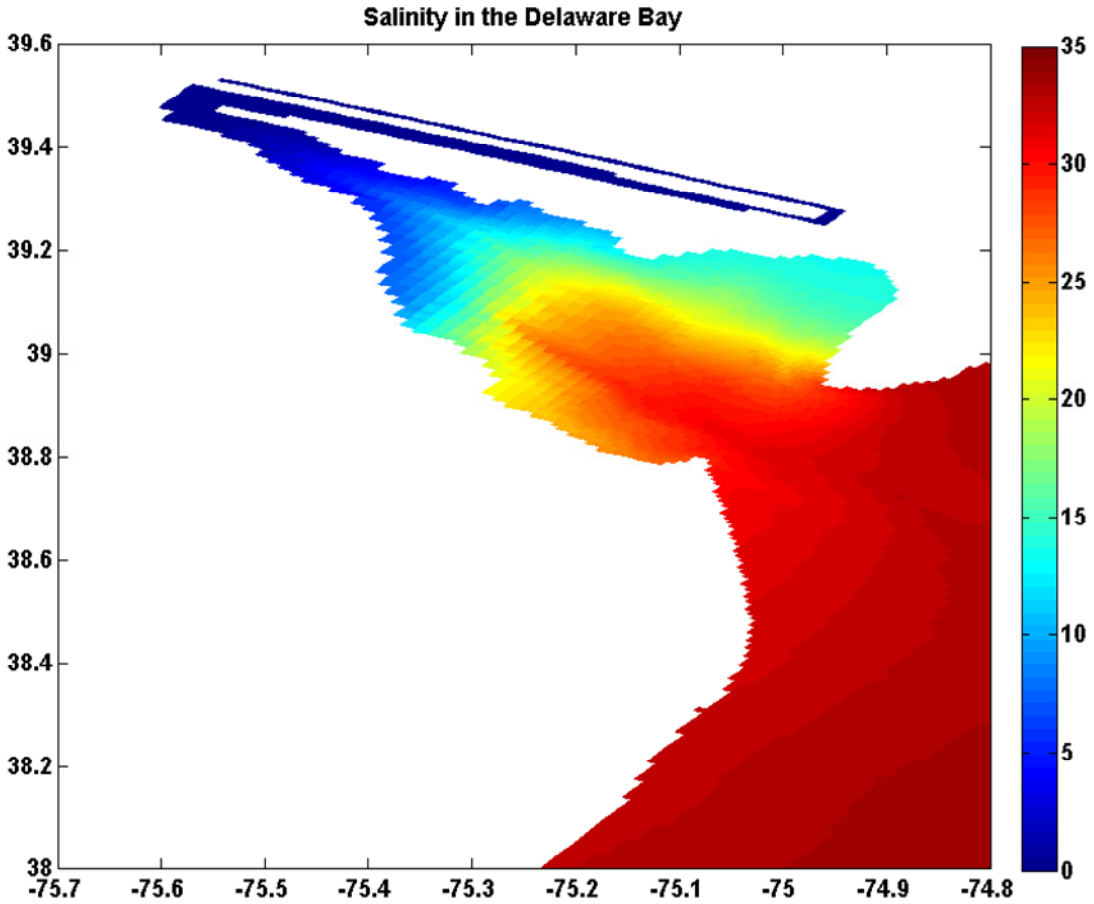

Figure 5.1 **Three year average of the depth averaged model salinity values from the beginning of 2007 to the end of 2009. The salinity is highly variable with the tides, river discharge, and winds.**

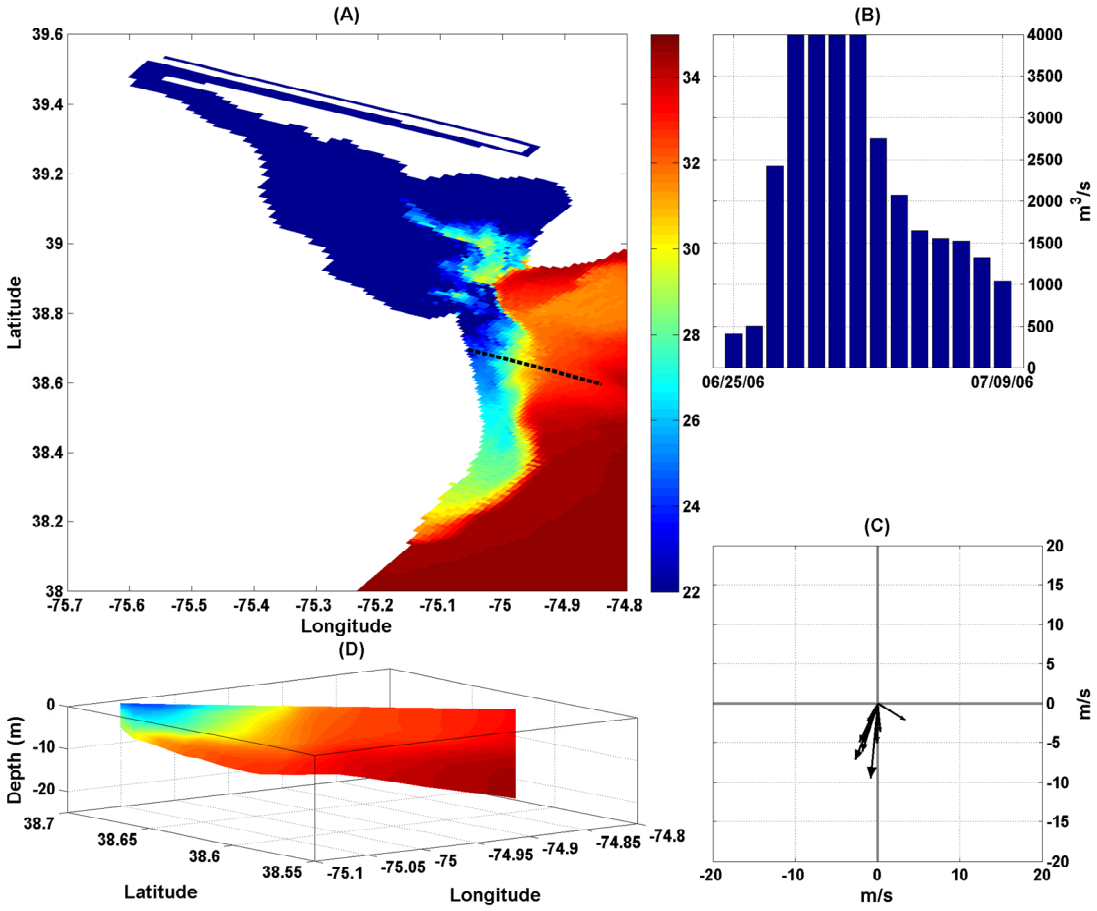

Figure 5.2 **09-July-2006 at 1:00:00. The buoyant plume that had developed during the early July 2006 significant discharge event. (A) Surface salinity in and around Delaware Bay. (B) Daily river discharge for the preceding two weeks. (C) Wind speed (m/s) and direction every for hours for the previous two days. (D) Salinity cross section. The dotted line in (A) is the location of the cross section. Colorbar units are in PSU.**

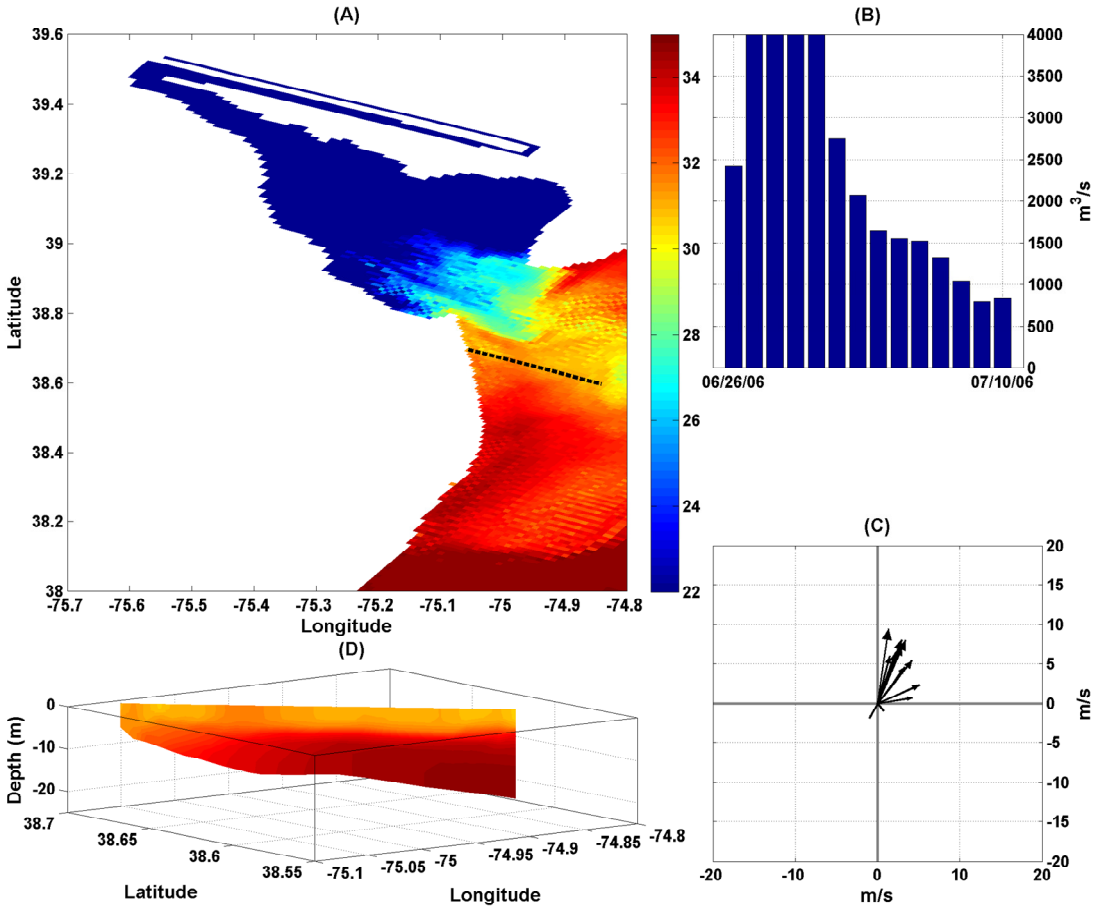

Figure 5.3 **10-July-2006 at 20:00:00. The dissolution of the plume shown in figure 5.2. (A) Surface salinity in and around Delaware Bay. (B) Daily river discharge for the preceding two weeks. (C) Wind speed (m/s) and direction every for hours for the previous two days. (D) Salinity cross section. The dotted line in (A) is the location of the cross section. Colorbar units are in PSU.**

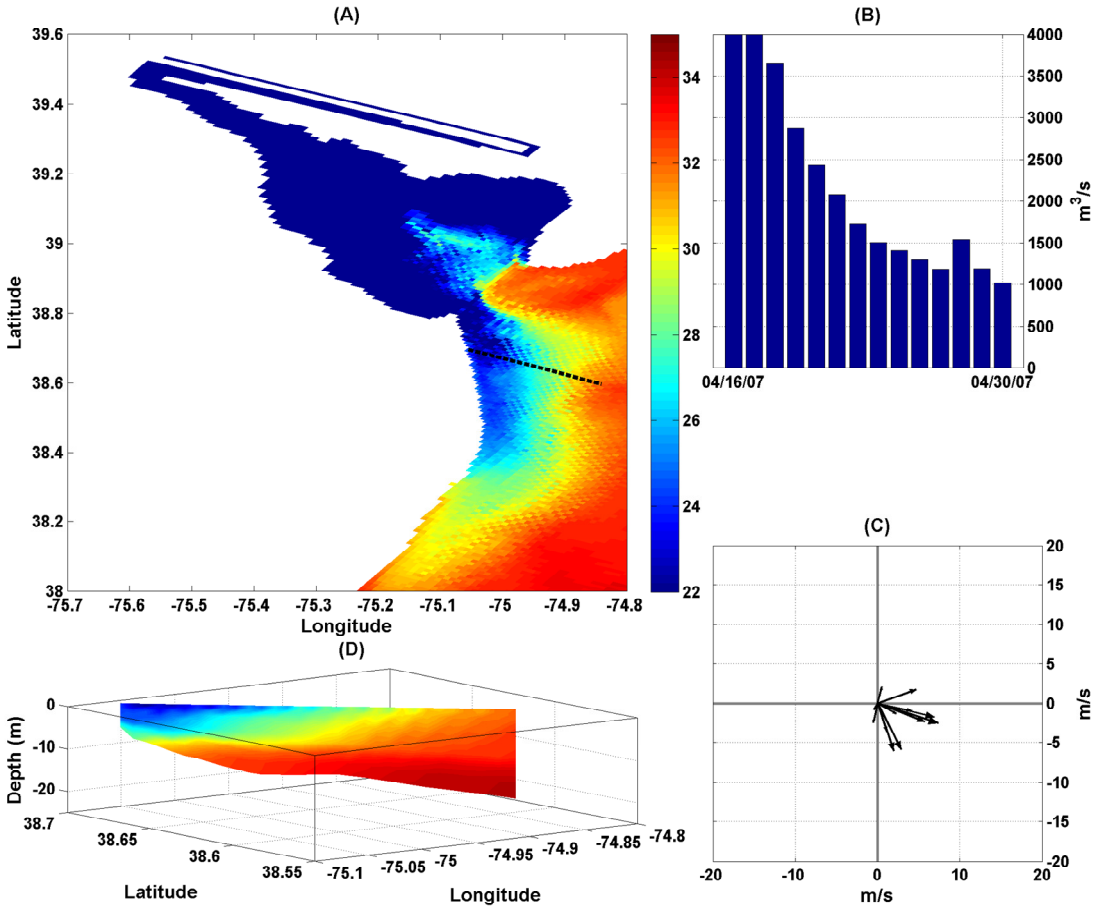

Figure 5.4 **30-April-2007 at 1:00:00. The buoyant plume that had developed during the late April 2007 significant discharge event. (A) Surface salinity in and around Delaware Bay. (B) Daily river discharge for the preceding two weeks. (C) Wind speed (m/s) and direction every for hours for the previous two days. (D) Salinity cross section. The dotted line in (A) is the location of the cross section. Colorbar units are in PSU.**

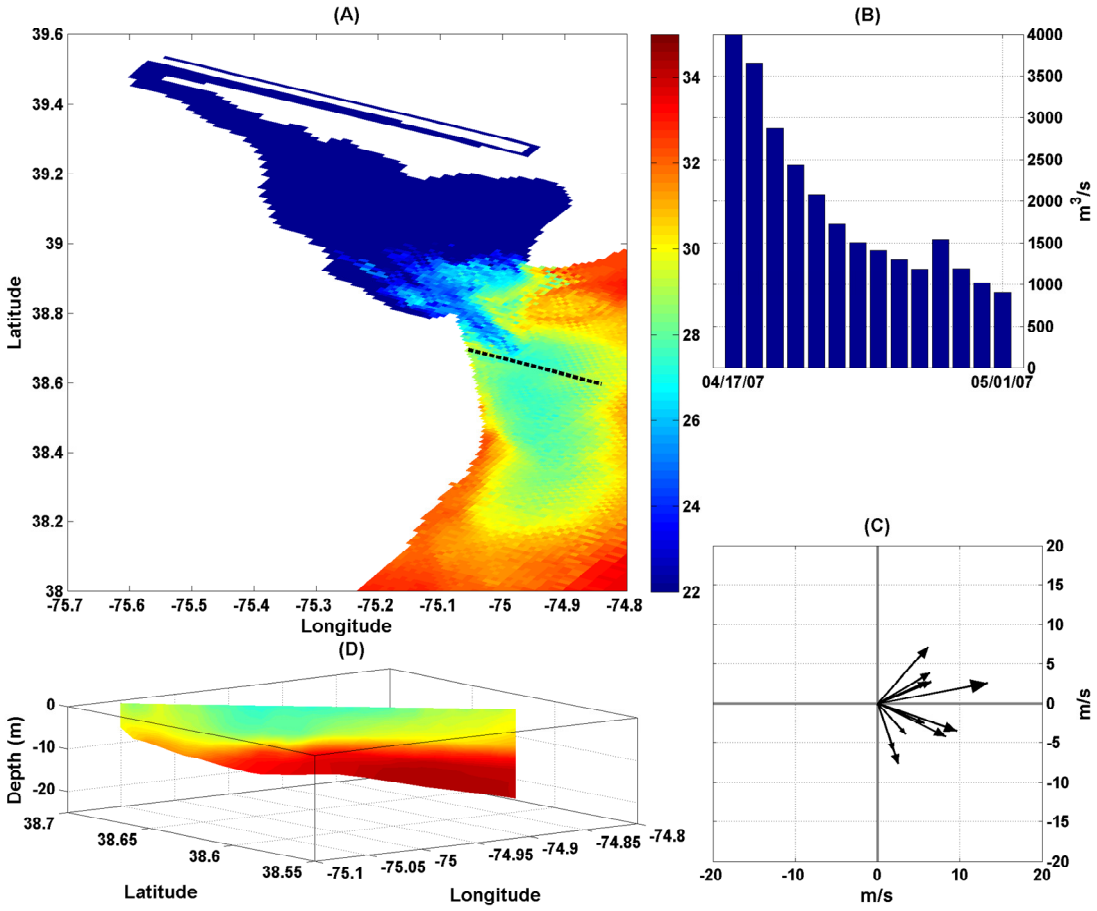

Figure 5.5 **01-May-2007 at 10:00:00. The widening of the plume in figure 5.4 due to shifting wind conditions. (A) Surface salinity in and around Delaware Bay. (B) Daily river discharge for the preceding two weeks. (C) Wind speed (m/s) and direction every for hours for the previous two days. (D) Salinity cross section. The dotted line in (A) is the location of the cross section. Colorbar units are in PSU.**

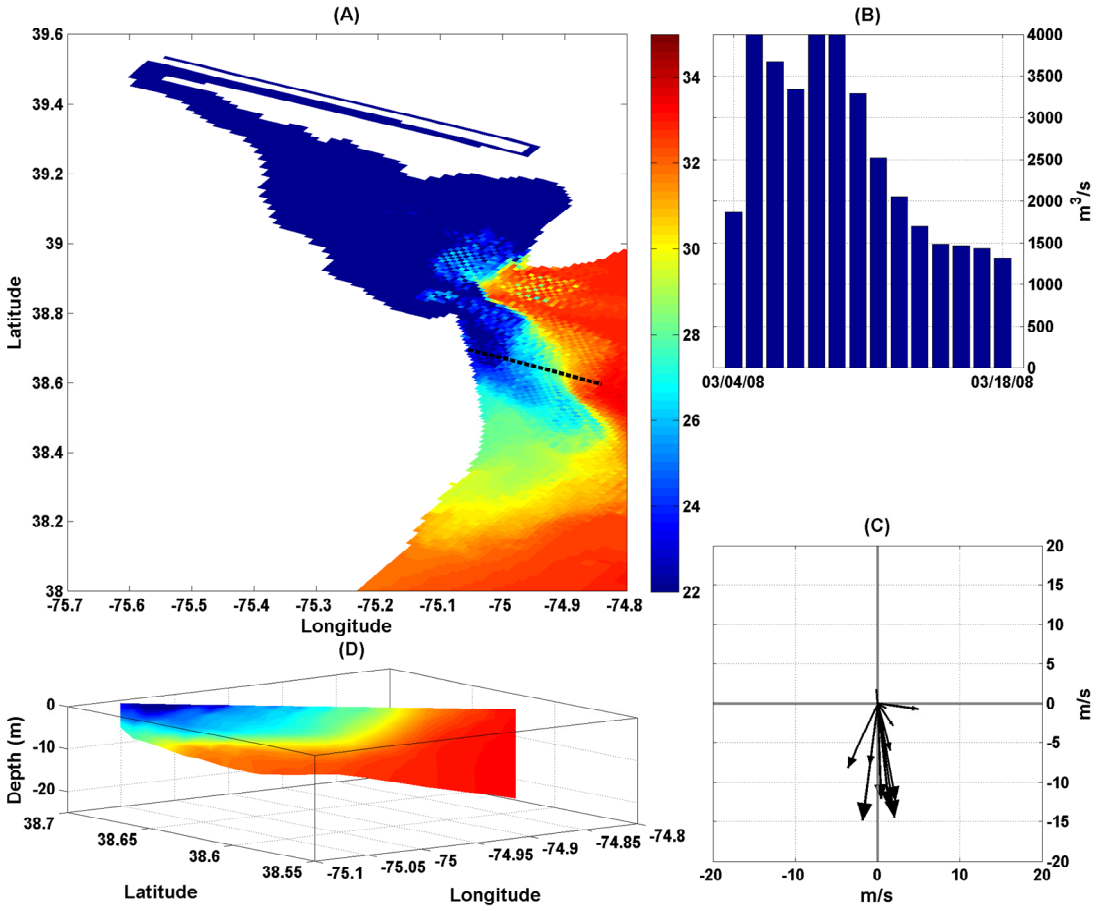

Figure 5.6 **18-March-2008 at 12:00:00. The buoyant plume that had developed during the early March 2008 significant discharge event. (A) Surface salinity in and around Delaware Bay. (B) Daily river discharge for the preceding two weeks. (C) Wind speed (m/s) and direction every for hours for the previous two days. (D) Salinity cross section. The dotted line in (A) is the location of the cross section. Colorbar units are in PSU.**

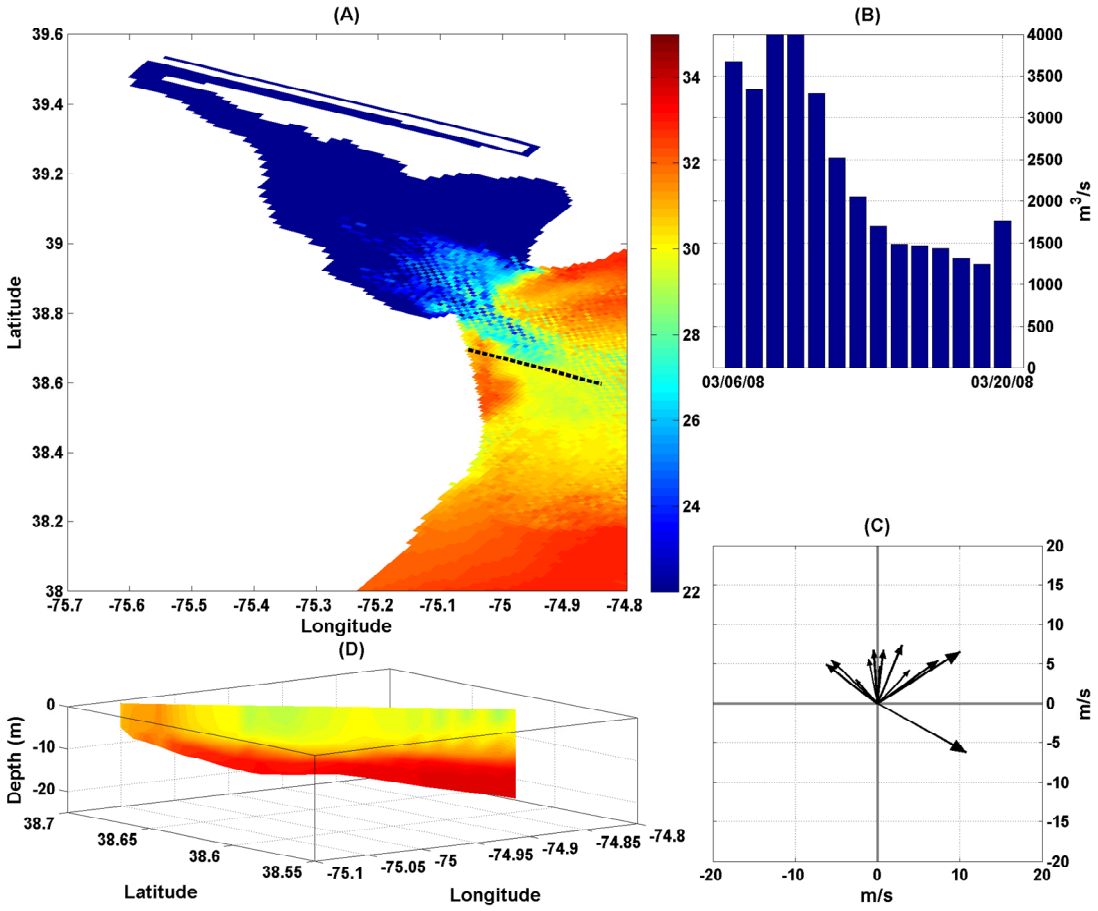

Figure 5.7 **20-March-2008 at 14:00:00. The spreading of the plume in figure 5.6. (A) Surface salinity in and around Delaware Bay. (B) Daily river discharge for the preceding two weeks. (C) Wind speed (m/s) and direction every for hours for the previous two days. (D) Salinity cross section. The dotted line in (A) is the location of the cross section. Colorbar units are in PSU.**

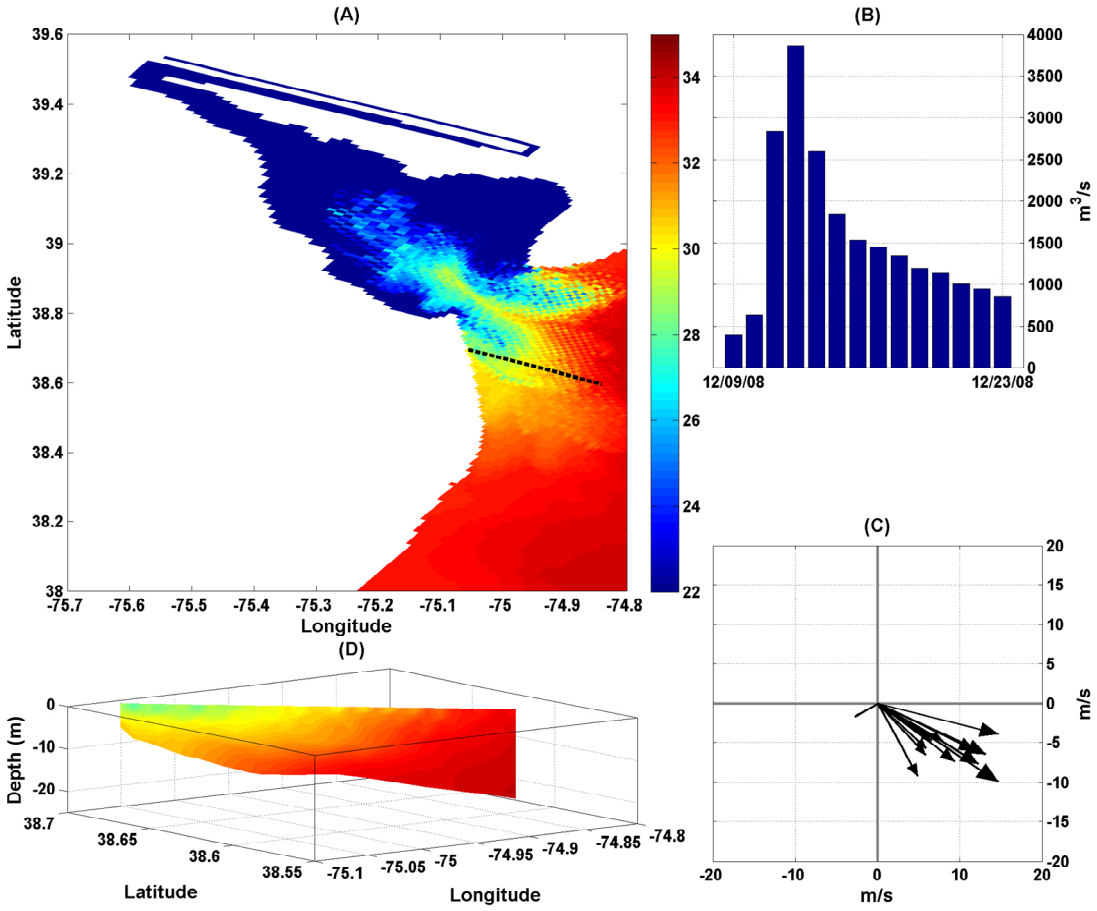

Figure 5.8 **23-December-2008 at 12:00:00. Mid December 2008 significant discharge event five. No noticeable plume developed. (A) Surface salinity in and around Delaware Bay. (B) Daily river discharge for the preceding two weeks. (C) Wind speed (m/s) and direction every for hours for the previous two days. (D) Salinity cross section. The dotted line in (A) is the location of the cross section. Colorbar units are in PSU.**

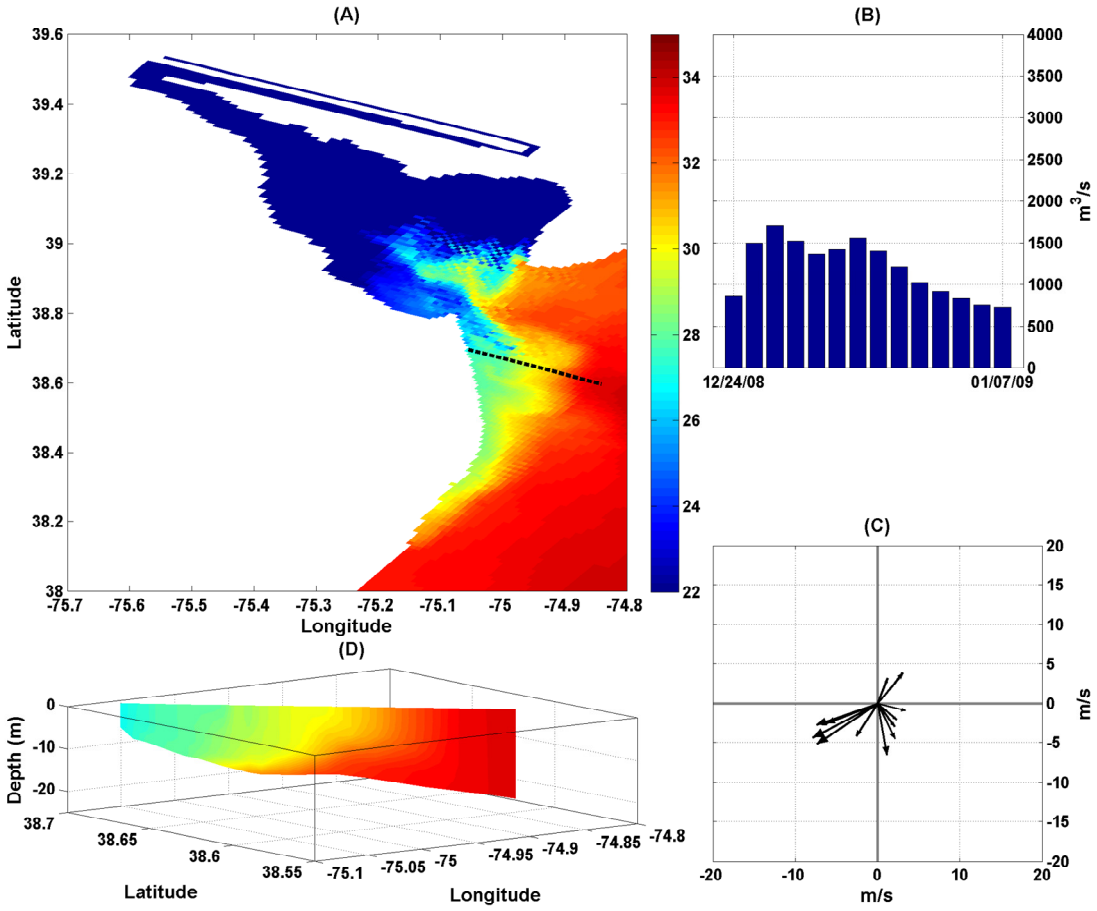

Figure 5.9 **07-Jan-2009 at 7:00:00. A plume that developed shortly after the mid December 2008 significant discharge event. (A) Surface salinity in and around Delaware Bay. (B) Daily river discharge for the preceding two weeks. (C) Wind speed (m/s) and direction every for hours for the previous two days. (D) Salinity cross section. The dotted line in (A) is the location of the cross section. Colorbar units are in PSU.**

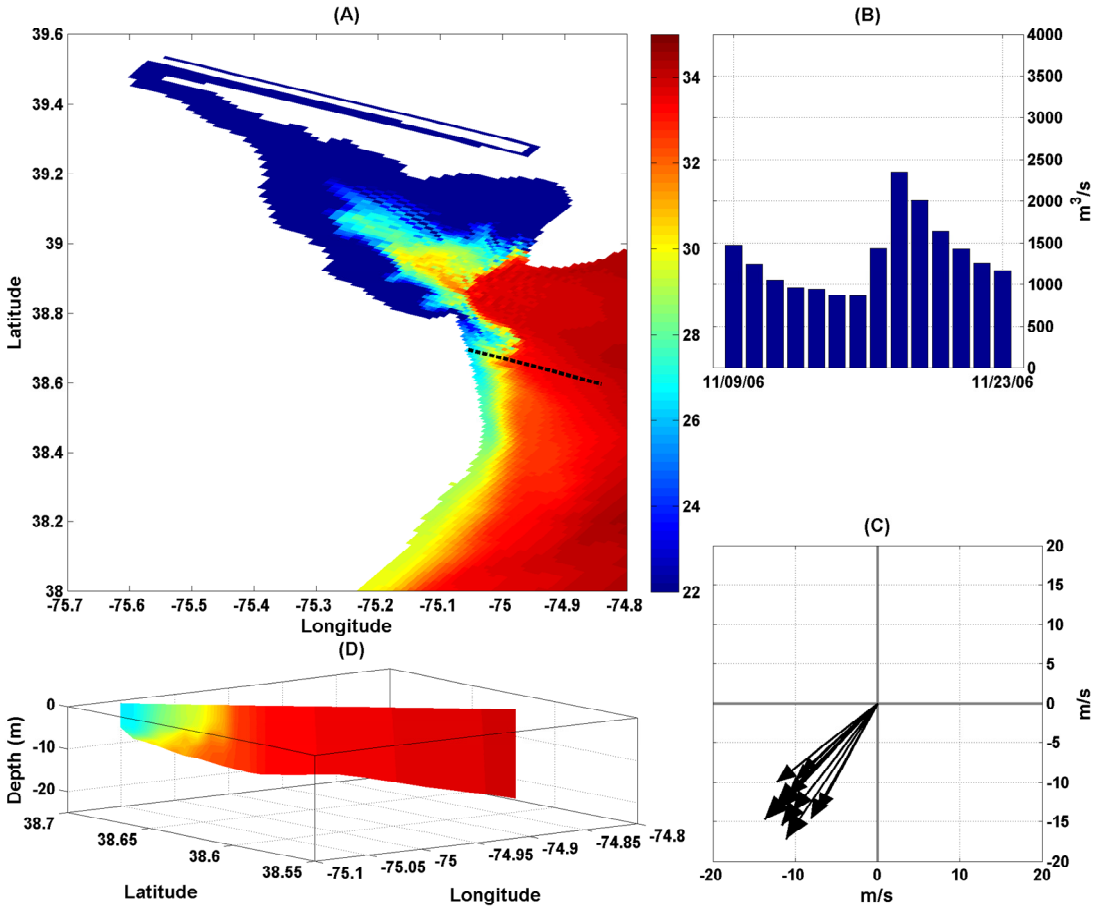

Figure 5.10 **23-November-2006 at 16:00:00. Shortly after the development of a coastal jet due to wind conditions. (A) Surface salinity in and around Delaware Bay. (B) Daily river discharge for the preceding two weeks. (C) Wind speed (m/s) and direction every for hours for the previous two days. (D) Salinity cross section. The dotted line in (A) is the location of the cross section. Colorbar units are in PSU.**

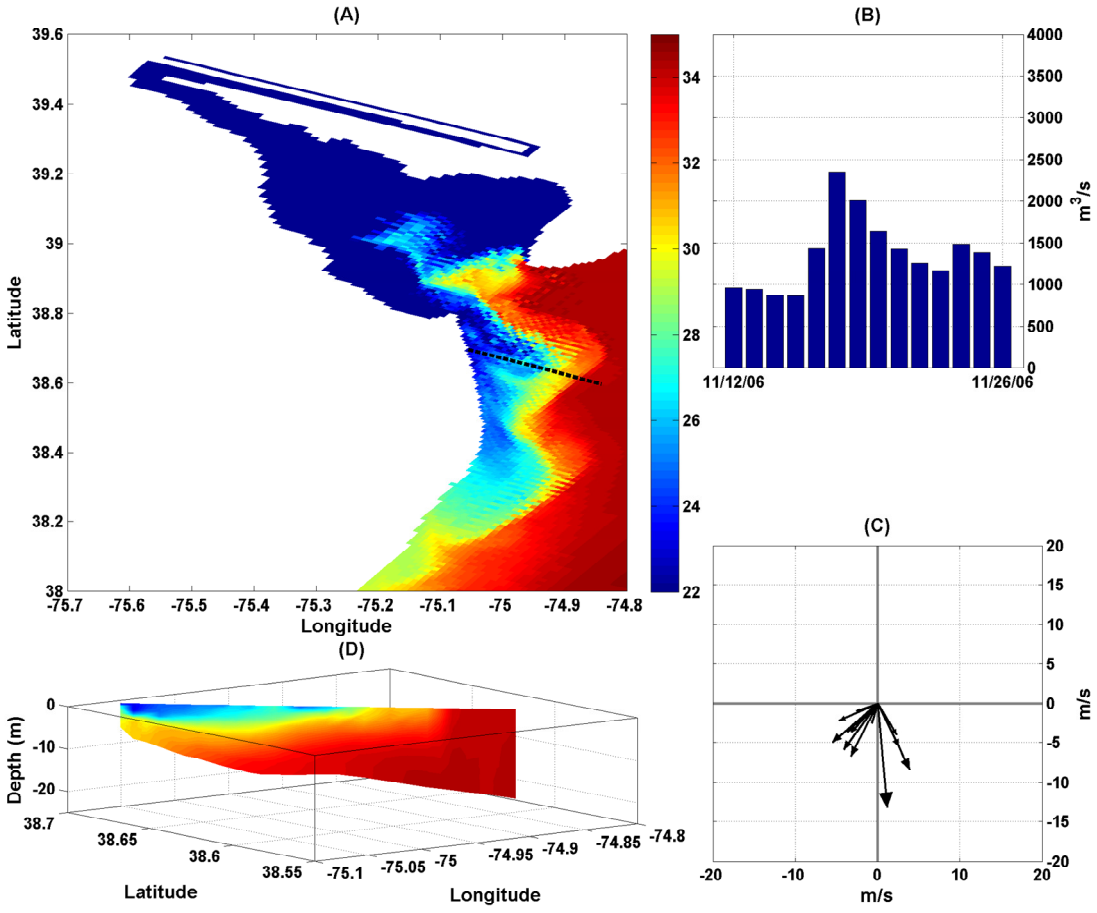

Figure 5.11 **26-November-2006 at 14:00:00. A more developed version of the coastal jet in figure 5.10 from a few days later. (A) Surface salinity in and around Delaware Bay. (B) Daily river discharge for the preceding two weeks. (C) Wind speed (m/s) and direction every for hours for the previous two days. (D) Salinity cross section. The dotted line in (A) is the location of the cross section. Colorbar units are in PSU.**

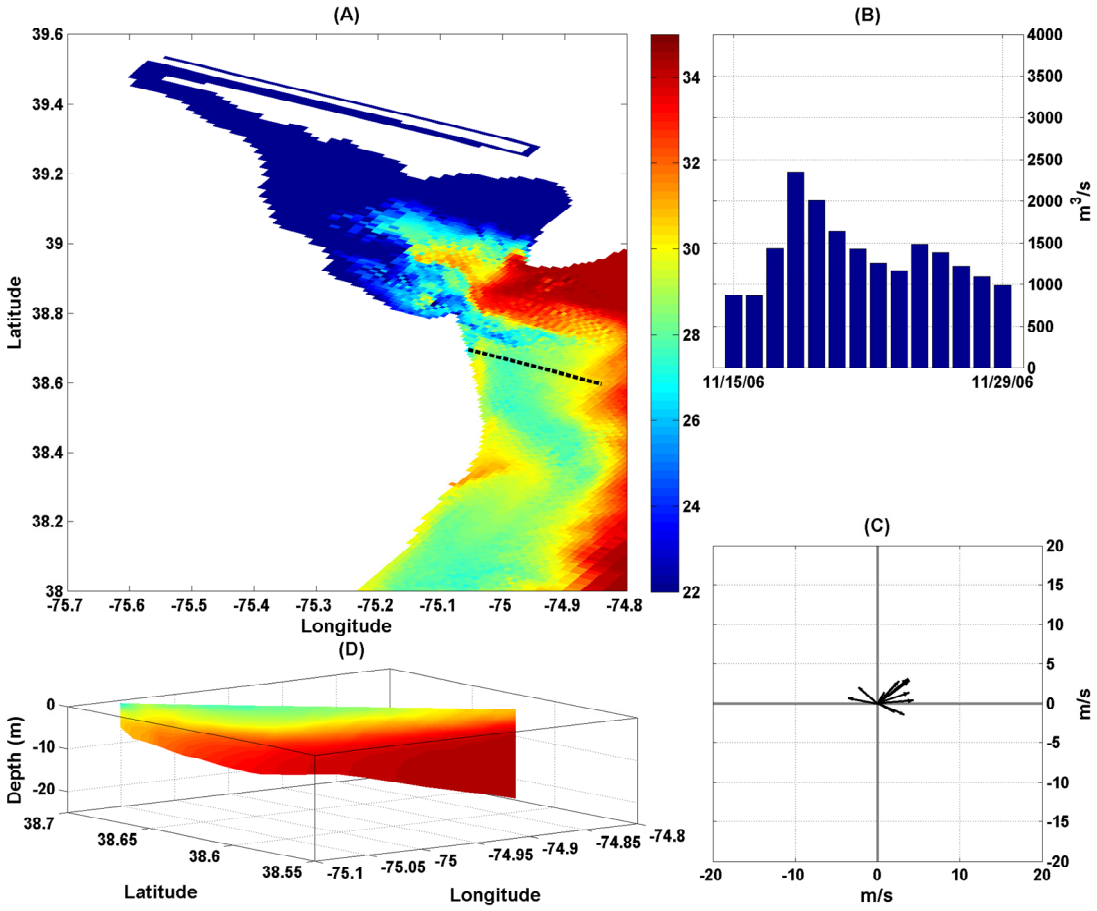

Figure 5.12 **29-November-2006 at 7:00:00. The widening of the plume from the previous figures shortly before it completely disappears. (A) Surface salinity in and around Delaware Bay. (B) Daily river discharge for the preceding two weeks. (C) Wind speed (m/s) and direction every for hours for the previous two days. (D) Salinity cross section. The dotted line in (A) is the location of the cross section. Colorbar units are in PSU.**

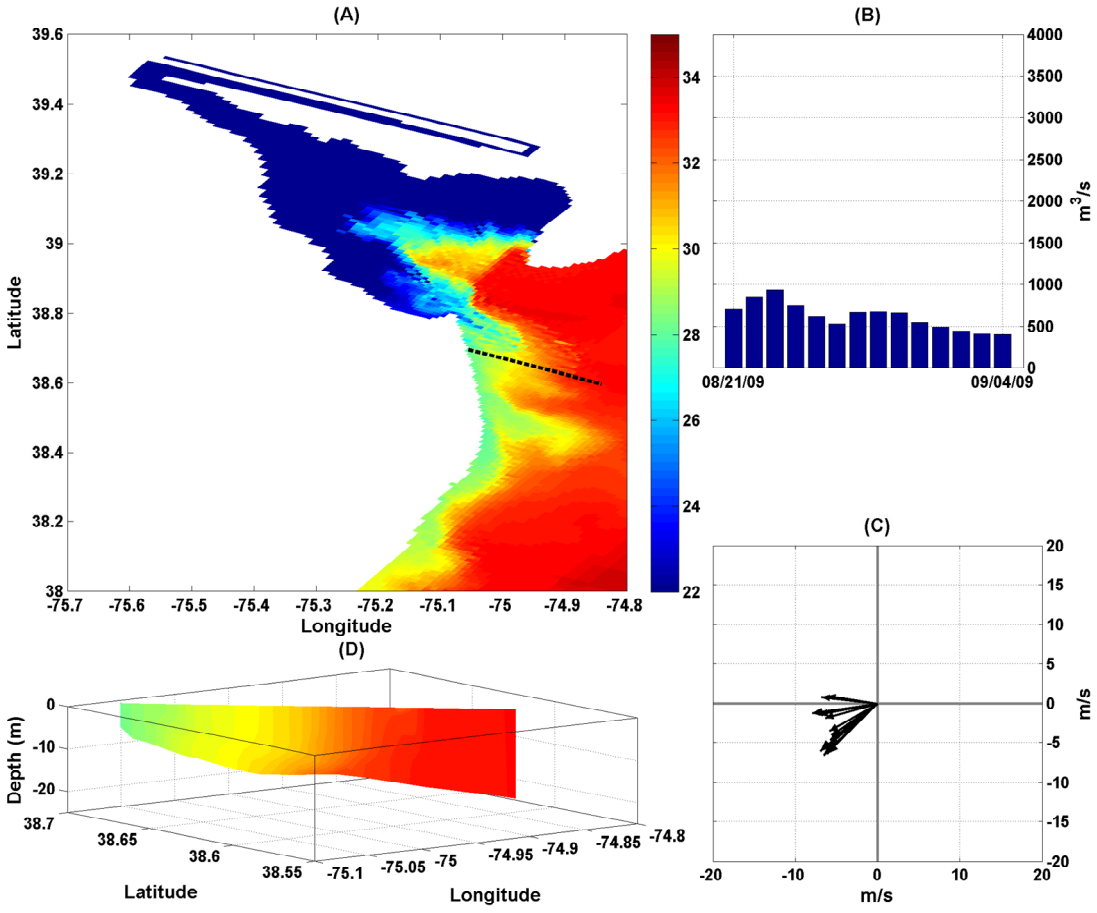

Figure 5.13 **4-September-2009 at 12:00:00. Another example of a coastal jet from a different time in the simulation. (A) Surface salinity in and around Delaware Bay. (B) Daily river discharge for the preceding two weeks. (C) Wind speed (m/s) and direction every for hours for the previous two days. (D) Salinity cross section. The dotted line in (A) is the location of the cross section. Colorbar units are in PSU.**

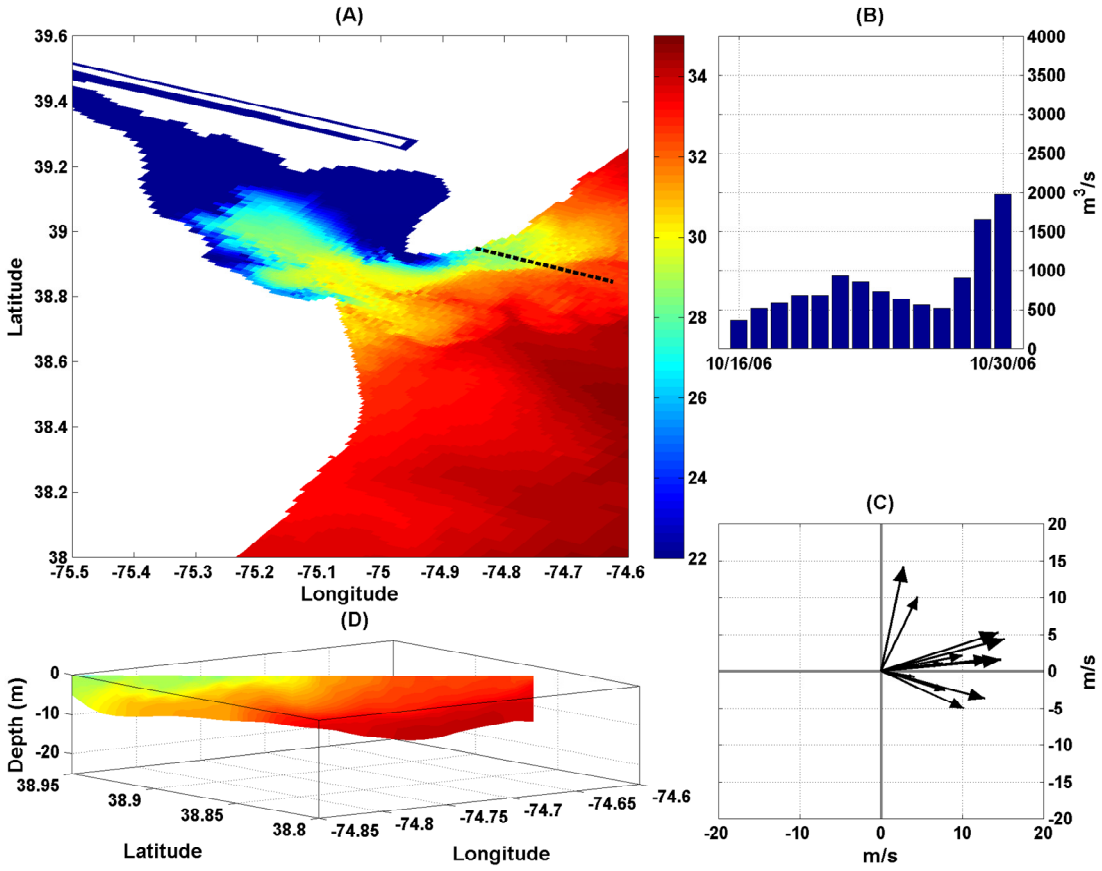

Figure 5.14 **30-October-2006 at 12:00:00. An example of a reversed plume developed from specific wind and discharge conditions. (A) Surface salinity in and around Delaware Bay. (B) Daily river discharge for the preceding two weeks. (C) Wind speed (m/s) and direction every for hours for the previous two days. (D) Salinity cross section. The dotted line in (A) is the location of the cross section. Colorbar units are in PSU.**

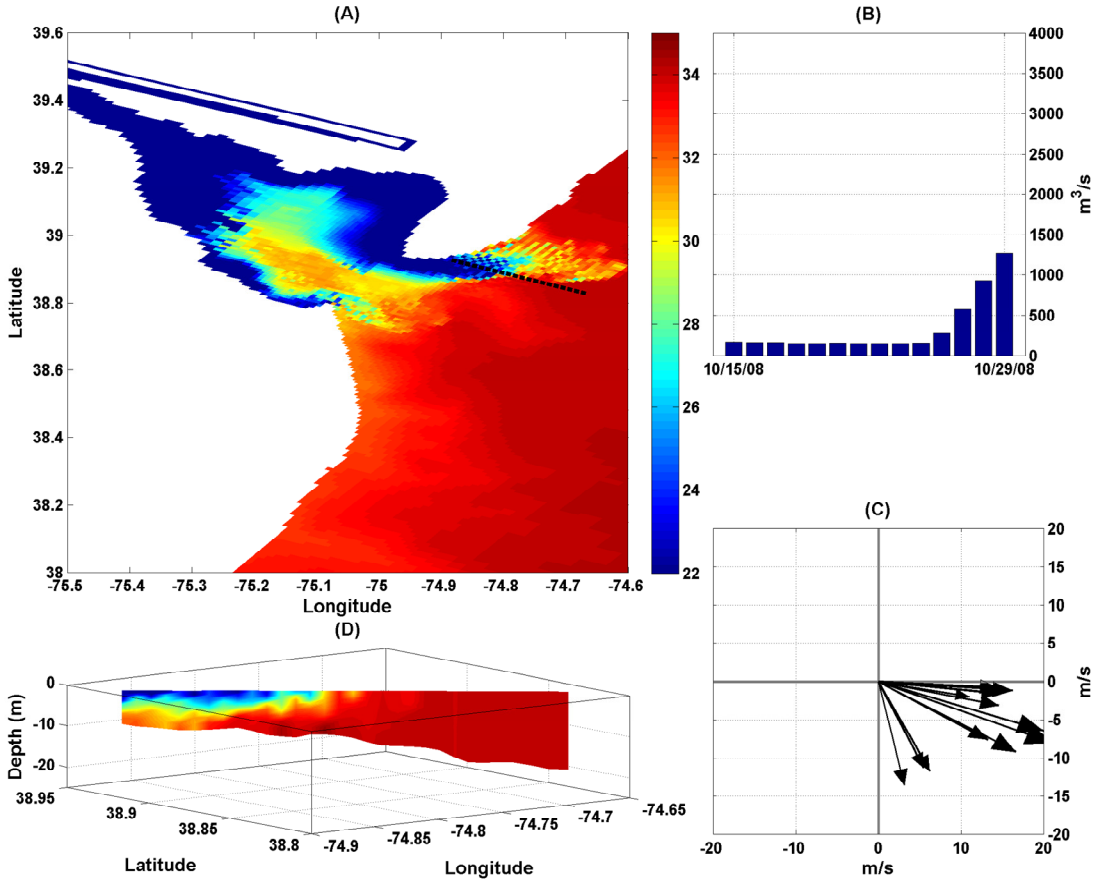

Figure 5.15 **29-October-2008 at 22:00:00. Another, more extreme reversed plume example. (A) Surface salinity in and around Delaware Bay. (B) Daily river discharge for the preceding two weeks. (C) Wind speed (m/s) and direction every for hours for the past two days. (D) Salinity cross section. The dotted line in (A) is the location of the cross section. Colorbar units are in PSU.**

Chapter 6

CONCLUSIONS

6.1 Summary of Model Performance

By looking at the results from the comparisons of model and measured data, it is clear the model demonstrates reasonable skill in predicting the hydrodynamic processes of Delaware Bay. The model predicts the measured currents based on CODAR data over a large area outside of the bay mouth to a high degree of accuracy, as well as providing an accurate picture of the 3D velocity based on point data taken from ADCPs. It also correctly predicts the free surface according to a comparison to the ADCP data.

6.2 Suggestions for Future Work

While this model serves as an appropriate base for a model of Delaware Bay, there are certainly ways it can be added to and improved. The next step would be to add wave information into the model by coupling to an existing wave model such as SWAN. More sophisticated atmospheric forcing and temperature information could be used in an attempted to improve the accuracy of the model as well.

The validation of the model can also be improved if there were more sources of measured data to compare to around the bay area. All of the comparisons from this effort have concentrated on the area around the bay mouth due to high

availability of measured data. Additional ADCP deployments into the bay could help further validate the performance of the model.

REFERENCES

Akima, H.. "On estimating partial derivatives for bivariate interpolation of scattered data", Rocky Mountain J. of Math, 14, 41-52 (1984).

Arakawa, A. and V. R. Lamb, "Methods of computational physics," Academic Press, 174-265, (1977).

Bissett, W.P., J.J. Walsh, D.A. Dieterle, K.L. Carder, "Carbon cycling in the upper waters of the Sargasso Sea: I. Numerical simulation of differential carbon and nitrogen fluxes", Deep-Sea Res., 46, 205-269, (1999).

Booij, N., R. C. Ris, and L. H. Holthuijsen, "A third-generation wave model for coastal regions. Part I - Model description and validation," Journal of Geophysical Research, 104, 7649-7666, (1999).

Budgell, W.P., "Numerical simulation of ice-ocean variability in the Barents Sea region", Ocean Dynamics, DOI 10.1007/s10236-005-0008-3 (2005).

Chapman, D. C., "Numerical treatment of cross-shelf open boundaries in a barotropic coastal ocean model", J. Phys. Oceanogr., 15, 1060—1075, (1985).

Chapman, R. D., L. K. Shay, H. C. Graber, J. B. Edson, A. Karachintev, C. L. Trump, and D. B. Ross, " On the accuracy of HF radar surface current measurements: Intercomparisons with ship-based sensors," J Geophys Res., 102, 18,737-18,748, (1997).

Chen Y. F., "Coupling of wave and circulation models for predicting storm-induced waves, surges, and coastal inundation," Masters Thesis, University of Delaware, DE, USA, (2010).

Choi, B.-J., and J. L. Wilkin, "The effect of wind on the dispersal of the Hudson River plume," *J. Phys. Oceanogr.*, **37**, 1878-1897, (2006).

Fairall, C. W., E. F. Bradley, D. P. Rogers, J. B. Edson and G. S. Young, " Bulk parameterization of air-sea fluxes for tropical ocean-global atmosphere Coupled-Ocean Atmosphere Response Experiment," J. Geophys. Res., 101, 3747-3764, (1996).

Fennel, K., J. Wilkin, J. Levin, J. Moisan, J. O'Reilly, and D. Haidvogel, "Nitrogen cycling in the Middle Atlantic Bight: Results from a three-dimensional model and implications for the North Atlantic nitrogen budget", Global Biogeochem. Cycles, 20, GB3007, doi:10.1029/2005GB002456 (2006).

Flather, R. A., "A tidal model of the northwest European continental shelf "Memoires de la Societe Royale de Sciences de Liege, 6, 141-164, (1976).

Freeman, N. G., A. M. Hale, and M. B. Danard, "A modified sigma equations' approach to the numerical modeling of great lake hydrodynamics," J. Geophys. Res., 77, 1050-1060, (1972).

Garvine, R. W., "Subtidal frequency estuary-shelf interaction: Observations near Delaware Bay. J. Geophysical Research., 90, 11,945-11,948, (1991).

Garvine, R. W., R. K. McCarthy, and K. -C. Wong, "The axial salinity distribution in the Delaware Estuary and its weak response to river discharge," Estuarine, Coastal, and Shelf Science, 35, 157-165, (1992).

Haidvogel, D. B., H. G. Arango, K. Hedstrom, A. Beckmann, P. Malanotte-Rizzoli, and A. F. Shchepetkin, " Model evaluation experiments in the North Atlantic Basin: Simulations in nonlinear terrain-following coordinates", Dyn. Atmos. Oceans, 32, 239-281, (2000).

Hansen, D.V. and M. Rattray, "New dimensions in estuary classification," Limnology and Oceanography, 11, 3, 319-325, (1966).

Harleman, D. R. F., "Real Estuaries, in Estuary and Coastline Hydrodynamics," Ippen, A. T., ed., 522-545, (1966).

Johnson, H. K., "Simple expressions for correcting wind speed data for elevation", Coastal Engineering, 36, 263-269, (1999).

Kosters, F., "Denmark Strait overflow: Comparing model results and hydraulic transport estimates," *J. Geophys. Res.*, **109**, C10011, doi:10.1029/2004JC002297, (2004).

Kundu, P. K., “Ekman veering observed near the ocean bottom,” Journal of Physical Oceanography, 6, 238-242, (1976).

Large, W. G., J. C. McWilliams, and S. C. Doney. “Oceanic vertical mixing: a review and a model with a nonlocal boundary layer parameterization”, Rev. Geophys., 32, 363-403, (1994).

Large, W.G., and S. Pond, “Open ocean momentum flux measurements in moderate to strong winds.” J. Phys. Oceanogr., 11, 324-336, (1981).

Luettich, R.A., Jr., J.J. Westerink, and N.W. Scheffner, “ADCIRC: an advanced three-dimensional circulation model for shelves coasts and estuaries, report 1: theory and methodology of ADCIRC-2DDI and ADCIRC-3DL”, Dredging Research Program Technical Report DRP-92-6, U.S. Army Engineers Waterways Experiment Station, Vicksburg, MS, 137p, (1992).

Marchesiello, P., J. C. McWilliams, and A. Shchepetkin, “Equilibrium structure and dynamics of the California Current System”, J. Phys. Oceanogr., 33, 753-783, (2003).

Mellor, G. L., “User’s guidefor a three dimensional, primitive equation, numerical ocean model,” Program in Atmospheric and Ocean Sciences report, Princeton University, pp. 41 (1998).

Mori, N., “ROMS memorandum- Open boundary conditions”, Kyoto University, Kyoto, Japan, (2007).

Münchow, A. and R. W. Garvine, “Dynamical properties of a buoyancy-driven coastal current,” J. Geophys. Res., 98, C11, 20,063-20,077, (1993a).

Münchow, A. and R. W. Garvine, “Buoyancy and wind forcing of a coastal current,” J. Mar. Res., 51, 2, 293-322, (1993a).

Muscarella, P., A. Skarke, B. L. Lipphardt, A. Trembanis, “Comparison of HF Radar and ADCP surface current measurements at Delaware Bay mouth,” In revision, (2010).

Ohlmann, C., P. White, L. Washburn, E. Terrill, B. Emery, and M. Otero, “Interpretation of coastal HF radar-derived surface currents with high-resolution drifter data,” J. Atmos. Ocean. Tech., 24, doi: 10.1175/JTECH1998.1, (2007).

Orlanski, I., “A simple boundary condition for unbounded hyperbolic flows” J. Comp. Sci., 21(3), 251-269, (1976).

Pawlowicz, R., B. Beardsley, and S. Lentz, "Classical Tidal Harmonic Analysis Including Error Estimates in MATLAB using T_TIDE", Computers and Geosciences, (2002).

Phillips, N. A., “A coordinate system having some special advantages for numerical forecasting,” J. Meteorology, 14, 184-185, (1957).

Powell T. P., C. V. W. Lewis, E. N. Curchitser, D. B. Haidvogel, A. J. Hermann, E. L. Dobbins, “Results from a three-dimensional, nested biological-physical model of the California Current System and comparisons with statistics from satellite imagery”, J. Geophys. Res., 111, C07018, doi:10.1029/2004JC002506, (2006).

Qin, W.., J. T. Kirby, and M. Badiey. “Application of the spectral wave model SWAN in Delaware Bay”, Research Report No. CACR-05-09, (2005).

Raymond, W. H. and H. L. Kuo, “A radiation boundary condition for multi-dimensional flows”, Quart. J. R. Met. Soc., 110, 535-551, (1984).

Rew, R. K. and G. P. Davis, "The Unidata netCDF: Software for Scientific Data Access," Sixth International Conference on Interactive Information and Processing Systems for Meteorology, Oceanography, and Hydrology, Anaheim, California, American Meteorology Society, pp. 33-40, (1990).

RD Instruments, “Workhorse Sentinel ADCP user’s guide,” P/N 957-6163-00, (January 2001)

Robertson, R., “Modeling tides and vertical tidal mixing: A reality check,” IOP Conf. Series: Earth and Environmental Science 11, (2010)

Sanders, T. M., “The fate of the Delaware Coastal Current on the continental shelf,” Ph.D. dissertation, University of Delaware, 177 pp, (1999).

Sanders T. M. and R. W. Garvine, “Fresh water delivery to the continental shelf and subsequent mixing: An observational study,” J. Geophys. Res., 106, C11, 27,087-27,101, (2001).

Shchepetkin, A. F., and J. C. McWilliams, “The Regional Ocean Modeling System: A split-explicit, free-surface, topography following coordinates ocean model”, Ocean Modelling, 9, 347-404, (2005).

Sharp, J., "The Delaware Estuary: Research as background for estuarine management and development," Delaware River and Bay Authority, (1984).

Skamarock, W. C., J. B. Klemp, J. Dudhia, D. O. Gill, D. M. Barker, W. Wang, and J. G. Powers, 2005, "A description of the Advanced Research WRF Version 2," NCAR Tech Notes-468+STR, (2005).

Smith, W. H. F., and D. T. Sandwell, "Global seafloor topography from satellite altimetry and ship depth soundings", Science, v. 277, p. 1957-1962, 26 Sept., (1997).

Song, Y. and D. B. Haidvogel, "A semi-implicit ocean circulation model using a generalized topography-following coordinate system," J. Comp. Phys., 115 (1), 228-244, (1994).

Teledyne RD Instruments, "Acoustic Doppler Current Profiler Principles of Operation: A Practical Primer," P/N 951-6069-00, (2006).

Thatcher, M. L. and D. R. F. Harleman. "Long-term salinity calculation in Delaware estuary", Journal of the Environmental Engineering Division, 107, EE1, 11-27, (1981).

Warner, J. C., C. R. Sherwood, R. P. Signell, C. K. Harris, and H. G. Arango, "Development of a three-dimensional, regional, coupled wave, current, and sediment-transport model", Computers & Geosciences, 34, 1284-1306 (2008).

Warner, J. C., N. Perlin, E. D. Skyllingstad, " Using the Model Coupling Toolkit to couple earth system models", Environmental Modelling & Software, 23, 1240-1249, (2008).

Warner, J.C., Armstrong, B., He, R., and Zambon, J.,"Development of a coupled-ocean-atmosphere-wave-sediment transport (COAWST) Modeling System", Ocean Modelling, 35, 230-244, (2010).

Whitney, M. M. "Simulating the Delaware coastal current", Ph.D. Dissertation, University of Delaware, DE, USA, (2003).

Wilkin, J. L., H. G. Arango, D. B. Haidvogel, C. S. Lichtenwalner, S. M. Durski, and K. S. Hedstrom, "A regional ocean modeling system for the long-term ecosystem observatory", J. Geophys. Res., 110, C06S91, doi:10.1029/2003JC002218, (2005).

Wilkin, J. and K. S. Hedstrom. ”User’s manual for an orthogonal curvilinear grid-generation package”, Institute for Naval Oceanography, (1991).

Wong, K. -C., “On the nature of transverse variability in a coastal plain estuary,” Journal of Geophysical Research, 99, 14, 209-14, 222, (1994).

Wong, K.-C., "The hydrography at the mouth of Delaware Bay: Tidally averaged distribution and intratidal variability". Estuarine, Coastal and Shelf Science 41:719-736, (1995).

Wong, K.-C., "On the relationship between long-term salinity variations and river discharge in the middle-reach of the Delaware estuary". Journal of Geophysical Research 100(C10):20705-20713, (1995).

Wong, K. –C. and A. Münchow, “Buoyancy forced interaction between estuary and inner shelf: observation,” Cont. Shelf Res., 15, 1, 59-88, (1995).

Xu, Z. “Ellipse parameters conversion and vertical velocity profiles for tidal currents,” Bedford Institute of Oceanography, (2000).